COMPUTATIONAL MODELLING OF ZEOLITE SYSTEMS.

A thesis submitted to the University of Manchester
for the degree of Doctor of Philosophy
in the Faculty of Science

By
Carl Mark Windsor
Department of Chemistry
2000

Contents

List of Figures

List of Tables

Abstract

UNIVERSITY OF MANCHESTER

ABSTRACT OF THESIS submitted by **Carl Mark Windsor** for the Degree of Doctor of Philosophy and entitled **Computational modelling of zeolite systems.**

Month and Year of Submission: September 2000

The chemical reactivity within a zeolite pore is highly dependent on the long-range electrostatic interactions of the periodic environment. Traditional Quantum Mechanical methods such as truncation of the zeolite framework (cluster modelling) neglect these interactions and thus incorrectly represent the electrostatic potential around the study cluster. This thesis presents a hybrid periodic QM/MM method for the embedding a QM cluster in the periodic electrostatic environment due to the extended Madelung field of a zeolite. Short range interactions are dealt with using standard molecular mechanical potentials whilst the periodic summation of the point charges is computationally dealt with by using an Ewald summation. The periodic charge density is directly interacted with the QM cluster allowing perturbation of the QM cluster by the external corrective potential.

Declaration

No portion of the work referred to in the thesis has been submitted in support of an application for another degree or qualification of this or any other university or other institute of learning.

Copyright

Acknowledgements

None of this would have been possible were it not for the following people:

My supervisor Professor Ian Hillier, for his support, guidance and funding throughout my research.

To all the members of the Manchester University Theoretical Chemistry group, who worked with me during my Ph.D. I'm sure I asked for help and took advice from everyone who worked here between October 1996 and September 2000. Most importantly Neil Burton, Joe McDouall, Andrew Masters, Richard Hall, Noj Malcolm, Martin Nygren, Richard Bryce, Sally Hindle, Mark Nichol, Dave Sheppard and Helen Steele.

To Liam Salsi, started off as a student and quickly became a teacher. Your discussions on Ewald theory were invaluable.

To Mark Vincent, thanks are due for the painstaking work done whilst proof-reading this thesis.

Thanks also to Julian Gale for the use of and support for GULP.

To my parents and brother for all their support.

Finally, a huge thank you to Tammy Bate for her support and encouragement. She made the difficult times much easier to handle, and had confidence in me

throughout.

Biography

The author graduated from UMIST in 1996 with an Upper Second Class honours degree in Chemistry and was awarded the Air Products prize for his third year dissertation on the subject of Computational modelling of aza Diels-Alder catalysis. Since then he has been engaged in research as a member of the Theoretical Chemistry group at the University of Manchester, under the supervision of Prof. Ian H. Hillier.

Publications

What makes a neutral imino dienophile undergo a thermal non-catalysed Diels-Alder reaction? Tetrahedron *54* (1998) 6035-6050

Ab-initio study of single and double point absorption of carbon monoxide on clusters representing zeolites. Phys. Chem. Chemical Physics *1* (1999) 507-512

Modelling of Zeolite Catalysis: An Overview. Online WWW Poster.

An Embedded Cluster Method To Model Zeolite Catalysis, WATOC 99 Poster presentation.

To Mum and Dad -
for all their hard work and sacrifices,
I would not be here otherwise.

"... do or do not, there is no try."

Yoda, Jedi Master.

Abbreviations

DFT	Density functional theory
ECP	Effective core potential
FTIR	Fourier transform infra-red
G9X	Gaussian9X
GULP	General utility lattice program
HF	Hartree-Fock theory
IR	Infra-red
LCSF	Localised self-consistent field
MAS	Magic angle spinning
MC	Monte Carlo
MD	Molecular dynamics
MM	Molecular mechanics
MO	Molecular orbital
MPX	Moller-Plesset purturbation theory (where X is the level of theory)
MTG	Methanol to gasoline
MUPPET	Manchester University periodic potential environment
NMR	Nuclear magnetic resonance
PDC	Potential derived charges
PEP	Positron emission profiling
PQM/MM	The periodic QM/MM method implimented in the MUPPET program

PWP	Plane wave pseudopotential
QM	Quantum mechanics
QM-MM	Interaction of the QM region with the MM region
QM/MM	Interaction of the QM region with itself and the MM region
SCF	Self-consistent field
TPD	Temperature programmed desorption
VDW	van der Waal(s)

Chapter 1

Introduction

1.1 The history of zeolites

The word 'zeolite' is of Greek origin, coming from the words 'zein' and 'lithos' meaning to boil and rock. The name was first used by the Swedish chemist Cronstedt who found that upon heating, the zeolite sample evolved steam.[6] There was little interest in zeolites until the late 1930's when the modern founder of zeolite chemistry, Richard Barrer began the characterisation of zeolite structure and chemistry. His initial studies of zeolites confirmed the molecular sieving properties of the microporous solids and was reported in a paper titled "The sorption of polar gases by zeolites" and published in the Proceedings of the Royal Society.[7] His subsequent papers gave details of the first method of laboratory synthesis of zeolites from silicate alumina gels, the changes that occur upon ion exchange and their use as strong environmentally friendly, shape selective catalysts. These discoveries sparked huge interest in the synthesis of shape selective zeolite catalysts in companies such as Union Carbide and Mobil. In the late 1950's, early 1960's Union Carbide made several discoveries which proved to be of great economic significance and propelled them to the forefront of zeolite science. Milton

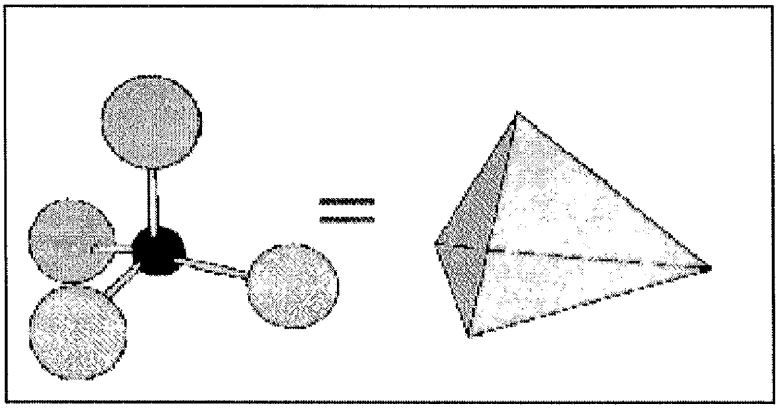

Figure 1.1: Tetrahedral T-Site

and Breck of the Linde division of Union Carbide, over a period of five years, developed and characterised three novel zeolites; Linde A, X and Y,[8] which have become the most profitable synthetic zeolites.

1.1.1 Zeolite structure

The classic definition of a zeolite is a crystalline, porous aluminosilicate composed of a linked framework of $[SiO_4]^{4-}$ and $[AlO_4]^{5-}$ edge sharing tetrahedra. The metal atoms are surrounded by four oxygen anions at the four corners of a tetrahedron, the tetrahedrally coordinated metals being known as T-sites.

The edge sharing tetrahedra associate to form a wide variety of rings and cages known as secondary building units (SBU's). The joining together of these SBU's gives rise to the huge number of different zeolites, all with intriguing properties. The SBU's join to form structurally and chemically important zeolite channels, known as oxygen windows that pass through the zeolite. It is the pore system of the zeolites that gives rise to their characteristic properties. The pores vary from one to three dimensions, vary in size and, in the case of ZSM-5, can also be sinusoidal. The rate of diffusion of a molecule through a zeolite will therefore

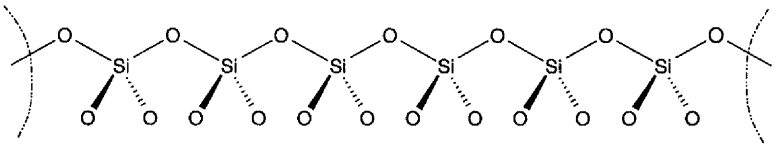

Figure 1.2: Neutral All-Silica Framework

be determined by a combination of the size of the sorbate and the type of zeolite used.

Recent discoveries of materials virtually identical to the classical zeolite *i.e.* oxides of metals other than silicon and aluminium, have stretched the definition. Virtually all oxide structures with a well defined porous structure are now included in the zeolite definition although some researchers prefer the name 'zeotypes'.[9] Further references to 'zeolites' within this text will be referring to the aluminosilicate family only with other such structures being called by their explicit name *e.g.* SAPO.

Each zeolite has an all silica polymorph and the type of zeolite is dependent on the percentage substitution of Aluminium (or other metal ion) in place of silicon when compared with the all silica form. In all-silica frameworks there is charge neutrality due to a 4^+ charge on the Si atoms and 2 oxygens per Si, each with a 2^- charge.

The Si:Al ratio is restricted to a maximum of 1:1. This is due to Loewensteins Rule[10] which forbids the existence of Al-O-Al linkages. This means that each aluminium tetrahedra must always be linked to four silicate tetrahedra.

1.2 Zeolite chemistry

There are two very different uses of zeolites

- As adsorbants or molecular sieves
- As industrially important chemical catalysts, most notably in the petrochemical industry where zeolites are used in oil refining as cracking catalysts

1.2.1 Molecular sieving properties

Zeolite molecular sieves are highly selective, high capacity adsorbants due to their large interior surface area and strong electrostatic interactions with their adsorbates. Molecules are selectively sieved based on their steric and chemical properties. Size and structure relative to the pore appertures in the zeolite, charge and dipole moments of the molecules[11] all affect the selectivity. For example, different polar molecules have differing strengths of interaction with the zeolite molecular sieve framework and hence can be separated.

To soften water and aid the work of washing powders, environmentally toxic polyphosphates are used as softeners. Softeners remove Ca^{2+} and Mg^{+} from washing water, which softens the water and prevents precipitation of the surfactants. Modern detergents use Zeolite A, which has no adverse effects on the environment and is better at removing Ca^{2+} ions. An Na^{+} exchanged version of the zeolite is used which readily swaps the soft Na^{+} ion for harder Ca^{2+} and Mg^{+} ions. Whilst it is good at removing Ca^{2+}, it is not quite as efficient at removing Mg^{+}, therefore some of the environmentally toxic polyphosphates are still used.

Zeolite A[8] is also used during the treatment of radioactive waste whereby radioactive isotopes of Caesium and Strontium are removed from nuclear waste into the zeolite cavity. All nuclear waste is mixed with zeolites before packaging and underground storage. This prevents radioactivity seeping into the ground after prolonged storage. Surprisingly, the zeolites are stable even when exposed to the highest levels of radiation, a fact proven after the fission reactor meltdowns

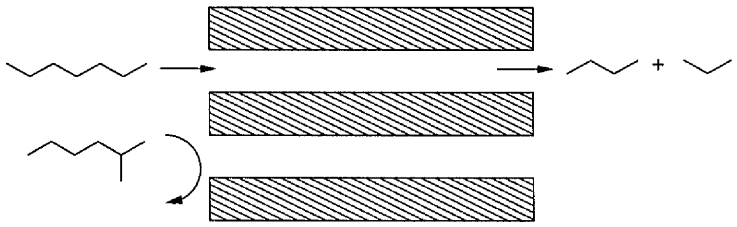

Figure 1.3: Schematic diagram of reactant shape selectivity: Rejection of branched chained hydrocarbons

at both Three Mile Island and Chernobyl where zeolites were used to absorb the waste caused by the accidents.[12] The natural zeolite clinoptilolite is commonly used in waste sewage sludge treatment[13] for the removal of toxic heavy metal ions such as cadmium, chromium, lead and zinc.

Another common use of zeolite A is in the separation of N_2 and O_2 from air.[11] The standard method relies on liquefaction of air and separating the resulting liquid by fractional distillation, a costly process which involves lowering the temperature of the gas to around -183°C. The alternative is to pass the gases over a zeolite bed at room temperature. Both N_2 and O_2 can fit through the pores of the zeolite but when under the influence of the electrostatic surroundings of the pore and binding effect of the acid sites, only the smaller N_2 molecule is able to leave. The zeolite bed eventually fills up and is unable to continue separation, at this point the bed is removed from the system and heated under pressure, which evolves the O_2 and regenerates the zeolite catalyst. This process is much more efficient than the liquefaction process.[14] The zeolites ability to preferentially sieve molecules can be used in a more useful way. If a reactant is sterically unable to enter the zeolite pores, where the reaction takes place, then the product resulting from that reactant is is also restricted (figure. 1.3). In the second case, if a product forms inside the zeolitic cavity but is unable to leave, again it is restricted (figure. 1.4).

Another example of the effect of shape selective catalysis is that which occurs in

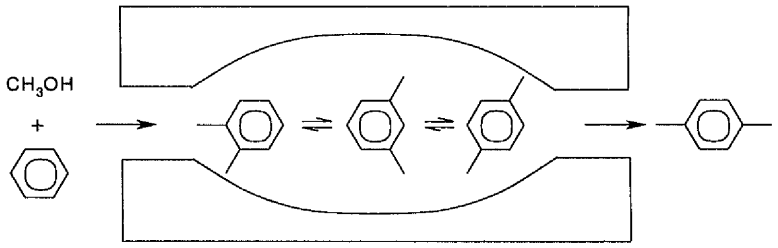

Figure 1.4: Schematic diagram of reactant shape selectivity: Para-xylene diffuses preferentially out of the zeolite channels

the methanol-to-gasoline (MTG) process[15] developed by the Mobil Oil Company. A stream of gaseous methanol is passed over a H-ZSM-5 catalyst bed, which results in a dehydration-polymerisation reaction inside the zeolite pore. The resulting effect is a sharp cut off of product distribution at C_{11} (gasoline) length fractions, the largest length of hydrocarbon that can fit inside the zeolite pore. The result of this cut-off is that no extra re-processing is needed to remove heavier residues. The impact of this has been immense for countries with no natural source of crude oil such as New Zealand generating their own gasoline via the MTG process. It is likely to become even more popular over the next few decades as crude oil supplies become depleted.

1.2.2 Zeolite catalysis

Steric catalysis

When molecules are absorbed into the zeolite pores, they are enveloped in a large electrostatic potential as they would be in a solvent, an enzyme cleft or in a cyclodextrin molecule but with the added advantage of a huge internal surface area. As well as this advantage, solvent molecules can be excluded from the zeolite pores to prevent reactant/solvent interactions which can greatly reduce subsequent reaction rates. Subsequently, if there is a high loading to supercage

ratio, the reactants will be much more highly concentrated than when solvated or when in the gas phase.

An example of this is the K^+ form zeolite Y catalysed cracking of hexane at 500°C.[12] The reaction can be catalysed by strong acid but in this case, the zeolite counter ion is K^+ and not H^+. The product distribution is found to be characteristic of a free-radical mechanism, rather than one proceeding via a carbenium ion intermediate. Hydrogen abstraction from the hydrocarbons by radical intermediate is favoured in the pores of the zeolite, whilst β-scission of the radicals is unaffected.

i.e. The bimolecular steps are accelerated whilst unimolecular steps are unaffected.

The catalytic mechanism of this reaction occurs due to the fact that the reactants are trapped in the microcavities of the zeolite, increasing the local reactant concentration. In addition to this, there are no solvent molecules to keep the reactants separated and play any part in side reactions.

Brønsted acidity

The isomorphous replacement of silicon with aluminium in a T-site gives rise to a charge imbalance due to the lower coordination number of the aluminium. This imbalance must be neutralised and this is achieved in two ways in naturally occurring zeolites:

- The Al-O bond lengthens.
- A coordination site is made available for an cation to counter the excess negative charge.

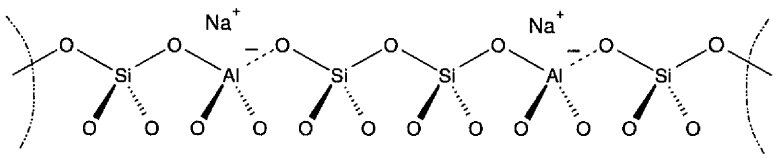

Figure 1.5: Neutral Sodium Balanced Zeolite Framework

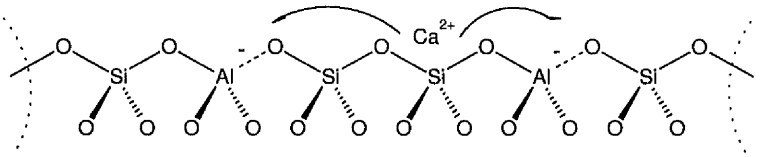

Figure 1.6: Neutral Calcium Balanced Zeolite Framework

In natural zeolites, the excess negative charge is balanced by the ions present in the surrounding environment, usually K^+, Na^+, Ca^{2+} and Mg^+ [†] . The type of counter ion used to balance the charge plays an important part in the use of the zeolite. This cannot be more true than on replacement of the cation with a proton by hydrothermal treatment to form a hydroxyl group at the oxygen bridge.

These acid sites behave as classic Brønsted acids which when combined with the high selectivity arising from shape selectivity and large internal surface area makes the zeolite an ideal industrial catalyst. The significance of this acidic proton can be shown by comparisons of experiments in H^+ exchanged zeolites and their equivalent cation form zeolite.

[†]Although they are drawn as fixed atoms, the counter anions are mobile (especially the Ca^{2+} which is shared between multiple sites). The negative charge on the zeolite is not localised to one tetrahedron but is smeared across the whole zeolite. This is an important factor in catalysis as it is thought that the delocalisation of the negative charge may stabilise cationic intermediates such as carbenium ions.

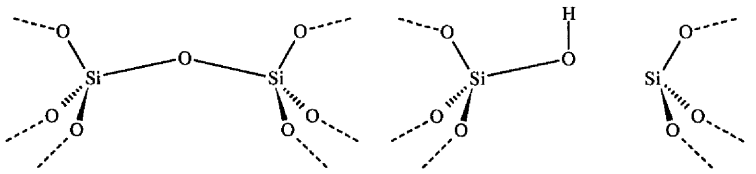

Figure 1.7: i) Siliceous zeolite ii) Zeolite Brønsted acid site

The reaction previously mentioned in section 1.2.1, the MTG (methanol-to-gasoline process), is dependent on the presence of the Brønsted proton, if the catalytic H-ZSM-5 is replaced by the purely siliceous analogue of ZSM-5, which has no Brønsted protons, the reaction does not take place at all. It is the initial steps of reactions such as this that we are interested in understanding so that zeolite structure and activity can be modified in order to increase the catalytic effect of the zeolites: a very economically important step for industry. As such, the initial steps of the MTG process are some of the most studied reactions in zeolite chemistry[16–25]

Catalytic cracking

Olefins readily undergo catalytic cracking via the carbenium ion intermediate pathway, however this is not the case for paraffins. The initiation step has been widely debated with several methods proposed for the initiation step. Most proposed initiation steps involve the generation of a carbenium ion on the paraffin by hydride abstraction. There are many suggestions for the route of the abstaction including the presence of trace amounts of readily protonated olefins which are able to perform such an abstraction from the parafin. It has also been claimed that the direct interaction of a proton on a C-H bond could result in a hydrogen molecule and a olefin as is possible in the presence a liquid superacid.[26] Also, direct abstraction has been postulated to occur via the Lewis acid site. In all cases, the initiation involved formation of a carbenium ion. Surprisingly, little though

has been given to other methods such as direct Brønsted acid attack on the C-C bond, forming a carboxonium ion-like activated complex.[27,28] Once formed, the complex is able to crack via protalytic cracking mechanism.

1.3 Experimental studies of zeolite structure

A great deal is known about the general zeolite structure and the chemistry of the acid site due to the wide range of experimental techniques that have been used to elucidate this information. Although a lot of general information exists concerning the systems as a whole, there is very little specific information about the co-ordination around the individual aluminium sites. X-ray crystallographic methods are only of use for framework determination as they do not elucidate the position of acidic hydrogens due to their low scattering factor. The absolute configuration of the aluminium is just as difficult to pin point, as relative to the silicon concentration, the aluminium concentration is usually low and although there are preferred T sites for it to occupy (except for the Si:Al=1 ratio), the site occupancy can be very low making overall occupancy pseudo-random. In addition to this, silicon and aluminium have such similar scattering factors that it is difficult to differentiate between the two. This prevents methods such as neutron diffraction from exactly positioning individual silicons and aluminiums and only an average T-site position from unit cell to unit cell can be calculated. This averaging effect loses any information about the specific acid sites.

A great deal of work has been performed to obtain acid site information such as proton affinity and heats of adsorption via direct chemical methods such as calorimetry,[29] titration,[30,31] FTIR.[30,32] These methods involve the reaction of a base at an acidic site but these methods are again fraught with difficulty. As with other methods, the results obtained are an average over all of the differing acid sites and there are other processes taking place inside the zeolite which can cause

the protonation energy to differ from probe to probe. It is well known that NH_3 in water is a stronger base than pyridine, yet in HY, H-ZSM-5 and M-ZSM-12 the pyridine consistently has a higher heat of adsorption (hence higher zeolite acid strength). Conversely, the proton affinity changes very little from zeolite to zeolite, suggesting that the structure has little effect on the acid strength but other effects come into play such as sorbate-framework interaction. More common are methods which interact the acidic proton with weak base probes such as Ar, N_2,[33] CO,[34,35] pyridene, tetramethylamine,[36] CD_3CN[37,38] and CCl_3CN[38] and then study the change in spectroscopic measurements, such as NMR chemical shifts and IR frequencies. Using these techniques, it has been found that the Brønsted acid sites are strong, but also that there are several sites of differing strengths. This arises due to the different positions in the zeolite lattice and a non-uniformity of Al substitution in the framework (except in the case of Si:Al = 1 where only the structural differences take effect).

One common factor with all zeolites is that a reduction in bridging proton density causes an increase in the average proton acidity. A consequence of this is that zeolites such as HY and HZSM-5, which have a low density of acidic protons act like an 'ideal' solution of non-interacting protons in a solid matrix. These zeolites are superacids, which at high temperatures, are able to protonate even paraffins. The acidity of the zeolite can be tuned to suit a specific experiment by varying the aluminium substitution.

1.4 Conclusion

Even after using all of these methods, it is still difficult to determine the exact position of aluminiums and hence acidic protons in the framework. It is therfore clear that experimental techniques are lacking in some respects in the determination of zeolite structure and that other methods are needed to complete the

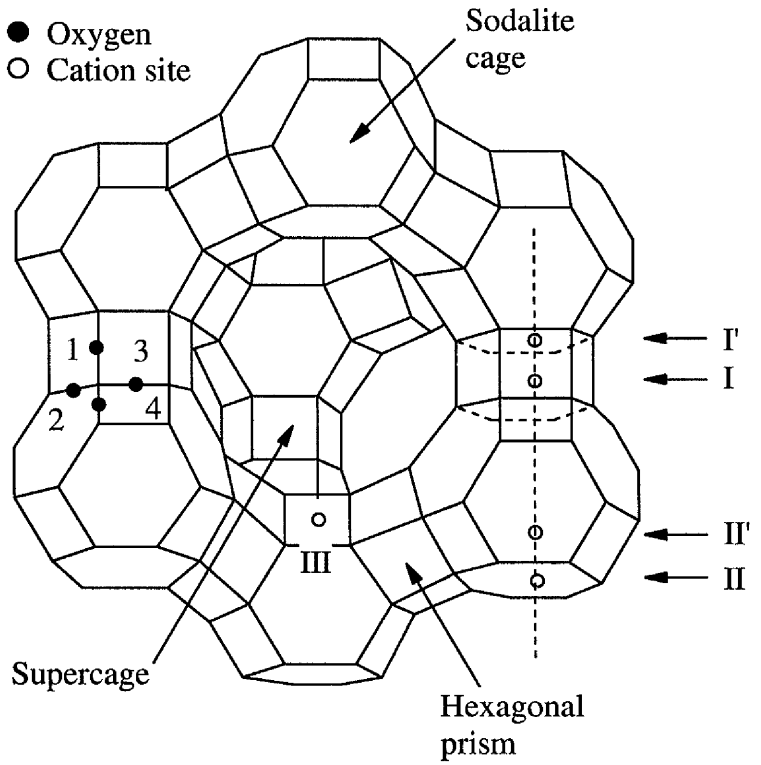

Figure 1.8: Diagram showing the differing oxygen and cation locations

picture. Computational modelling is an ideal candidate to bridge this gap. Computational methods have proven to be invaluable in this area especially when used in collaboration with experimental work to verify the results. The majority of work published today in the zeolite field has an amount of theoretical calculation associated with it in one form or another. In cases where spectroscopic and crystallographic methods have failed to completely resolve a crystal structure, empirical force field methods have been used to calculate minimum structures with aluminiums explicitly placed.[39] Molecular or lattice dynamics techniques have been used to measure sorption processes through the zeolite pore channels.[40–46] Electronic structure methods have also been used on small clusters to elucidate reaction pathways so that our understanding of zeolite chemistry can be increased with the aim of being able to predict how structural changes will affect reactions. Modern computational methods also allow NMR shifts[45,47–50] and IR frequencies[51] to be calculated, the results will have the advantage of being specific to the arrangement of T-sites used in the calculation.

Chapter 2

Computational modelling techniques

There are number of points to consider when beginning a computational study. The computational method must be chosen carefully depending on the size of system and the properties which are of interest. If a reaction is under study, an electronic structure technique must be used to allow explicit consideration of electrons, but on the other hand, if a diffusion process is under study, a dynamical simulation technique is the most informative. If too few atoms are used, the calculation may not reproduce the full system, conversely too many atoms and the calculation becomes computationally prohibitive. Due to their periodic nature, crystalline systems also require the inclusion of the long range electrostatic contribution of the lattice for accurate representation.[52]

The aim of this chapter is to review some of the methods commonly employed in the field of computational chemistry and ultimately in the rest of this thesis.

2.1 *Ab-initio* methods

Ab-initio is a term used to describe an accurate (although only exact for the hydrogen atom) solution of the non-relativistic, time-independent Schrödinger equation.[53] The following approximations are, as standard, made to simplify the solution of the Schrödinger equation.

- Time independence assumption

  The Hamiltonian operator does not explicitly depend on time, so the wavefunction corresponds to a stationary geometry and therefore is a function of only spatial and spin coordinates.

- Neglect of relativistic effects

  An assumption is made that electrons have the same mass regardless of how fast they travel.

- Born-Oppenheimer approximation

  Because of the vastly differing magnitudes of the electronic and nuclear motions within the molecule one may separate the equation into two parts. The first treats the purely quantum mechanical behaviour of the electrons within the field of the relatively slow (and therefore approximately fixed) nuclei; whilst the second part describes the motions of the nuclei within the rapidly changing field of the wave-like electrons.

- Orbital approximation

  The true wavefunction is represented as a combination of mathematical functions (orbitals), each dependent on the coordinates of only one electron. The orbitals are assembled using what is called a Slater determinant, which mathematically preserves the electron spin restrictions of the system.

2.1.1 Hartree-Fock theory

$$\hat{H}_{elec} = \sum_{i=1}^{n} -\frac{h^2}{8\pi^2 m} \nabla_i^2 - \sum_{i=1}^{n}\sum_{\alpha=1}^{N} \frac{Z_\alpha e^2}{4\pi\epsilon_0 r_{i\alpha}} + \sum_{i}^{n}\sum_{<j}^{n} \frac{e^2}{4\pi\epsilon_0 r_{ij}} \tag{2.1}$$

In equation 2.1 the first term contributing to the electronic Hamiltonian is the electronic kinetic energy where n is the number of electrons, the second term is the electron-nuclear attraction energy, and the third, electron-electron repulsion. The equation can be greatly simplified by working in atomic units, where electron charge (e) and mass (m_e) are defined as unity. The equation then becomes

$$\hat{H}_{elec} = \sum_{i=1}^{n} -\frac{1}{2} \nabla_i^2 - \sum_{i=1}^{n}\sum_{\alpha=1}^{N} \frac{Z_\alpha}{r_{i\alpha}} + \sum_{i}^{n}\sum_{<j}^{n} \frac{1}{r_{ij}} \tag{2.2}$$

Another approximation is the description of the wavefunction in terms of the one electron functions Φ, i.e. orbitals. This approximation gives the Hartree product.

$$\Psi(r_1, r_2, \ldots r_n) = \Phi_1(r_1)\Phi_1(r_2)\ldots\Phi_1(r_n) \tag{2.3}$$

This is still not an acceptable representation of the wavefunction as it contravenes Pauli's anti-symmetry principle,[54,55] which only allows a spatial orbital to contain 2 electrons of opposite spins ($\pm \frac{1}{2}$), also the electrons must be indistinguishable. These restrictions on the wavefunction behaviour are taken into account by use of a Slater determinant.

$$\Psi = \frac{1}{\sqrt{n!}} \begin{vmatrix} \Phi_1(r_1)\alpha(1) & \Phi_1(r_1)\beta(1) & \Phi_2(r_1)\alpha(1) & \ldots & \Phi_{\frac{n}{2}}(r_1)\beta(1) \\ \Phi_1(r_2)\alpha(2) & \Phi_1(r_2)\beta(2) & \Phi_2(r_2)\alpha(2) & \ldots & \Phi_{\frac{n}{2}}(r_2)\beta(2) \\ \Phi_1(r_3)\alpha(3) & \Phi_1(r_3)\beta(3) & \Phi_2(r_3)\alpha(3) & \ldots & \Phi_{\frac{n}{2}}(r_3)\beta(3) \\ \vdots & \vdots & \vdots & \ddots & \vdots \\ \Phi_1(r_n)\alpha(n) & \Phi_1(r_n)\beta(n) & \Phi_2(r_n)\alpha(n) & \ldots & \Phi_{\frac{n}{2}}(r_n)\beta(n) \end{vmatrix} \tag{2.4}$$

This simplified method of separating the many body problem, which cannot be solved, into the soluble sum of single body problems was postulated by Hartree[56] and Fock.[57]

The system is then described by $\frac{n}{2}$ equations of the Schrödinger form

$$\hat{F}_i(1)\Phi_i(1) = \epsilon_i\Phi_i(1) \tag{2.5}$$

Roothaan[58] and Hall[59] suggested a method that allows computational solution of the Hartree-Fock equation to give a molecular wavefunction Ψ. This is done by expanding the unknown molecular orbitals Φ in terms of a linear combination of atomic orbitals (LCAO).

$$\Phi_i = \sum_{\mu=1} c_{\mu i}\chi_\mu \tag{2.6}$$

Substituting equation 2.6 into 2.10 gives

$$\hat{F}\sum_{\mu} c_{\mu i}\chi_\mu = \epsilon_i \sum_{\mu} c_{\mu i}\chi_\mu \tag{2.7}$$

Multiplying through by the basis function χ_l and integration over all electronic space (dν) gives the secular equation

$$\sum_{\mu} c_{\mu i}\left(\int \chi_l F \chi_\mu d\nu\right) = \epsilon_i \sum_{\mu}\left(\int \chi_l \chi_\mu d\nu\right) \tag{2.8}$$

$$\sum_{\nu=1} \left(F_{\mu\nu} - \epsilon_i S_{\mu\nu}\right) C_{\nu i} = 0 \tag{2.9}$$

Where ϵ_i are the orbital eigenvalues (energies). The solution then becomes

$$FC = SC\epsilon \tag{2.10}$$

where F is the Fock matrix, S the overlap matrix in the atomic orbital basis and ϵ a diagonal matrix containing the orbital eigenvalues. The Fock matrix is given by

$$F_{\mu\nu} = H_{\mu\nu}^{core} + \sum_{\lambda=1}^{N}\sum_{\sigma=1}^{N} P_{\lambda\sigma}\left[(\mu\nu|\lambda\sigma) - \frac{1}{2}(\mu\lambda|\nu\sigma)\right] \tag{2.11}$$

$$P_{\lambda\sigma} = 2\sum_{i=1}^{occ.} c_{\lambda i}c_{\sigma i} \tag{2.12}$$

From equation 2.10, it can be seen that both sides of the equation depend on the atomic orbital coefficients (C). In practice, an initial guess is made for the set of coefficients. An iterative procedure is used to refine them until they do not change. They are then said to be self-consistent. This method is known as a self-consistent field (SCF) procedure.

2.1.2 Møller-Plesset perturbation theory

Møller-Plesset perturbation theory is a method of improving Hartree-Fock theory by adding electronic excitation into the wavefunction. The Hamiltonian operator is written as

$$\hat{H} = \hat{H}_0 + \lambda V \tag{2.13}$$

where the unperturbed Hamiltonian $\hat{H}_0$ is given as the sum of the one-electron Fock operators, V is a small perturbation to $\hat{H}_0$ and λ is an arbitrary parameter. If the perturbation is sufficiently small, the energy and wavefunction can be expressed as a power series.

$$E = E_0 + \lambda E^{(1)} + \lambda^2 E^{(2)} + \ldots + \lambda^n E^{(n)} \tag{2.14}$$

$$\Psi = \Psi^{(0)} + \lambda\Psi^{(1)} + \lambda^2\Psi^{(2)} + \ldots + \lambda^n\Psi^{(n)} \tag{2.15}$$

Substituting equations 2.14 and 2.15 into the time independent Schrödinger equation gives

$$(\hat{H}_0 + \lambda V)(\Psi^{(0)} + \lambda\Psi^{(1)} + \ldots) = (E_0 + \lambda E^{(1)} + \ldots)(\Psi^{(0)} + \lambda\Psi^{(1)} + \ldots) \tag{2.16}$$

First order Møller-Plesset[60] theory gives energy and wave function identical to that of the unperturbed Hartree-Fock energy and wavefunction. Second (MP2) and fourth (MP4) order Møller-Plesset theory are standard levels of theory for use in calculating small systems, implemented in most *ab-initio* codes.

2.1.3 Density functional theory

For many years, Hartree-Fock theory has been the method of choice when performing electronic structure calculations on chemical systems. However, the Hartree-Fock approximation and its use of a single determinant to describe the exact wavefunction of a system has its limitations. The area where the theory has its biggest failing is in describing the correlated motion between electrons of opposite spin, due to the averaging of inter-electronic interactions through the Coulomb and exchange terms. Within the last few years, density functional theory[61] (DFT) has experienced a rise in its popularity for calculating structures and properties of chemical systems,[62–64] including zeolites.[65–72] This increase in popularity can be attributed to the need to include electron-correlation in calculations on large systems and the new and more accurate approximations to the exchange-correlation energy density functional (see below).

In density functional theory the ground state of a multi-electron system is fully determined by the electron density. The electronic energy, E_{tot}, can be obtained

as an electron density functional[73,74]

$$E_{tot}[\rho] = V_{ne}[\rho] + T[\rho] + J[\rho] + E_{xc}[\rho] \tag{2.17}$$

where $V_{ne}[\rho]$ is the interaction energy of the electrons with the nuclei and $J[\rho]$ is the Coulomb energy. The second term, $T[\rho]$, is defined as the kinetic energy of a system of noninteracting electrons with the same density as the real system of interacting electrons being studied. This may be seen to introduce a severe error. However, this is not the case, because the final term, $E_{xc}[\rho]$, contains, in addition to the exchange and correlation (XC) contributions to the energy, the difference between $T[\rho]$ and the true electronic kinetic energy of the system. The so called 'Kohn-Sham'[75] equations, formulated by varying E_{tot} with respect to ρ, are solved in an iterative manner similar to the solutions of the Hartree-Fock equations.

The quality of any DFT calculation is limited by the quality of its approximation to the true XC energy functional, $E_{xc}[\rho]$ and it is therefore not surprising that a great deal of effort has been invested in development of ever more sophisticated XC functionals. The simplest and most popular approximation to $E_{xc}[\rho]$ is the local density approximation (LDA). Density gradient corrections are typically applied to correct the assumed homogeneous nature of the molecular density in the LDA approximation. The main functional used in this thesis is denoted B-LYP, and is the Becke gradient corrected exchange functional[76] combined with the Lee-Yang-Parr correlation functional.[77] A hybrid functional (B3-LYP)[78,79] is a widely used functional in zeolite chemistry[65–67] and has also been used throughout this thesis, and includes some Hartree-Fock exchange.

2.1.4 Basis sets

LCAO theory approximates an unknown molecular orbital to be the linear combination of atomic orbitals. Each molecular orbital will be in the form of equation 2.6 and can be expanded using a set of analytically derived (fitted) exponential functions known as Slater functions to describe the atomic orbitals.

$$\chi_\mu = Ce^{-\zeta r}Y_{lm}(\theta, \phi) \tag{2.18}$$

Where C is a normalising constant, Y_{lm} is a spherical harmonic angular function, and ζ is the orbital exponent. The Y_{lm} and ζ exponent values are available in the literature for $1s, 2s, 2p, 3s, etc$ in the form of basis sets. If one of these functions is used per atomic orbital, it is known as a 'minimal basis' calculation. If double this number are used per atomic orbital, it is referred to as 'double zeta' quality. Although accurate, these Slater functions are not widely used due to the difficulties involved in their integration. Instead, Boys[80] suggested the use of standard Gaussian functions as they are easier to evaluate. To obtain the accuracy of Slater functions with the simplicity of Gaussians, several Gaussians are fitted to reproduce a Slater function. Calculations are often reported to have been calculated using an STO-3G basis. This indicates that a minimal basis set of Slaters was used but for each integral the exponential function was fitted by 3 Gaussians. Fixed combinations of these Gaussian functions are known as contractions, for example, a 6-31G basis set uses 6 contracted Gaussian functions to represent the core electrons and the valence shell represented by two contractions, one of 3 primitive Gaussians and one single primitive Gaussian.

Polarization and diffuse functions

The quality of a basis set can be increased by the addition of extra basis functions. Polarisation functions can be added to include an extra electronic shell

not normally considered. For example in the case of oxygen at 6-31G basis, the basis set contains a p-type function as the maximum quantum shell (where l=1). When the electronegative oxygen is brought near a more electropositve atom *e.g.* carbon, polarisation can occur and the s an p orbital shape is distorted and need to change shape. This is achieved by mixing with higher angular momentum orbitals *i.e.* the d-orbitals. It would be advantageous therefore, for a polarisation function to be included. This would be represented as 6-31G* where the * indicates inclusion of a polarisation function. A second asterisk would indicate the presence of a p-type polarisation function on the hydrogens. An accurate description of anionic systems requires diffuse functions *i.e.*, functions with smaller exponents than the standard functions. These are indicted by a +, 6-31+G, indicating diffuse functions on heavy atoms, 6-31++G indicating diffuse functions on heavy atoms and hydrogens. Diffuse functions are implemented as standard s and p functions but with smaller than usual exponents.

2.2 Semi Empirical Molecular Orbital Theory

As described in section 2.1 the most reliable quantum mechanical method is the *ab-initio* method due to its non-empirical nature. There are systematic ways of correcting for the deficiencies of any level applied by progressing to a higher level of theory. The problem with this is knowing what level of theory is sufficient to study a system. What is seldom known in advance is which level of theory is sufficient to models the molecular properties of the system under study. Therefore, *ab-initio* calculations are not always successful in reproducing experimental observations.

Once a sufficiently accurate level of theory has been identified, it is often found that *ab-initio* calculations are time consuming and prohibitively so for large systems. It is often stated that *ab-initio* calculations scale as the fourth power of

the number of basis functions for ground-state, closed-shell systems. This scaling factor arises because each two-electron integral $(\mu\upsilon|\lambda\sigma)$ involves four basis functions, so the number of two-electron integrals would be expected to increase in proportion to the fourth power of the number of basis functions. In practice, *ab-initio* calculations often scale as a significantly smaller power than four because the two-electron integrals can be related by symmetry and the number of integral calculations can be reduced in direct SCF by not recalculating integrals from iteration to iteration if their contribution does not significantly alter.

Semi-empirical calculations take this approximation one step further by removing certain parts of the calculation and addressing other parts empirically, without fundamentally disturbing the character of the results.

Most of the two-electron integrals can be safely neglected in the calculation because of their small contribution, while others can be assigned empirically determined values. Semi-empirical calculations make further approximations by considering only the valence electrons of the atoms given that the inner-shell electrons do not participate in the formation of chemical bonds. These calculations are significantly faster than *ab-initio* and because of this the size of system that may be examined can be increased considerably.

2.2.1 Zero Differential Overlap Methods

As discussed above, *ab-initio* methods are too costly for large systems due to the number of two-electron integrals calculated. These integrals are, in many cases numerically small and can be neglected or approximated, thus reducing the number requiring evaluation drastically.

Before an integral is removed or approximated, it is necessary to adopt a consistent and justifiable criterion for their rejection.

$$(\mu\upsilon|\lambda\sigma) = \int\int \varphi_\mu(\mathbf{r}_1)\varphi_\upsilon(\mathbf{r}_1)\frac{1}{r_{12}}\varphi_\lambda(\mathbf{r}_2)\varphi_\sigma(\mathbf{r}_2)d\mathbf{r}_1 d\mathbf{r}_2. \tag{2.19}$$

The two-electron integral expression (equation 2.19) may be interpreted physically as the energy of the electrostatic repulsion between two electronic charge clouds distributed in space according to the products $\varphi_\mu(\mathbf{r}_1)\varphi_\upsilon(\mathbf{r}_1)$ and $\varphi_\lambda(\mathbf{r}_2)\varphi_\sigma(\mathbf{r}_2)$ respectively. Its value depends on the extent of the spatial overlap that exists between the two diatomic orbitals representing the distribution of an electron within the molecule. All semi-empirical molecular orbital models developed over the years have been based on the acceptance that all two-electron integrals involving charge clouds arising from the overlap of two diatomic orbitals on different centres are ignored.

The first and most stringent semi-empirical method is the zero differential overlap (ZDO) model[81,82] in which the only two-electron integrals evaluated are the Coulomb integrals $(\mu^2|\upsilon^2)$. Any overlap of different orbitals, even if the orbitals are centred on the same atom, is treated as though it were zero.

This model can only be applied to π-electron systems and there was a considerable time period before the development of similar theories for all-valence electrons. If the full SCF equations are solved without any approximations then the calculated energies and electron distribution will be the same whatever the choice of coordinate axes. The results must also be the same whether we choose to take a linear combination of atomic orbitals, or a linear combination of hybridized orbitals which are themselves linear combinations of atomic orbitals. We say that the results of the SCF calculation are invariant to an orthogonal transformation of the atomic orbital basis. If one makes approximations to the SCF equations then the conditions of rotational and hybridization invariance may not necessarily be satisfied. This was not a problem in the ZDO π-electron method because

the molecular symmetry of π-electron systems leads to a natural choice of axis, namely perpendicular to the plane. For a molecule with no symmetry, however, one would not want the results to depend on the choice of axis when none is obvious.

The all-valence SCF approximation in which all integrals $(\mu\upsilon|\lambda\sigma)$ are neglected unless $\mu = \upsilon$ and $\lambda = \sigma$, is called CNDO (Complete Neglect of Differential Overlap).[83] For invariance to orthogonal transformations of the basis, it is required that integrals like $(\mu^2|\lambda^2)$ are the same for all valence orbitals μ on atom A and λ on atom B. These integrals are put equal to $(s_A^2|s_B^2)$, the value of the s-orbital Coulomb repulsion. Examination of calculated values for these integrals suggests, however, that by adopting this approximation we may be losing a feature which has an important influence on molecular shape; that is the repulsions between p-orbitals and s-orbitals are not generally the same.

The dependence of the Coulomb integrals on orbital shape was allowed for in a method called PNDO (Partial Neglect of Differential Overlap).[84] The most important feature of the PNDO method is that integrals between two atoms A and B are evaluated only after transforming to a set of symmetry axes for the diatomic fragment AB. Thus, the two-centre terms are calculated by a method which is independent of the choice of axes for the molecule as a whole. The integrals are transformed to linear combinations of ones constructed from the diatomic set of orbitals. Most of these diatomic two-electron integrals vanish by virtue of the axial symmetry of the AB fragment. There are 22 remaining integrals of the form shown below. These are evaluated using an empirical expression.

In the PNDO method only the first ten integrals of this kind are considered because all two-electron integrals which depend on the overlapping of charge densities of different basis orbitals are neglected.

The one-centre exchange integrals $(\mu\upsilon|\mu\upsilon)$ are therefore neglected and this is

1	$(ss\|ss)$	12	$(sp_\sigma\|p_\pi p_\pi)$
2	$(ss\|p_\pi p_\pi)$	13	$(sp_\sigma\|p_\sigma p_\sigma)$
3	$(ss\|p_\sigma p_\sigma)$	14	$(ss\|sp_\sigma)$
4	$(p_\pi p_\pi\|ss)$	15	$(p_\pi p_\pi\|sp_\sigma)$
5	$(p_\sigma p_\sigma\|ss)$	16	$(p_\sigma p_\sigma\|sp_\sigma)$
6	$(p_\pi p_\pi\|p_\pi p_\pi)$	17	$(sp_\pi\|sp_\pi)$
7	$(p_\pi p_\pi\|p'_\pi p'_\pi)$	18	$(sp_\pi\|sp_\sigma)$
8	$(p_\pi p_\pi\|p_\sigma p_\sigma)$	19	$(sp_\pi\|p_\pi p_\sigma)$
9	$(p_\sigma p_\sigma\|p_\pi p_\pi)$	20	$(p_\pi p_\sigma\|sp_\pi)$
10	$(p_\sigma p_\sigma\|p_\sigma p_\sigma)$	21	$(p_\pi p_\sigma\|p_\pi p_\sigma)$
11	$(sp_\sigma\|ss)$	22	$(p_\pi p'_\pi\|p_\pi p'_\pi)$

clearly a limitation in spectroscopic terms, because the implicit assumption is that all atomic states from a given electronic configuration have the same energy. The retention of these two-electron integrals was the modification to CNDO that became known as INDO (Intermediate Neglect of Differential Overlap) .[85]

The closest approximation to the full SCF equations of Roothaan is the NDDO (Neglect of Diatomic Differential Overlap)[86] method. In all the ZDO methods an integral $(\mu\upsilon|\lambda\sigma)$ is taken to be zero if μ and υ are orbitals of different atoms of if λ and σ are orbitals of different atoms. The NDDO method differs from those described previously in that all integrals $(\mu_A\upsilon_A|\lambda_B\sigma_B)$ are retained in the calculation , and not just those for which $\mu = \upsilon$ and $\lambda = \sigma$, as in the CNDO and INDO methods. The modern semi-empirical methods are based on this scheme so that MNDO (Modified Neglect) and its third generation variations, AM1 and PM3, all use the NDDO formalism .[87]

2.2.2 The MNDO method and the AM1 Model

Given the NDDO assumption referred to in the previous section,[82] it is straightforward to derive the following expressions for the MNDO Fock matrix elements. The resulting equations are:

$$F_{\mu\mu} = H_{\mu\mu}^{core} + \sum_{\upsilon \; on \; A} \left[P_{\mu\mu}(\mu\mu|\upsilon\upsilon) - \frac{1}{2} P_{\upsilon\upsilon}(\mu\upsilon|\mu\upsilon) \right]$$

$$+ \sum_{B \neq A} \sum_{\lambda \; on \; B} \sum_{\sigma \; on \; B} P_{\lambda\sigma}(\mu\mu|\lambda\sigma) \tag{2.20}$$

where

$$H_{\mu\mu}^{core} = U_{\mu\mu} - \sum_{B \neq A} V_{\mu\mu B} \tag{2.21}$$

$$F_{\mu\upsilon} = H_{\mu\upsilon}^{core} + \frac{3}{2} P_{\mu\upsilon}(\mu\upsilon|\mu\upsilon) - \frac{1}{2} P_{\mu\upsilon}(\mu\mu|\upsilon\upsilon)$$

$$+ \sum_{B \neq A} \sum_{\lambda \; on \; B} \sum_{\sigma \; on \; B} P_{\lambda\sigma}(\mu\upsilon|\lambda\sigma) \quad \mu \; and \; \upsilon \; both \; on \; A. \tag{2.22}$$

where

$$H_{\mu\upsilon}^{core} = - \sum_{B \neq A} V_{\mu\upsilon B} \tag{2.23}$$

$$F_{\mu\upsilon} = H_{\mu\upsilon}^{core} - \frac{1}{2} \sum_{\lambda \; on \; B} \sum_{\sigma \; on \; A} P_{\lambda\sigma}(\mu\sigma|\upsilon\lambda) \quad \mu \; on \; A \; and \; \upsilon \; on \; B. \tag{2.24}$$

where

$$H_{\mu\upsilon}^{core} = \beta_{\mu\upsilon} \tag{2.25}$$

The MNDO scheme is semi-empirical and so these various expressions require parameterization at some level.

The MNDO and AM1 one-centre two-electron integrals are derived from experimental data on isolated atoms. For each atom there are five one-centre two-electron integrals which do not vanish by symmetry and these are the Coulomb and exchange integrals:

$$\begin{aligned} G_{ss} &= (ss|ss); \\ G_{sp} &= (ss|pp); \\ H_{sp} &= (sp|sp); \\ G_{pp} &= (pp|pp); \\ G_{p^2} &= (pp|p'p'). \end{aligned} \tag{2.26}$$

where p and p' are two different p-type atomic orbitals. G signifies a Coulomb integral and H an exchange integral.

In a local diatomic frame AB there are 22 unique two-electron two-centre integrals for each pair of heavy (non-hydrogen) atoms and an alternative treatment is required in order to account for the different types. These two-centre repulsion integrals represent the energy of interaction between the charge distributions at atom A and atom B. Classically, they are equal to the sum over all interactions between the electric multipoles $M^A_{l_1m}$ and $M^B_{l_2m}$, representing the charge distributions, $\varphi_\mu(\mathbf{r}_1)\varphi_\upsilon(\mathbf{r}_1)$ and $\varphi_\lambda(\mathbf{r}_2)\varphi_\sigma(\mathbf{r}_2)$, on the two centres A and B respectively. The subscripts l and m specify the order (monopole, dipole, quadrupole, etc.) and the orientation of the multipoles respectively. The formulae

$$(\mu^A\upsilon^A|\lambda^B\sigma^B) = \sum_{l_A,l_B} \sum_{m_A=-l_A}^{+l_A} \sum_{m_B=-l_B}^{+l_B} \left[M^A_{l_1m_A}, M^B_{l_2m_B}\right] \tag{2.27}$$

expresses the representation of the two-centre two-electron repulsion integral by the interactions of the set of electric multipoles.[87,88] Each multipole is treated as

a configuration of point charges each of magnitude 2^{-l} a.u. These integrals show the correct limiting behaviour as $R_{AB} \rightarrow 0$ and $R_{AB} \rightarrow \infty$. Next, we turn our attention to the one-electron terms. The core-Hamiltonian in equation 2.11 has been rendered into four parts in the MNDO scheme. Firstly there is the quantity

$$U_{\mu\mu} = \int \varphi_\mu(-\frac{1}{2}\nabla^2 + V_A)\varphi_\mu d\mathbf{r} \tag{2.28}$$

which is the energy of the orbital φ_μ in the field of its own nucleus (A) and core electrons. In the MNDO scheme these one-centre one-electron terms are treated as parameters. The second part is the core-electron attraction integral

$$V_{\mu\upsilon B} = \int_V \varphi_\mu V_B \varphi_\upsilon d\mathbf{r}. \tag{2.29}$$

This is the expression for the potential energy due to the Coulombic attraction between the charge distribution $\varphi_\mu\varphi_\upsilon$ and the core of a distant atom B. Similarly there is a term in which the overlap cloud is distributed according to φ_μ^2. In the MNDO formalism these are expressed as follows:

$$\begin{aligned} V_{\mu\mu B} &= -z_B(\mu_A\mu_A|s_Bs_B) \\ V_{\mu\upsilon B} &= -z_B(\mu_A\upsilon_A|s_Bs_B) \end{aligned} \tag{2.30}$$

where z_B is the charge of the core of atom B (and is equal and opposite to the total charge of the valence electrons of that atom). This expression can be justified in the following way. If atom A and B are far apart then the integral in equation (2.29) will approximately be equal to $-z_A R_{AB}^{-1}$, the attraction of an electron to a positive core. A two-centre repulsion integral shows a similar dependence at large separations of the two atoms, when it approaches the value

$$(\mu\upsilon|ss) = R_{AB}^{-1}, \tag{2.31}$$

which is the electrostatic repulsion of two electrons, with the s-orbital centred on atom A. We can therefore write that

$$V_{\mu\upsilon B} = -f(R)z_B(\mu_A\upsilon_A|s_Bs_B), \tag{2.32}$$

where $f(R)$ is a *penetration function* which allows for the deviation of $V_{\mu\upsilon B}$ and $(\mu\upsilon|ss)$ from R_{AB}^{-1} at small R_{AB}. It has been found, however, that acceptable results are achieved for all the ZDO methods by ignoring this effect and allowing $f(R) = 1$. Equation (2.30) is therefore obtained.

The final one-electron term is the so called resonance integral,

$$\beta_{\mu\upsilon} = \int_V \varphi_\mu(-\frac{1}{2}\nabla^2 + V_A + V_B)\varphi_\upsilon d\mathbf{r} \tag{2.33}$$

which represents the energy of attraction of the overlap cloud (between orbitals φ_μ and φ_υ on atoms A and B respectively) with the two participating cores A and B. To take this integral as zero in a strictly zero-overlap model would be logical, but if this were done then the essential term in bond formation would be lost. This therefore violates the NDDO approximation, but since resonance integrals are large, this integral is retained. This is the origin of 'modified' in MNDO. The interaction of this overlap cloud with the cores on which the two orbitals are not centred is regarded as insignificant, so that the exclusion of such interactions from expression (2.33) is justified.

In the MNDO scheme these one-electron core resonance integrals $\beta_{\mu\upsilon}$ are expressed in terms of the overlap integrals $S_{\mu\upsilon}$, which are calculated analytically, and atomic parameters β_μ^A and β_υ^B such that

$$\beta_{\mu\upsilon} = -\frac{1}{2}S_{\mu\upsilon}(\beta_\mu^A + \beta_\upsilon^B). \tag{2.34}$$

In physical terms the expression represents the extent of the bonding between atoms A and B which is proportional to the orbital overlap between them, or in other words, to the amount of electronic charge found between the two cores.

The above equations account for the evaluation of the electronic energy within the MNDO method. The addition of this electronic energy to the positive repulsion energy due to the interactions of the atomic cores represents the total energy. From the Coulomb law the core-core repulsion energy is

$$E_{AB}^{core} = \frac{z_A z_B}{R_{AB}}. \tag{2.35}$$

The forms chosen for the electron-electron and electron-core integrals, however, do not follow a simple $1/R$ law for distances greater than the van der Waals radius. One way to correct the fundamental problems such as the repulsion between two hydrogen atoms (or indeed any neutral molecule) at all distances is to change the core-core repulsion term from a simple Coulombic expression to:

$$E_{AB}^{core} = z_A z_B (s^A s^A | s^B s^B). \tag{2.36}$$

In fact while this correction gives the desired behaviour at relatively long separations, it does not account for the fact that as two nuclei approach each other the screening by the core electrons decreases. In MNDO an extra term is added to the basic repulsive term of equation 2.36 to give

$$E_{AB}^{core} = z_A z_B (s^A s^A | s^B s^B)(1 + e^{-\alpha_A R_{AB}} + e^{-\alpha_B R_{AB}}) \tag{2.37}$$

where α_A and α_B are parameters dependent upon the nature of the atoms A and B. For OH and NH bonds a slightly different core-core interaction was found to be more appropriate

$$E_{XH}^{core} = z_X z_H (s^X s^X | s^H s^H)(1 + R_{XH} e^{-\alpha_X R_{XH}} + e^{-\alpha_H R_{XH}}). \tag{2.38}$$

A serious limitation of MNDO is its ability to accurately model intermolecular systems involving hydrogen bonds (for example, the heat of formation of the water dimer is far too low in MNDO). This is because of a tendency to overestimate the repulsion between atoms when they are separated by a distance approximately equal to the sum of their van der Waals radius. To overcome this deficiency third generation modifications, called Austin Model 1 (AM1)[89] and PM3,[90,91] have been developed. The strategy adopted was to modify the core-core term in equation 2.38, using Gaussian functions. Both attractive and repulsive Gaussian functions were used; the attractive Gaussians were designed to overcome the repulsion directly and were centred in the region where the repulsions were too large. Repulsive Gaussian functions were centred at similar inter-nuclear separations. The additional term may be considered as a van der Waals attraction term. With this modification the expression for the core-core term was related to the MNDO expression by:

$$E_{AB}^{core} = E_{MNDO}^{core} + \frac{z_A z_B}{R_{AB}} \left\{ \sum_i K_{A_i} e^{-L_{A_i}(R_{AB}-M_{A_i})^2} + \sum_j K_{B_j} e^{-L_{B_j}(R_{AB}-M_{B_j})^2} \right\}. \quad (2.39)$$

The additional terms are spherical Gaussian functions with a width determined by the parameter L. It was found that the values of these parameters were not critical and many were set to the same value. The M and K parameters were optimized for each atom, together with the α parameters in the exponential terms in equations (2.37) and (2.38). In AM1 there are between two and four Gaussians per atom, while for PM3 there are just two.

The AM1/MNDO method is a good choice over other semi-empirical methods because it has been established that it is an effective method because it as able,

with reasonable accuracy, to reproduce experimental results for a diverse range of chemical applications. The scientific literature concerning the AM1 method is large and comprehensive so that a confident assessment has been made of its merits and defects.[88,92] The results have been quite (qualitatively) impressive when compared to experimental and *ab initio* calculations. It should be noted that geometries and heats of formation are obtained in these methods for compounds corresponding to standard conditions at 25°C and 1 atm. Thus correlation and zero point energy are implicitly included in the parameters.

2.3 Molecular mechanics

Molecular mechanics is a method which represents molecules as charged spheres connected by springs. Observable data is used to parameterise constants related to Hooke's law, allowing systems to be represented by Classical physics and simple potential energy functions. This method ignores the explicit presence of electrons which enables larger systems to be calculated but the drawback is that it is only useful for the description of molecular ground states, making it difficult to follow reaction paths. It is a relatively cheap method although the accuracy of the calculation is highly dependent on the system used to parameterise the constants and its similarity to the system under study. There are tried and tested parameter sets available for general zeolites and for many organic compounds, allowing minimisation to local minima and Monte Carlo searching methods to search for the global minima.

The term "molecular mechanics" refers to a set of classical potential energy functions used to represent a chemical system. There are many functional forms used in the field of molecular mechanics and many sets of parameterised force fields that use them. This section will describe those specific to the systems under study as part of this thesis, namely zeolites and crystalline lattices and small

organic molecules which may take part in reactions within those systems.

2.3.1 Functional forms

There is a large difference between the ionic crystalline lattices and their covalently bonded organic sorbates that we wish to study. As a result they are usually treated using totally different potential functions.

Crystalline lattices

As two ions are brought together, they first feel an attractive force due to London dispersive forces caused by the formation of instantaneous dipoles in the charge clouds. As the ions get closer together (past the equilibrium geometry) the force quickly become repulsive so that a small decrease in separations gives rise to a large increase in the repulsion. The source of this repulsive force is attributed to the Pauli exclusion principal where electrons with the same spin are forbidden from occupying the same region of space. This is often referred to as exchange or overlap force.

To model these interactions analytical pair potentials are used, the most common form used in modelling of ionic systems being the Buckingham Potential:

$$V(r_{ij}) = Ae^{-r_{ij}/\rho_{ij}} - C_{ij}r_{ij}^{-6} \tag{2.40}$$

Where r_{ij} is the interatomic separation, A_{ij}, ρ_{ij} and C_{ij} are constants. The $Ae^{-r_{ij}/\rho_{ij}}$ term is the repulsive term whilst the $C_{ij}r_{ij}^{-6}$ term represents the attractive force contribution. The only drawback with the use of this potential is the fact that at very small separation the potential term becomes attractive so checks must be made to ensure that ions do not come too close together otherwise they will crash onto the same site.

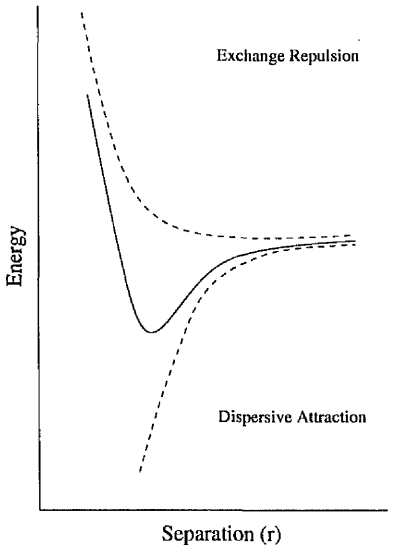

Figure 2.1: Schematic representation of the van der Waal interactions involved in bringing two ions together

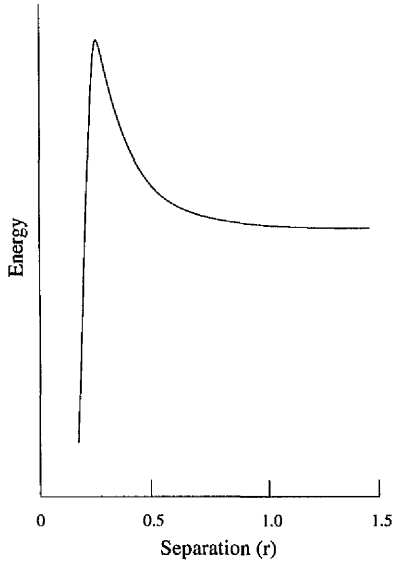

Figure 2.2: Example of a Buckingham potential

It is common for a three-body (angle bending) term to be included in zeolite force fields.

$$E_{3-body} = \frac{1}{2}\sum_{i}\sum_{j,k} K_i(\theta_{ijk} - \theta_0)^2 \tag{2.41}$$

An angle term is defined for the zeolite force-field between the shells of the oxygen atoms, j and k, bonded to a T atom i. The purpose of this term is to reduce the flexibility of $\widehat{OTO}$ angle by taking into consideration the partial covalency of the T-O bond and the fact that the T site is sp^3 hybridised.

Long range interactions are modelled entirely by a classical Coulomb term. Each charge on each ion interacts with every other charge according to equation 2.42. This term gives the largest contribution to the total lattice energy.

$$E_{coulomb} = \frac{1}{2}\sum_{i,j} q_i q_j / r_{ij} \tag{2.42}$$

This summation is a function of 1/r which converges very slowly with increasing separation (r). This causes problems in periodic calculations which will be discussed in section 4.6.

Electronic polarisability of the ions is modelled by incorporation of the shell model.[93] This method allows the ions charge cloud to become polarised by a surrounding electrostatic field and become non-spherical which creates a net dipole (μ) on the ion.

The ion is represented by a massless shell and a massive core which are connected by a harmonic spring (figure 2.3). The charge on the shell is negative whilst that of the core is positive so that the sum of the two is the integer ionic charge. The shell is representative of the negative charged cloud of valence electrons.

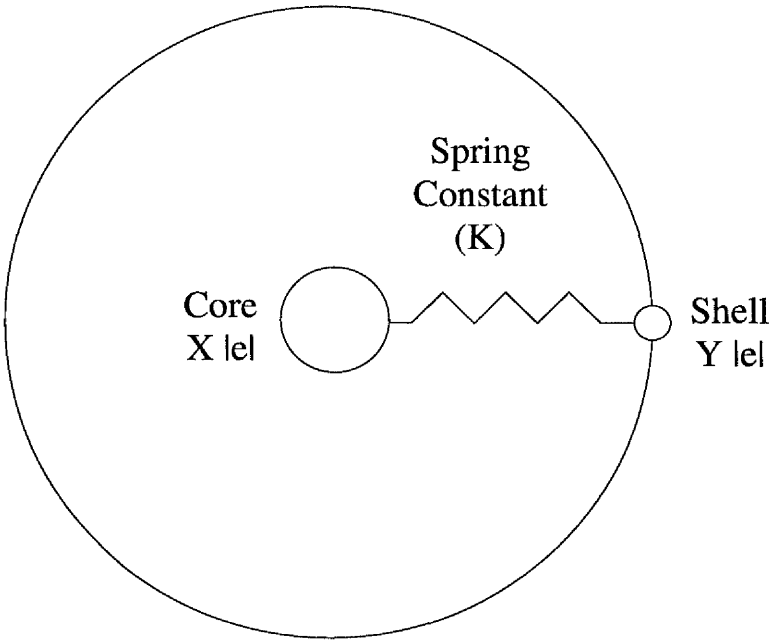

Figure 2.3: Dick & Overhauser shell model. Ions are modelled as a massive core connected to a massless shell via a harmonic spring.

The dipole moment can then be shown to be

$$\mu = \alpha E_{ext} \tag{2.43}$$

where α is the polarisability of the ion, and E_{ext} is the electric field strength.

$$\alpha = \frac{Y|e|^2}{K} \tag{2.44}$$

where $Y|e|$ is the shell charge, and K the spring constant.

The core shell interaction is then calculated by

$$\phi_{i_c i_s} = \frac{1}{2} K_i (r_c - r_s)^2 \tag{2.45}$$

where $r_c - r_s$ is the core shell separation.

All short-range forces are now assumed to act between the ion shells, this allows for an important coupling of the short range forces to the electronic polarisation. The long range forces act both on the core and the shell, further polarising the charge cloud.

In systems which are largely ionic but show some covalency, such as zeolites, an additional term must be included to account for the directionality imposed by the covalent character. This is usually done by the addition of a harmonic angle term, as shown in equation 2.41.

The force on an ion can be now evaluated as the derivative of the total potential energy function with respect to r.

$$U_L(r_{ij}) = \sum_{i,j} V(r_{ij}) + \sum_{i,j} \frac{q_i q_j}{r_{ij}} + \sum_{i,j} \varphi_{ij} + \sum_{i,j,k} \theta_{ijk} + nx \tag{2.46}$$

$$\frac{\delta U}{\delta r} = -F(r) \tag{2.47}$$

Organic sorbates

Due to their high degree of covalency, organic molecules (or any other covalant systems) are better represented by bonded potentials. The simplest and most commonly used of these potentials are harmonic spring potentials derived from Hooke's law where atoms are considered to be hard spheres connected by harmonic springs.

The harmonic bonded potential is written in the form of Hooke's law

$$E_b = \frac{1}{2}\sum_{i,j} k_{ij}^b (r_{ij} - r_0)^2 \tag{2.48}$$

Where k_{ij}^b is the spring constant, r_0 the equilibrium separation and r_{ij} the interatomic separation.

Angle terms are usually implemented in the same way as the bonded potential, with a harmonic term as shown in equation 2.49. Higher terms can also be included in this term.

$$E_\theta = \frac{1}{2}\sum_{i,j} k_\theta (\theta - \theta_0)^2 \tag{2.49}$$

Where K_θ is the harmonic three-body force constant, and θ and θ_0 are the calculated and equilibrium angles.

The dihedral term was neglected in early force fields and it was assumed that the *trans*-gauche energy differences would arise from non-bonded interactions. This was not the case, so, the dihedral angle term was introduced to reproduce the effect.

$$E_\phi = \frac{1}{2}\sum_{i,j} k_\phi (1 + \cos(n\phi - \phi_0)) \tag{2.50}$$

Although the Buckingham potential is often used in solid state systems to describe the dispersive and exchange repulsive interactions between atoms and molecules it is more common to employ the Lennard-Jones potential in modelling of molecular systems (equation 2.51).

It is common for a 6-12 version of the potential to be employed even though a more suitable description of the actual potential would be a 6-9 form. The reason for the use of the less appropriate form is that for large systems it is more computationally favourable to evaluate r^{12} as it is just r^6 squared so a trade-off between expense and accuracy is made.

$$\Psi(r_{ij}) = \sum_{i,j} \frac{A_{ij}}{r_{ij}^{12}} + \frac{B_{ij}}{r_{ij}^{6}} \tag{2.51}$$

Where A_{ij} and B_{ij} are constants related to the well depth and collision parameter. The first term is the short range repulsive term, the second part is the attractive term arising from the dispersive effects within electron clouds.

As for the crystalline system, the electrostatic contribution is calculated using a standard Coulombic term.

$$E_{coulomb} = \frac{1}{2} \sum_{i,j} q_i q_j / r_{ij} \tag{2.52}$$

Conclusion

With the bonding in silica and zeolites being mainly ionic in nature, the ion pair force-field seems to be the ideal method of describing the crystal structure. This has been proven to be the case in the work by Schröder et al.[94] A great deal of work was undertaken, testing the different zeolite force-fields to check the advantages and disadvantages. When compared to the shell model potential, the zeolite CFF force-field predicts structure and energy accurately for silicas,[95,96]

aluminosilicates[97,98]and ALPO's[99] but is poor at predicting infra-red frequencies. One problem with partially covalent systems such as zeolites is the assignment of charges. The charges can be obtained by fitting to a quantum mechanical potential energy surface or by fitting to experimental data. There are other methods such as electronegativity equalisation[100,101] which can be used to calculate charges, this method is embodied in the GULP code.[102] Although other force-fields have a problem with the assignment of charges, the shell model does not. The charges can be assigned as the formal charges, the dipolar shell model being efficient enough to adsorb any partial covalency.

The zeolite Shell Model Potential of Sauer et al[103] was used in all Molecular Mechanics work in this thesis as it had been used successfully in several previous studies[103]

There are many force-fields available to model the small absorbed molecules in the zeolite pores. It was decided that the parameters would be taken from the AMBER[104] force-field when explicit parameters were unavailable.

2.4 Combined or hybrid methods

Ab-initio methods provide high accuracy but at a high cost. Molecular mechanics methods sacrifice accuracy and flexibility for reduced computational cost. One solution to this problem would be to combine the good points of the two methods in a 'hybrid' methodology and study the reaction site using a high level electronic structure method, whilst representing the longer range interactions using an approximate method such as molecular mechanics.

One of the earliest implementations of a combined QM/MM potential was that of Warshel et al.[105] The method employed a quantum mechanical method to describe the small reactive centre and the rest of the system was modelled using

a less accurate empirical force-field method. More recently the work of Singh et al[106] implemented a combined QM/MM potential using *ab-initio* methods and the AMBER molecular mechanics force-field.[104] This was the basis of the work done at Manchester embodied in the MUQMMM code.

The basic idea behind this method is to partition the system into several regions which can then be evaluated by using appropriate levels of accuracy. Atoms which play a part in electron transfer processes or which are better described using electronic methods such as electron rich transition metals are treated with *ab-initio* methods. The rest of the system can then be treated using an approximate empirical force-field method.

2.4.1 Mechanical embedding methods

The simplest of these methods is when the system is partitioned into multiple regions and as the distance from the reaction centre increases, less accurate methods are employed. These types of methods, commonly called 'onion' methods due to their layered construction, have been implemented by Morokuma et al [107,108] and are available in the standard Gaussian98 package.[109] The drawback with these methods is that the quantum mechanical centre is not polarised by its surroundings *i.e.* it only feels a force due to the environment.

2.4.2 Full QM/MM potentials

In the simplest case a system is partitioned into two regions. If the system consists of a small molecule reaction in solution, such as the dissociation of methanoic acid in water, the system can be partitioned easily. The reactive molecules, CH_3COOH + H_2O, are made quantum mechanical whilst the surrounding water solvent is studied molecular mechanically.

The system becomes more complicated for larger systems such as enzymes. In this case the whole enzyme cannot be treated quantum mechanically so when divided into QM and MM sections some covalent bonds between the two regions will be 'broken'. If the QM region was evaluated as it was divided, it would be unrepresentative of the real system as the broken bonds and missing electrons would make the system into an unnaturally high spin state. To avoid this problem, all broken bonds are terminated with junction or link atoms to saturate the dangling bonds and preserve the local environment. These can be any atom or functional group such as a methyl group but are more commonly protons for simplicity. Further work by Rivail et al[110] has been done to eliminate the use of the termination atom, which can cause errors in the local potential, by substituting it with an empty localised orbital along the site of the missing bond. This allows the more natural representation of electron delocalisation without the use of the termination atom.[111]

2.5 Stationary point location on potential energy surfaces

The dynamics of chemical systems, within the fixed nucleus approximation, are governed by the form of the potential energy surface (PES). However, complete characterisation of the surface, which is a function of 3N-6 coordinates for an N-atom system, is too large a task in most instances. Fortunately it is possible to gain much information from just a few selected regions of the PES; in particular, from minima and first order saddle points. The first order or lowest energy saddle point connecting two local valleys or minima is a fundamental point on the PES. The saddle point is the highest point on a lowest energy pathway connecting these minima. The significance of the saddle point is that it is an approximate dynamic bottleneck, a point of no return, for a transformation from the vicinity of one local minima or valley to another. The rate of the reaction is very strongly

influenced by the relative energy of this saddle point or transition state, especially if the energy barrier is high and peaked. This section describes ways in which minima and transition states can be found.

The simplest optimization methods require no gradient evaluation (*i.e.* function-only methods) and are generally slow to converge, and may perform very poorly on complex potential energy surfaces.[112] Most methods in quantum chemistry therefore require the calculation of gradients (first derivatives of the energy with respect to the nuclear coordinates) and the Hessian matrix (the matrix of second derivatives of the energy with respect to nuclear coordinates).[113,112] Either first or second derivatives may be obtained numerically or analytically. In practice, it is usual to employ analytical first derivatives, as they can be obtained without excessive computational cost. However, a numerical Hessian is commonly used, as analytical second derivatives are difficult and expensive to obtain. All stationary points have all first derivatives equal to zero, this is a requirement of being at the top of a peak (a maximum) or the bottom of a well (minimum) of the surface. To distinguish between a minimum, a maximum or a saddle point the second derivatives must be evaluated. These second derivatives give the harmonic force constants for displacements in any direction. The Hessian matrix will have all positive eigenvalues if the stationary point is a minimum, negative eigenvalues indicate a maximum and a first order saddle point (a transition structure) will have only one negative eigenvalue.

2.5.1 Optimization procedures

Since first derivatives are now available for almost all *ab-initio* methods, the discussion will focus on methods where first derivatives are available. The most efficient methods, called variable metric or quasi-Newton methods, require an approximate matrix of second derivatives that can be updated with new information during the course of the optimization. Some of the more common methods have

different equations for updating the second derivative matrix.

The PES, a function of 3N Cartesian coordinates or 3N-6 internal coordinates (3N-5 for linear molecule) can be expanded about an arbitrary point such that the energy at a displaced point $\mathbf{x}$ is given by the Taylor series.

$$E(\mathbf{x}) = E_0 + \sum_i \frac{\partial E}{\partial x_i}|_0 x_i + \frac{1}{2}\sum_{i,j} \frac{\partial^2 E}{\partial x_i \partial x_j}|_0 x_i x_j + ... \tag{2.53}$$

If the series is truncated after the quadratic term, in vector notation, the series becomes

$$E(\mathbf{x}) = E_0 + \mathbf{g}_0^\dagger \cdot \mathbf{x} + \frac{1}{2}\mathbf{x}^\dagger \cdot \mathbf{F}_0 \cdot \mathbf{x} \tag{2.54}$$

where $\mathbf{F}$ and $\mathbf{g}$ have elements

$$\mathrm{g}_i = \frac{\partial E}{\partial x_i}|_0 \quad F_{i,j} = \frac{\partial^2 E}{\partial x_i \partial x_j}|_0 \tag{2.55}$$

Taking the derivative of $E(\mathbf{x})$

$$\frac{\partial E}{\partial \mathbf{x}} = \mathbf{g}_0 + \mathbf{F}_0 \cdot \mathbf{x} \tag{2.56}$$

At a stationary point $\partial E/\partial \mathbf{x} = 0$ and $\mathbf{x} = -\mathbf{F}_0^{-1} \cdot \mathbf{g}_0$ or $\mathbf{x} = -\mathbf{H}_0 \cdot \mathbf{g}_0$ where $\mathbf{H}_0$ is the approximate inverse Hessian matrix $\mathbf{F}_0^{-1}$ In subsequent steps $\mathbf{H}_0$ is updated by an updating formula to yield a new $\mathbf{H}_0$. Various updating schemes have been proposed. The default algorithm used in the Gaussian series of molecular orbital programs is the Berny algorithm.[114]

2.5.2 Redundant internal coordinates

The choice of coordinate system plays an important role in the efficiency of optimizations. The simplest choice of coordinates is Cartesian. The potential energy

as a function of Cartesian coordinates contains large couplings, both quadratic terms and higher order ones. Due to these large couplings, a simple initial estimate of the Hessian **F** in Cartesian coordinates, such as the diagonal (unit) matrix sometimes used, is very poor and the algorithm needs many steps to build up a reasonable approximation to it. A better choice can be to estimate **F** from a lower level calculation or from an empirical force field (note that the latter are based on valence coordinates). If a good initial Hessian is used, the Cartesian coordinates should be nearly as good as any other coordinate system for small displacements, *i.e.* close to the equilibrium, where the higher order anharmonic terms are unimportant. Internal coordinates have been used in optimization from the earliest application of gradient theory.[115,116] These coordinates minimize coupling, both harmonic and anharmonic, and therefore should work better in general for geometry optimization than Cartesian coordinates. There are two principal types of internal coordinate systems. A simpler choice of internal coordinates is used in the 'Z-matrix' method employed in many molecular orbital programs. The Z-matrix is a connectivity-type definition of the molecular geometry in terms of individual bond lengths, angles and dihedrals. Although the Z-matrix works reasonably well in many cases, the use of this method introduces strong linear and nonlinear couplings between the coordinates and so is undesirable for geometry optimizations. The treatment of rings is particularly unsatisfactory in that the last bond that closes a ring is necessarily missing. The second type of internal coordinates used are redundant internal coordinates. Pulay[117–119] demonstrated clearly that redundant internal coordinates are the best choice for minimizing polycyclic molecules. Pulay and co-workers defined a natural internal coordinate system that is similar to the coordinates used by vibrational spectroscopists. Most redundancies can be eliminated by using pseudo-symmetry coordinates about each atom and special coordinates for ring deformations, spiro ring fusions, *etc.* However, in molecules with complex topology, it is difficult to find physically reasonable non-redundant coordinates.

The use of the redundant internal coordinate method within the Gaussian94 package has enabled much more efficient optimisation of the quantum chemical region using the hybrid QM/MM code. Prior to using redundant internal coordinates, non-redundant coordinates were used within Gaussian92. These had the problem of the user having to specify which bonds, angles and dihedrals would best describe the system.

Gaussian94 uses a set of redundant internal coordinates composed of all bond lengths, valence angles, and dihedral angles to reduce the number of special cases. This coordinate set, however, has somewhat greater redundancy than the coordinates used by Pulay, but this does not seem to affect the efficiency of the optimisation.[120] The redundant internal coordinate set using Gaussian94[121] is defined in the following manner. First, the inter-atomic distances are examined, using a variety of methods, to determine which atoms are bonded.[120] A bond stretching coordinate is assigned to each regular, inter-fragment, and hydrogen bond. A valence angle bend coordinate is assigned for any two atoms bonded to the same third atom. A dihedral angle coordinate is assigned for each pair of atoms bonded to opposite ends of a bond or bonded to a linear array of atoms. The coordinate system defined is based on the identification of bonds. All of the remaining coordinates (valence angles and dihedral angles) are generated from the bonding information.

The first difficulty in working with redundant coordinates is the suitable definition of the force (or gradient) vector. If $\mathbf{B}$ is the Wilson B matrix[122] ($B_{ij} = \partial q_i / \partial x_j$) defining the transformation from Cartesian displacements, δx_i, to redundant internal displacements, δq_i,

$$\delta \mathbf{q} = \mathbf{B} \delta \mathbf{x} \tag{2.57}$$

then the transformed gradient is given by

$$\mathbf{B}^t\mathbf{g}_q = \mathbf{g}_x \tag{2.58}$$

where $\mathbf{g}_x$ is the gradient in Cartesian coordinates and $\mathbf{g}_q$ is the gradient in redundant internal coordinates. Since $\mathbf{B}$ is rectangular, the inverse of this transformation is a little more complicated and can be written

$$\mathbf{g}_q = \mathbf{G}^{-1}\mathbf{B}\mathbf{u}\mathbf{g}_x \tag{2.59}$$

where $\mathbf{G} = \mathbf{B}\mathbf{u}\mathbf{B}^t$ and $\mathbf{u}$ is an arbitrary non-singular matrix. In Gaussian94 a unit matrix is used for $\mathbf{u}$ by default. However, in the QM/MM scheme this matrix was taken as a diagonal matrix containing the reciprocal of each atomic mass three times in the appropriate positions. Any fixed atoms (later described as 'frozen atoms' in Chapter 6) in the QM/MM scheme are given infinite mass and so remain anchored at the same position. The generalised inverse of $\mathbf{G}$ ($\mathbf{G}^-$) is obtained by diagonalizing $\mathbf{G}$ and inverting only the non-zero diagonal elements, and transforming it back. An initial estimate of the Hessian is required in quasi-Newton optimization methods. The default in Gaussian94 is an empirical estimate that is diagonal in the redundant internal coordinate space. The Cartesian Hessian can also be calculated analytically at any number of levels of theory and then can be transformed to redundant internal coordinates (see Peng *et al.*[120] for full discussion). The Hessian in redundant internal coordinates is updated iteratively for minimizations by applying the Broyden, Fletcher, Goldfarb, Shanno (BFGS) formula[123–126] using the current point and all previous points, rather than using just the current and the next most recent point. Bofill's update[127] (a mixture of the symmetric Powell[128] and the Murtagh-Sargent[129] updates) is used for transition states.

In generating the Newton step in redundant coordinates, displacements are generated primarily in the non-redundant part of the internal coordinate space.

A projector $\mathbf{P}$ is constructed from the $\mathbf{G}$ matrix and its generalised inverse:

$$\mathbf{P} = \mathbf{G}\mathbf{G}^{-} = \mathbf{G}^{-}\mathbf{G} \tag{2.60}$$

Both the gradient and the Hessian have to be projected to prevent displacements in the remainder of the space by setting the corresponding matrix elements of the Hessian to arbitrarily large values. The Newton step is then given by

$$\Delta\mathbf{q} = -\tilde{\mathbf{H}}_0\tilde{\mathbf{g}}_q, \tag{2.61}$$

where $\tilde{\mathbf{H}}_0$ is the projected inverse Hessian matrix and $\tilde{\mathbf{g}}$ is the projected gradient. The final step in geometry optimization using internal coordinates is the generation of the new Cartesian coordinates. Because of the nonlinear nature of this transformation, this is usually done iteratively.[117] The first estimate of the new Cartesian coordinates is given by

$$\mathbf{x}_1 = \mathbf{x}_0 + \mathbf{u}\mathbf{B}^t\mathbf{G}^{-}\Delta\mathbf{q}. \tag{2.62}$$

The values of the internal coordinates are computed from the Cartesian coordinates, and $\mathbf{q}_1 - \mathbf{q}_0$ is compared with $\Delta\mathbf{q}$. The process is repeated until there is no further change in the Cartesian coordinates.

Choice of the search direction and control of step size are also of importance in determining the efficiency of the optimization.[112] Trust radius and eigenvector following methods[130] have been shown to be effective.

2.5.3 Summary

From this discussion we can see that the efficiency of an optimization will depend on a number of factors:

- The initial geometry,
- the choice of coordinate system,
- the initial estimate of the Hessian,
- the Hessian updating method, and
- control of the search direction and step size.

Gaussian94 is flexible enough to be able to maximize the effect of these factors in controlling semi-empirical and *ab-initio* molecular orbital calculations. It is also capable of predicting many properties of molecules and reactions, and is now widely acknowledged as an efficient, powerful tool for exploring areas of chemical interest like reaction mechanisms and potential energy surfaces. It is for these reasons that all quantum chemical calculations, be they stand alone or integrated into the QM/MM hybrid code, are evaluated using the Gaussian94 package.

Chapter 3

Chiral Modifiers

3.1 Introduction

Commonly, drugs and other chemicals which have an effect on the body tend to be chiral in nature. It is normally only one of these drug enantiomers that is active, yet the manufacturing process usually produces a racemic mixture of the drug. In some cases the non-active enantiomer can have other more dangerous effects, as in the case of R and S thalidomide. It can be clearly seen that it would be advantageous and profitable to recover the wasted enantiomer or better; not to produce it in the first place. It is well known that zeolites are sterically specific, only allowing molecules of a certain size and shape in and out, but if a zeolite could be made stereo-specific, this would be extremely useful.

This has been achieved in 2 ways:

- Construction of a chiral zeolite
- Introduction of a chiral agent into an achiral zeolite support

3.1.1 Chiral zeolites

A great deal of attention has been focused on zeolite β due to the ability of it to be constructed in such a way that causes it to become a chiral environment. Newsam et al working for the oil company Exxon[131] elucidated the structure of the zeolite using X-ray defraction, and found it to consist of two structural isomorphs, A and B. Both forms are constructed from a basic building block that has a left (L) or right (R) orientated stacked planes. All left, LLLLL, or all right, RRRRR orientated stacked planes will give rise to a chiral (left or right) form of polymorph A. A mix of orientations of the planes *e.g.* LRLRLR, will give rise to the achiral polymorph B.[132,133] The energy of the 2 stacking configurations are the same so that without special processing, the zeolite will be a mixture of all three polymorphs and hence achiral. Purification of the mixture to enrich the amount of one of the enantiomers of polymorph A gives rise to an chirally active zeolite.

3.1.2 Adsorption of a chiral agent into the achiral zeolite framework

The more interesting aspect of zeolite chirallity is the induction of chiral environment into an achiral zeolite by adsorption of a chiral agent. This is interesting due to the ability to tailor a chiral centre to meet the requirements to the reaction. This gives researchers the ability to mimic the chiral environment found in biological enzymes. This has been done in the work of Jacobs et al.[134] where the phthalocyanins were encapsulated within the supercage of zeolite Y. This mimiced the biological oxidation catalyst, cytochrome P450 which, amongst others, plays a part in the photosynthesis process. These enzyme mimics are commonly referred to as 'zeozymes'.[132,133]

3.2 Chiral Modification of Zeolite Y

Some of the most interesting work on the subject of chiral modification involves the adsorption of a chiral agent into the achiral zeolite-Y pores. This forms a stable complex, able to discriminate between isomers of butan-2-ol in a dehydration reaction.[132,133,135–139]

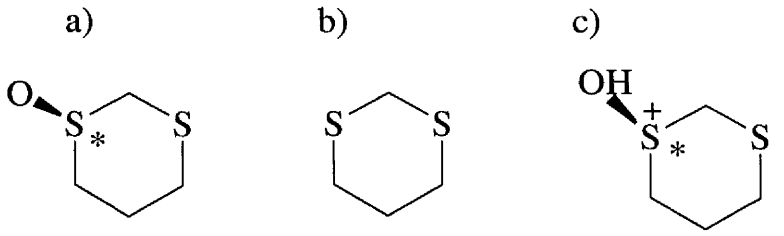

Figure 3.1: The 3 dithiane molecules used in the study, asterisk indicates chiral centre. (a) chiral R-1,3-dithiane 1-oxide (b) achiral dithiane (c) chiral R-1,3-dithiane 1-oxide cation.

3.2.1 Experimental

Willock et al[135] found that on introduction of the chiral molecule, R-1,3-dithiane 1-oxide (figure 3.1(a)) into the achiral zeolite Y, the complex was able to act as a chiral catalyst in the enantioselective dehydration of butan-2-ol. In fact, the chiral complex was able to dehydrate S-butan-2-ol up to 19 times faster than the R enantiomer. It is thought that the R-1,3-dithiane 1-oxide (figure 3.1(c)) forms a ion-pair chemisorbed species with the framework, *i.e.* proton transfer occurs from the zeolite to the R-1,3-dithiane 1-oxide, the molecule becoming a framework counter-cation. The presence of the chiral dithiane is important in the reaction as addition of the achiral 1,3-dithiane (figure 3.1(b)) to zeolite Y had no effect on the activity of dehydration. The presence of the acidic proton is also of importance as the reaction is not catalysed by R-1,3-dithiane 1-oxide in the analogous all-silica

framework. This suggests that the important interaction in the process is that of the R-1,3-dithiane 1-oxide with the acidic proton. Cluster calculations were performed on a T4 cluster using the semi-empirical AM1 method from which the results in table 3.2.1 were obtained.

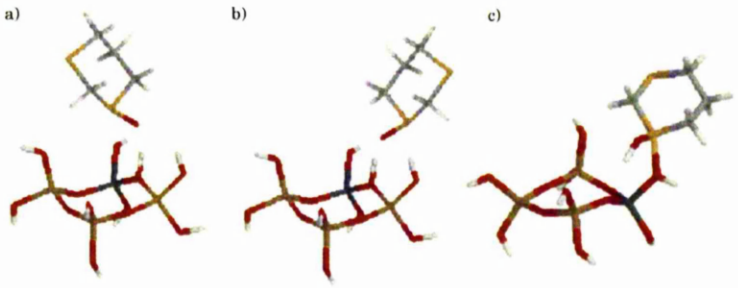

Figure 3.2: (a)T4(H) / R-1,3-dithiane 1-oxide (b) T4 / R-1,3-dithiane 1-oxide TS (c) T4 / R-1,3-dithiane 1-hydroxide

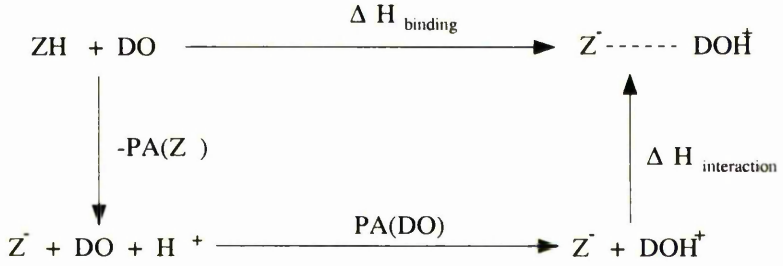

Figure 3.3: Thermodynamic cycle for the binding of 1,3-dithiane-1-oxide (DO) to a T4 zeolite (Z) cluster via proton transfer. PA stands for proton affinity

To study the stability of the cation complex for both the R and S 1,3-dithiane 1-oxide, the results were used to calculate the proton affinities using the thermodynamic cycle (figure 3.3).

The proton affinity (PA) can be calculated using equation 3.1

$$-PA_{(DO)} = E_{HF(DOH)} + E_{ZP(DOH)} - E_{HF(DO)} - E_{ZP(DO)} \tag{3.1}$$

Molecules	Energy (AM1) (Hartree)	ZPE	Corrected Energy
T4	-157.20357	0.12991	-157.07366
T4(H)	-157.62265	0.14152	-157.48113
R-1,3-dithiane 1-oxide	-48.942156	0.11739	-48.824766
R-1,3-dithiane 1-hydroxide	-49.207812	0.12656	-49.081257
S-1,3-dithiane 1-oxide	-48.942156	0.11739	-48.824766
S-1,3-dithiane 1-hydroxide	-49.207812	0.12655	-49.081263
R-butan-2-ol	-35.696610	0.13689	-35.559718
S-butan-2-ol	-35.696610	0.13690	-35.559711
Transition States			
T4 / R-1,3-dithiane 1-oxide TS	-206.56653	0.25564	-206.31090
T4 / S-1,3-dithiane 1-oxide TS	-206.56755	0.25569	-206.31186
Complexes			
T4(H) / R-1,3-dithiane 1-oxide	-206.58593	0.26142	-206.32451
T4(H) / S-1,3-dithiane 1-oxide	-206.58087	0.26008	-206.32078
T4 / R-1,3-dithiane 1-hydroxide	-206.58580	0.26122	-206.32458
T4 / S-1,3-dithiane 1-hydroxide	-206.58671	0.26101	-206.32570
T4 / R-1,3-dithiane 1-hydroxide / R-butan-2-ol	-	-	-
T4 / R-1,3-dithiane 1-hydroxide / S-butan-2-ol	-	-	-
T4 / S-1,3-dithiane 1-hydroxide / R-butan-2-ol	-242.291644	0.399384	-241.89226
T4 / S-1,3-dithiane 1-hydroxide / S-butan-2-ol	-242.293876	0.399585	-241.89429

Table 3.1: Energies of the molecules involved in the interaction of R and S 1,3-dithiane 1-oxide with a T4 cluster. T4(H) / R-1,3-dithiane 1-oxide represents R-1,3-dithiane 1-oxide bound to a T4 ring cluster with a proton on the bridging oxygen.

where $PA_{(DO)}$ is the proton affinity of the dithiane oxide molecule, $E_{HF(DOH)}$ and $E_{HF(DO)}$ are the energies of the protonated and non-protonated dithiane oxide molecules. $E_{ZP(DOH)}$ and $E_{ZP(DO)}$ represent the zero point energies of the respective dithiane molecules, obtained from infra-red frequency evaluations.

This gives a proton affinity of 673.9 kJ mol^{-1} for both R and S 1,3-dithiane 1-hydroxide. Figures 3.5 and 3.6, show the potential energy surface of adsorption of R and S 1,3-dithiane 1-oxide onto a T4 zeolite cluster.

The energies plotted are given relative to the most favourable combination of molecules, which in both cases is the dithiane hydroxide bound to the zeolite cluster, 44.91kJ mol^{-1} more favourable in the case of the R enantiomer and

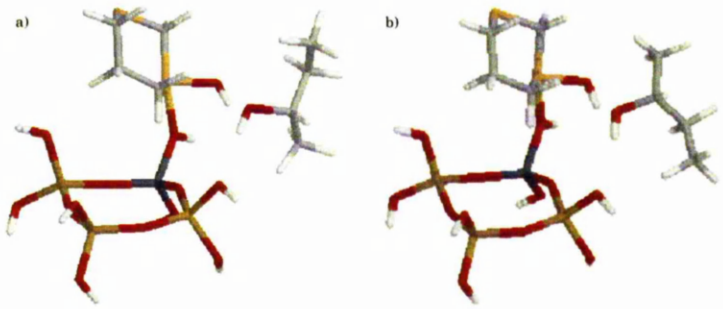

Figure 3.4: (a) T4 / S-1,3-dithiane 1-hydroxide / R-butan-2-ol (b) T4 / S-1,3-dithiane 1-hydroxide / S-butan-2-ol

37.08kJ mol^{-1} for the S enantiomer. There is a large barrier for proton transfer from the zeolite to the dithiane, 35.75kJ mol^{-1} R enantiomer and 23.42kJ mol^{-1} for the S enantiomer, the resulting dithiane hydroxide being more stable in both cases 0.18kJ mol^{-1} and 12.92kJ mol^{-1} respectively.

It is worthy of note that the energy required to overcome the transition state barrier for proton transfer is more than compensated for by the energy dissipated on association of the reactants. This supports the experimental work in which it is seen that adsorbed dithiane exists in a strongly bound cation form and the 1,3-dithiane 1-oxide is only regenerated on solvent extraction.[137,138]

Further work was undertaken to calculated the binding of R and S butan-2-ol to the T4 / S-1,3-dithiane 1-hydroxide complex. The S-1,3-dithiane 1-hydroxide complex is most active to the dehydration of R-butan-2-ol, and therefore it is thought that the R-butan-3-ol would bind more tightly as suggested in the work of Feast et al.[137] The results of this work do not reproduce experimental data, the S enantiomer was found to bind 5.356kJ mol^{-1} more tightly than the R enantiomer contrary to experimental work.

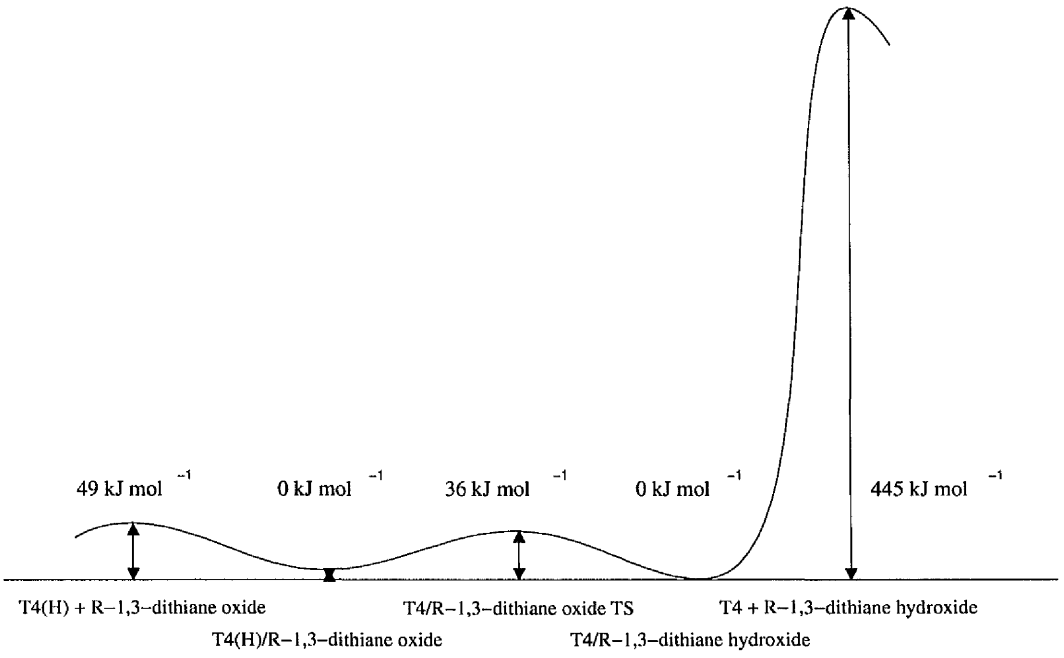

Figure 3.5: The potential energy surface for the adsorption of R-1,3-dithiane 1-oxide on to a T4 zeolite cluster

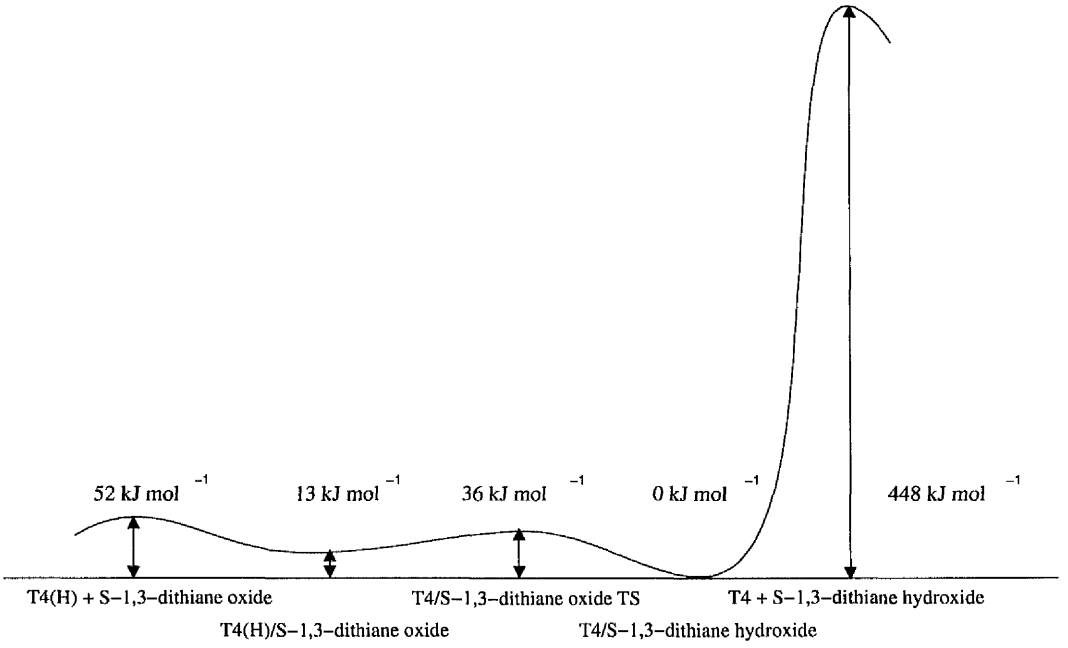

Figure 3.6: The potential energy surface for the adsorption of S-1,3-dithiane 1-oxide on to a T4 zeolite cluster

3.3 Conclusion

Although a relatively large zeolite cluster was used in this study, it can clearly be seen that a larger zeolite system needs to be utilised to include all the contact interactions between the absorbants and the zeolite framework. This is born out by the theoretical results which, in areas, contradict the experimental data. It is clear that a larger system with a more accurate computational method is required to accurately represent this system. The computational method can simply be improved as AM1 is a semi-empirical method. The next progression would therefore be to use an non-empirical method such as *ab-initio* Hartree-Fock theory. The next failing; the lack of the surrounding environment can be addressed by increasing the cluster size. The problem with this is that if both the cluster size and the methods are improved, the calculation will become prohibitively expensive. In this example, the cluster would have to become prohibitively large in order to totally surround the cluster. The solution to this problem is to calculate the important regions where the *chemistry* occurs using an accurate method such as Hartree-Fock with a large basis-set. The surrounding region can then be evaluated using a less accurate method. The development of methods to address these problems will be discussed in subsequent chapters.

Chapter 4

Computational methods for modelling of periodic systems

4.1 Introduction

The methods mentioned in Chapter 2 such as molecular mechanics and *ab-initio* methods are commonly applied to molecular systems. Due to the periodic nature of crystalline lattices, these methods cannot be applied in the same way to model this type of system. The main problem is that the finite summation over the atoms in the system, in the case of a molecular system becomes infinite in the periodic case. In their normal form these infinite summations are incalculable so several methods have been developed to avoid or remove the problem.

4.2 Finite cluster calculations

Cluster Calculations are the most common *ab-initio* calculations; they are performed by selecting the most important section of the zeolite and reactant, then

discarding the rest. Trailing T-site bonds on the zeolite are commonly terminated with hydrogens.

This type of calculation is used due to simplicity as it has the low computational overhead of a small number of atoms. Additionally, this method is readily available in all modelling programs as no modifications of the standard MM or *ab-initio* methodology are required. The problem with this type of calculation is that the important features of the zeolite are neglected such as the long range crystal structure. All of the long range interactions are ignored in cluster calculations and it has been proven in the field of enzyme catalysis that it is often these interactions that make a reaction viable.

The neglect of the surrounding environment causes further problems when excising clusters from zeolites such as Zeolite-Y. It has been shown both experimentally and computationally that there are 4 chemically different oxygen sites at which the proton can reside and each of these sites will have a different energy of deprotonation. When the clusters are taken out of the zeolite, the surrounding environment which differentiates these clusters is lost and therefore the cluster energies become identical.[140–142]

Nevertheless, this type of calculation has proven to be a valuable starting point for more complex calculations. However, there is an important point to consider; how large a cluster to use over how much computational time is available, a balance must be made between the two. If the cluster is too small, the calculation will be inaccurate, too large a cluster and it will be computationally prohibitive.[143,144] Even though this type of calculation is widely used and provides a good basis for further work, it has been proven to be inaccurate due to the lack of long range potential provided by the infinitely periodic framework. Cluster approximation grossly underestimates the acidity of the proton, which is the site of interest in most zeolite reactions such as the MTG process. Methods of countering this have been suggested, where the length of the terminating hydrogens are varied to fit

the proton affinity of the acidic proton to reproduce experiment.

4.3 Periodic molecular mechanics

The molecular mechanical description of a group of atoms is conveniently partitioned into different terms which when summed give rise to a reasonable approximation of the system.

- Bonded terms between neighboring atoms
- Non-bonded interactions such as the van der Waal terms
- Electrostatic interactions

The above representation is the same whether the system is an organic molecule or a periodic solid. In addition, the bonded terms are treated the same in both the periodic and non-periodic cases unless the interaction traverses a unit-cell boundary. In this case, standard periodic boundary conditions are applied to the system.

In the case of non-bonded, non-electrostatic interactions, the energy decays rapidly, as a function of r (r^{-12} and r^{-6} in the case of the van der Waal term). This tends towards zero very quickly with increasing r and can be dealt with by applying a cut off in the region of 10Å with little of no loss in accuracy. Once again periodic boundary conditions are applied if an interaction occurs across a cell boundary.

The electrostatic term is entirely different as it is a slowly decaying function of $\frac{1}{r}$ and therefore still significant at large values of r. For non-periodic systems this is not a problem as all the electrostatic interactions can be summed over the finite space. In the periodic case on the other hand, this would involve an impossible sum over an infinity distance. This problem is solved by the use of

a mathematical technique known as the Ewald summation. It will be discussed in section 4.6 as it is equally applicable to quantum mechanical methods as it is to molecular mechanical methods. These methods have been embodied in the 3 dimensional molecular mechanics package GULP (General Utility Lattice Program)[102] and the 2 dimensional, surface analysis package MARVIN.

Introduction of periodicity to a calculation brings with it added variables that require minimisation, such as the unit cell parameters and the strains on the unit cell. They must be dealt with and optimised as would any other variables.

4.3.1 Constant pressure minimisation

In the constant pressure minimisation method, both the ionic positions and the lattice vectors are relaxed to minimise the forces on both the atoms and the unit cell. The cell vectors are minimised using the same method as in the constant volume minimisation for the coordinates, the lattice vectors being treated as extra variables.

The bulk strains (the strains on the whole unit cell) are defined as

$$r' = (\mathbf{I} + \epsilon).r \tag{4.1}$$

where $\mathbf{I}$ is the identity matrix, ϵ is the strain on the lattice vectors,r and r' are the transformed lattice vectors such that

$$\begin{bmatrix} x' \\ y' \\ z' \end{bmatrix} = \begin{bmatrix} 1+\varepsilon_1 & \frac{1}{2}\varepsilon_6 & \frac{1}{2}\varepsilon_5 \\ \frac{1}{2}\varepsilon_6 & 1+\varepsilon_2 & \frac{1}{2}\varepsilon_4 \\ \frac{1}{2}\varepsilon_5 & \frac{1}{2}\varepsilon_4 & 1+\varepsilon_3 \end{bmatrix} \begin{bmatrix} x \\ y \\ z \end{bmatrix} \tag{4.2}$$

The static pressure can be found as the first derivative of the lattice energy with respect to the strain by using the chain rule relationship

$$P_{static} = \frac{\partial U}{d\varepsilon_j} = \frac{\partial U}{\partial r} \cdot \frac{\partial r}{\partial r^2} \cdot \frac{\partial r^2}{\partial \varepsilon_j} \tag{4.3}$$

where the 1st term $(\frac{\partial U}{\partial r})$ represents the 1st derivative of the energy, the second term $(\frac{\partial r}{\partial r^2})$, equates to 1/2r and the third term is solved by squaring the equation defining the bulk strains and differentiating to give

$$\frac{\partial r'^2}{\partial \varepsilon_j} = 2r^{\alpha}.r^{\beta} + 2r^{\alpha}.\varepsilon.r^{\beta} \tag{4.4}$$

applying equilibrium conditions, *i.e.* strain is zero, $\varepsilon = 0$

$$\frac{\partial r'^2}{\partial \varepsilon_j} = 2r^{\alpha}.r^{\beta} \tag{4.5}$$

4.3.2 Constant volume minimisation

This type of minimisation relaxes the ion position whilst keeping the cell dimensions fixed. Standard optimisation methods such as Newton-Raphson variable matrix methods are used to minimise the lattice energy $U(r)$ with respect to the ionic coordinates.

In this approach $U(r)$ is expanded to the second order

$$U(r') = U(r) + g^T.\delta r + \frac{1}{2}\delta r^T.\mathbf{W}.\delta r \tag{4.6}$$

where δr is the displacement (or strain) of the ions, g is the first derivatives whilst $\mathbf{W}$ is the second derivatives with respect to r.

At equilibrium, when the change in energy with strain is zero

$$\frac{\partial U}{\partial \delta r} = 0 = \mathrm{g} + \mathbf{W}.\delta r \tag{4.7}$$

$$\delta r = -\mathbf{W}^{-1}.\mathrm{g} \tag{4.8}$$

For a perfectly harmonic system in r, the equilibrium position should be reached in one step. This is rarely the case but a small step usually gives rise to a lower energy. The minimum is then found via an iterative scheme. Usually this is the most efficient method of optimisation but the use of second derivatives can prove expensive for large systems. For this reason it is often advantageous to use first derivative only methods such as conjugate gradients for the early cycles when the system is most anharmonic and far from equilibrium.

4.4 Periodic Quantum Mechanics

One of the most widely used[145] implementations of a Periodic Quantum mechanics package is that embodied in the Crystal92,[146] 95,[147] and 98 series of programs. The theory and methodology behind this program is beyond the scope of this thesis so only a brief comment will be made on the subject

4.4.1 Periodic Hartree-Fock Theory

Basis functions and orbitals

As with standard Hartree-Fock calculations, the periodic method requires the use of orbitals which are eigenfunctions of the one-electron Hamiltonian. To maximise the efficiency of the calculation the Crystal Orbitals utilise the translational

symmetry of the crystal. The local atomic orbital basis is thus defined as:

$$\chi_{\alpha}^{\mathbf{g}}(\mathbf{r}) \equiv \chi_{\{n,l,m\}}(\mathbf{r} - \mathbf{g} - \mathbf{s}_{\alpha}) \tag{4.9}$$

where $\mathbf{g}$ is a vector referencing the general cell, α represents the α'th atomic orbital in that cell. n, l, m refers to the quantum numbers which characterise the atomic orbital and $\mathbf{g} - \mathbf{s}_{\alpha}$ represents the position of the atom in the form of a fractional vector. $\mathbf{r}$ is the position at which the wavefunction is evaluated.

Bloch functions are used to express the atomic orbitals in a form which incorporates the translational symmetry of the periodic system.

$$\phi_{\alpha\mathbf{k}} = \sum_{\mathbf{g}} e^{i\mathbf{k}.\mathbf{g}} \chi_{\alpha}^{\mathbf{g}}(\mathbf{r}) \tag{4.10}$$

The crystal orbitals can be expressed as a linear combination of the Bloch functions, where $C_{n\alpha}^{(k)}$ is a variational coefficient.

$$\varphi_{n\mathbf{k}} = \sum_{\alpha} C_{n\alpha}^{(k)} \phi_{\alpha\mathbf{k}} \tag{4.11}$$

Basis sets in the form of Bloch function are generally used as they are simply expressed in terms of atom centred local functions. Methods exist where plane-waves are used in place of Bloch functions. The advantage of this is that a single plane wave provides the exact solution to the homogeneous electron gas problem, the archetype for all solid-state studies.

Computational method

A periodic Hartree-Fock calculation performed using the CRYSTAL program can be broken down into several steps as detailed below.

The Fock matrix is constructed in direct space with exactly the same contributions as in the non-periodic case.

$$\mathbf{F}_{12}^{\mathbf{g}} = \mathbf{T}_{12}^{\mathbf{g}} + \mathbf{Z}_{12}^{\mathbf{g}} + \mathbf{C}_{12}^{\mathbf{g}} + \mathbf{X}_{12}^{\mathbf{g}} \tag{4.12}$$

Where $\mathbf{g}$ represents a direct lattice vector by which a given unit cell is referenced, $\mathbf{T}_{12}^{\mathbf{g}}$ is the kinetic energy matrix and $\mathbf{Z}_{12}^{\mathbf{g}}$ and $\mathbf{C}_{12}^{\mathbf{g}}$ are the interactions of the AO overlap distribution, $\chi_1^{\mathbf{g}}(\mathbf{r})\chi_2^{\mathbf{g}}(\mathbf{r})$, with the full nuclear and electronic charge distributions respectively.

This representation of the Fock matrix differs little from the non-periodic representation. It is only on further consideration of the $\mathbf{C}_{12}^{\mathbf{g}}$ term that it can be seen that electronic overlap can take place between different cells. Again for the $\mathbf{X}_{12}^{\mathbf{g}}$ term or the exchange contribution it can be shown that basis functions formally located on the four centres can each be in different cells. These are problems that are not encountered in typical QM systems and must be tackled appropriately. This is done by transforming the direct space Fock matrix into reciprocal space via Fourier transforms and iterating until self-consistency is achieved.

Periodic electrostatic potential

In the same way as in with the molecular case, the quantum mechanical electrostatic potential at a point, $V(r)$, is evaluated from the electronic charge density, $\rho(r)$, of the converged wavefunction. In standard molecular Hartree-Fock methods, the potential of the system containing N atoms, at a point $\mathbf{r}$, where Z, is the nuclear charge of the i'th atom can be written as

$$V(\mathbf{r}) = \sum_{\mathbf{i=1}}^{\mathbf{N}} \frac{\mathbf{Z_i}}{|\mathbf{r} - \mathbf{R_i}|} - \int \frac{\rho(\mathbf{r}')}{|\mathbf{r} - \mathbf{r}'|} \mathbf{dr}' \tag{4.13}$$

The same method cannot be directly applied to periodic systems as the evaluation will be for an infinite number of atoms, N. Techniques are available to circumvent

this problem such as the Ewald summation method. This will be discussed in depth in section 5.3. One other method is the multipole expansion method which will briefly be described.

In a similar way to the Ewald method, the short range contributions to the electrostatic potential are evaluated exactly, longer range contributions are evaluated using a multipole expansion of the shell charges .[148]

$$\rho(\mathbf{r}) = \sum_{\mathbf{h}} \sum_{\lambda} \rho_{\lambda}^{\mathbf{h}} = \sum_{\mathbf{h}} \sum_{\lambda} \rho_{\lambda}(\mathbf{r} - \mathbf{h}) \tag{4.14}$$

The shell contributions are taken to be 'short-range' if $e^{\alpha_\lambda(\mathbf{r}-\mathbf{s}_\lambda-\mathbf{h})} > 10^{-\xi}$, where α_λ is the exponent of the adjoined Gaussian, $\mathbf{S}_\lambda$ is the fractional vector which references the shell λ, and ξ the integral penetration parameter. For high multipole order, e.g. $l = 6$, with an appropriate choice of penetration parameter, the resulting *approximate* periodic electrostatic potential can be shown to be within 0.1% of the exact value but at a greatly reduced computational cost.

4.5 Combined or hybrid methods

Ideally we would like to study all of our systems at the highest level of theory possible and employ the largest basis set. In reality calculations are limited by the amount of computing resources that are available. The amount of computing time, memory and disk space consumed are dependent on the number of basis functions in the system and the method employed so we have to try to limit both. The molecular mechanics method is computationally inexpensive but does not allow calculation of electronic processes, whilst quantum mechanical methods are more accurate but also more expensive. One solution to this problem is the hybrid method. Hybrid methods have been implemented to allow the study of the reaction site using a high level electronic structure method, whilst representing

the longer range interactions using an approximate method. There are currently 2 main methods of doing this for zeolites.

4.5.1 Embedded cluster methods

Embedding in a field of point charges

The embedding of a quantum mechanical cluster in point charges is the next step up from the bare calculation. With this method a finite layer of point charges surrounding the cluster is included in the quantum mechanical calculation, and the effect of the classical point charges is included in the evaluation of the 1 electron Hamiltonian. Although this method may be a step up from a bare cluster calculation it has severe drawbacks. To prevent the cluster from crashing into the charges upon optimisation, the atoms surrounding the charges must be fixed in space causing an unnatural distortion around the boundary. This will be a minor problem if the fixed geometry is at or close to equilibrium but will be inaccurate otherwise. In addition to this the finite nature of the point charge array can lead to inaccuracies in the long range electrostatics.

Embedding in the potential due to a field of point charges

This method uses a periodic *ab-initio* code such as Crystal92 to calculate the electrostatic potential generated by the periodic zeolite structure. The potential due to the quantum mechanical cluster is then evaluated and subtracted from the periodic potential according to the scheme in figure 4.1.

The QM cluster is then surrounded by a cube to which a set of point charges is fitted to represent the calculated 'difference' potential. The potential derived charge grid (PDC) is then combined with the non-periodic *ab-initio* cluster calculation 'fooling' the reacting site into experiencing a long range interaction with

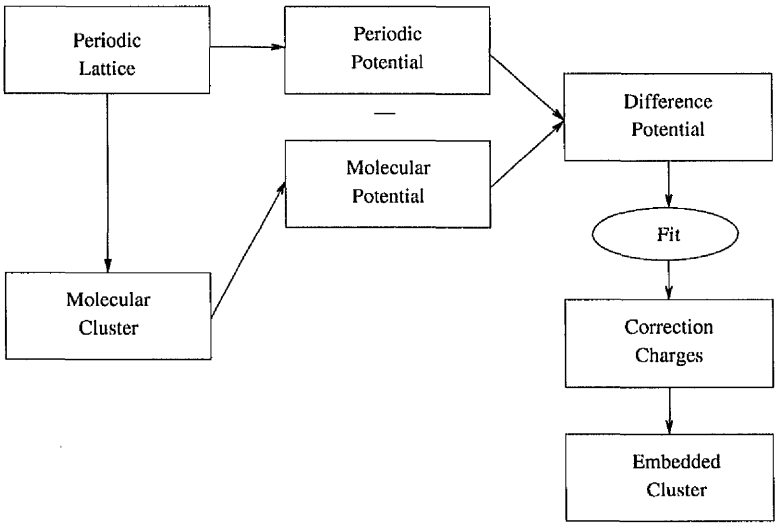

Figure 4.1: Schematic representation of the potential derived charge model

a periodic zeolite framework.[149] The advantage of this method is its simplicity which allows standard features of the *ab-initio* code to be used as normal but experiencing the effect of the periodic framework. Information such as NMR shielding tensors can be calculated with the correction caused by the periodic structure.

4.5.2 Periodic QM-MM method

As stated in sections 2.1 and 2.3 respectively, *ab-initio* is accurate but costly, whilst Molecular Mechanics sacrifices accuracy for cost. The combined method uses the expensive *ab-initio* method for the reacting site, but Molecular Mechanics for the longer range interactions. This method uses the MM methodology to calculate the long range contribution of the periodic zeolite to the reacting centre which is calculated quantum mechanically.

QMPot

The QMPot method was implemented by Sauer et al[150,151] and has been utilised in many studies of zeolites.[103,152–155] It is a 'mechanical' embedding method *i.e.* the interaction between the MM and the QM regions does not include polarisation of the QM electron density by the MM environment.

The Energy is partitioned according to the following scheme.

$$E(S) = E_{QM}(I) + E_{MM}(O) + E(I-O) \tag{4.15}$$

where

S = the entire system
I = the inner region
O = the outer region
$E(S)$ = energy of the entire system
$E_{QM}(I)$ = QM energy of the inner region
$E_{MM}(O)$ = MM energy of the outer region
$E(I-O)$ = Interaction term

The interaction term can be calculated in different ways, it is this that makes the method an 'electronic' or 'mechanical' embedding method.

Commonly the interaction term is given by

$$E(I-O) = E_{QM}(I-O) + E_{MM-QM}(I-O) \tag{4.16}$$

where $E_{QM}(I-O)$ is often calculated by interacting the outer region point charges with the QM electron density adding the charges to the QM Hamiltonian.

$E_{MM-QM}(I-O)$ covers the interactions between the 2 systems not included in the QM calculation, such as the bonded and short range non-bonded interactions.

This can be further approximated by neglecting the $E_{QM}(I-O)$ term and instead including a totally classical interaction of the inner and outer region charges.

$$E(I-O) = E_{MM}(I-O) \tag{4.17}$$

The interaction of the 2 sets of charges is then included via the energy and force contribution from the analytical potential. Hence the total energy of the system becomes:

$$E(S) = E_{QM}(I) + E_{MM}(I-O) + E_{MM}(O) \tag{4.18}$$

To simplify the application of this method further we can evaluate the MM contributions in a slightly different way

$$E_{MM}(I-O) + E_{MM}(O) = E_{MM}(S) - E_{MM}(I) \tag{4.19}$$

this reduces the calculation to one of the whole system and one of the cluster which we can be evaluated without any significant changes to the programs being used.

The energy term is therefore based upon the equation

$$E(S) = E_{QM}(I) + E_{MM}(S) - E_{MM}(I) \tag{4.20}$$

The inclusion of termination atoms in the QM cluster will be compensated for if the MM calculation exactly reproduces their potential as calculated quantum mechanically. This is done by parameterising the force field using the same basis

set and method that will be used for the hybrid study. Although this does account for the effect of termination atoms (assuming the mm force-field exactly reproduces the QM potential), however it makes the calculations impractical. Calculations are restricted to the method and the basis set that was used for the fitting of the force-field and a new force-field has to be fitted for each new target system.

4.6 The periodic Madelung summation

The electrostatic potential of a finite set of point charges, also known as the Madelung potential can be shown as

$$V_{(\boldsymbol{r})} = \frac{1}{2}\sum_{i}\sum_{j}\frac{q_i q_j}{4\pi\epsilon_0 r_{ij}} \tag{4.21}$$

or in the case of a system containing a finite number of unit cells

$$V_{(\boldsymbol{r})} = \frac{1}{2}\sum_{n}\sum_{i=1}^{N}\sum_{j=1}^{N}\frac{q_i q_j}{4\pi\epsilon_0 r_{ij}|\boldsymbol{r_{ij}}+\boldsymbol{n}|} \tag{4.22}$$

Where:
i, j are ion positions
q_i and q_j are the charges on ions i and j respectively
r_{ij} is the separation of i and j
n is the number of unit cells to be included in the summation

The problem with the summation in this form is that the periodic environment has to be truncated for the equation to be evaluated as it is impossible to evaluate a sum over an infinite number of unit cells containing an infinite number of charges. The electrostatic potential decays very slowly with increasing distance

as it is a function of $1/r$, therefore truncating the potential would give rise to large errors.

A second problem with this truncation of the potential is that on examination of equation 4.22, it can be shown that the summation is conditionally convergent. This means that the convergence of the summation is dependent on where the cut-off is made. This effect is shown in figure 4.2 and occurs due to the fact that the total energy of the crystal is highly dependent on how it is cut.

These problems can be circumvented by using several mathematical techniques, one of which is a method originally suggested by Madelung [156] and further developed by Ewald .[157]

For each point charge in the cell, a surrounding screening charge distribution of opposite sign is added as shown in Figure 4.3 b).

For convenience the charge distribution is given the form of a Gaussian function.

The addition of the screening charge distribution has the effect of screening the interaction between neighbouring point charges and making their interactions short-ranged. The potential of the point charges and the screening charge distribution can now be summed in the real space lattice of the simulation box.

To compensate for the addition of the screening charge distribution, a second charge distribution of the same charge as the original point charge and of the same form as the previous charge distribution is added as shown in Figure 4.3 c). The cancelling distribution can be evaluated in reciprocal space by summing the Fourier transforms of each of the charge distributions and then transforming back into real space.

Further technical details of this method can be found in chapter 5, section 5.3.

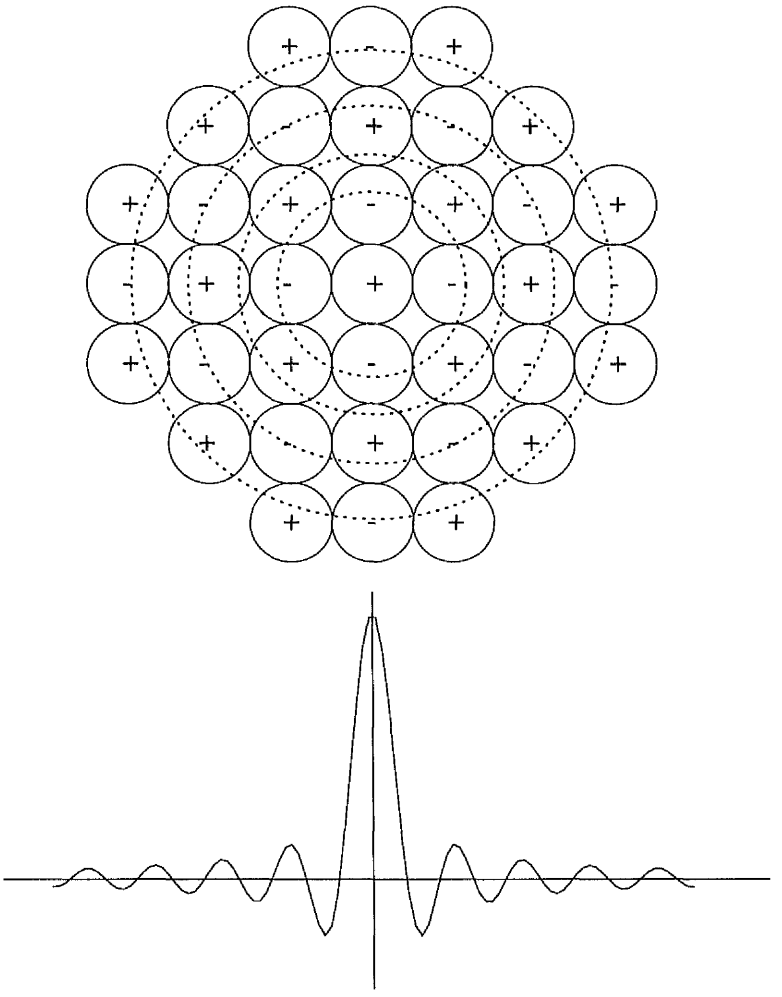

Figure 4.2: Schematic representation of conditional convergence effects when using truncation methods for long range electrostatics

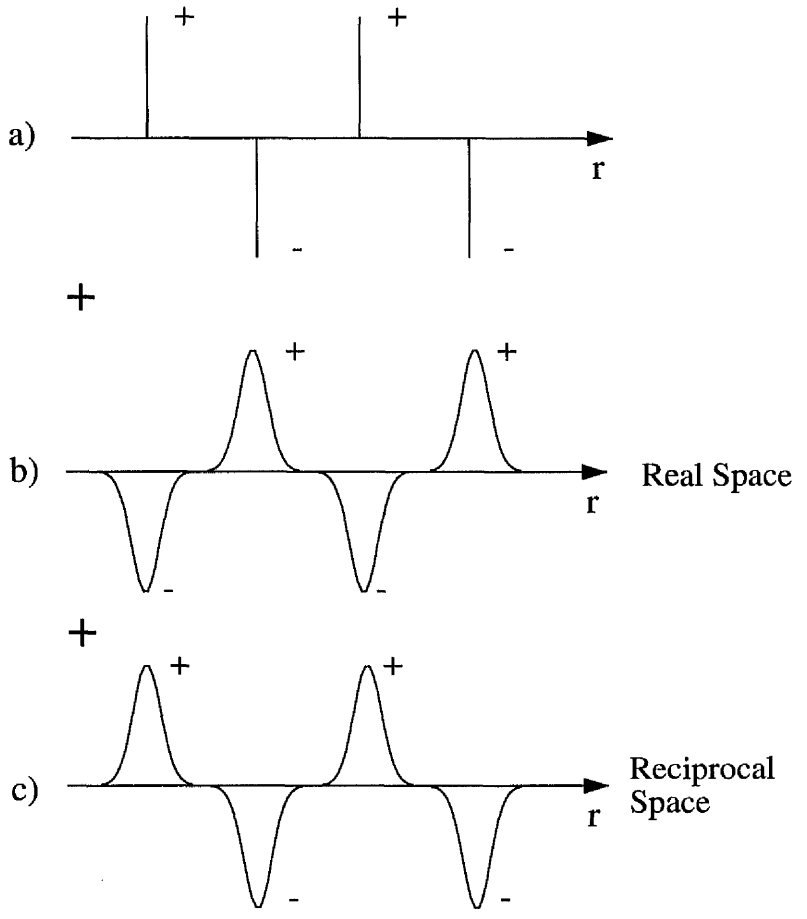

Figure 4.3: Schematic representation of Ewald summation method

Chapter 5

A Combined QM/MM potential for periodic modelling

5.1 Introduction

As noted in Chapter 4, there are currently several methods for modelling of periodic systems. The notable exception from the list is a periodic implementation of the QM/MM methodology. This chapter details the implementation of such a method, from both a theoretical and a practical perspective and presents a general method for combined quantum chemical and molecular mechanics geometry optimisations of zeolites and other periodic crystalline solids.

The methodology is relatively straight forward when the QM and MM atoms are divided between separate regions as shown in Figure 5.1. In this case the calculation is simply of a QM cluster embedded in a periodic MM solvent. The problem becomes more difficult if the QM region consists of a cluster which is part of a larger system such as a zeolite fragment. This involves coupling of the two disparate modelling techniques and the truncation of bonds to form the

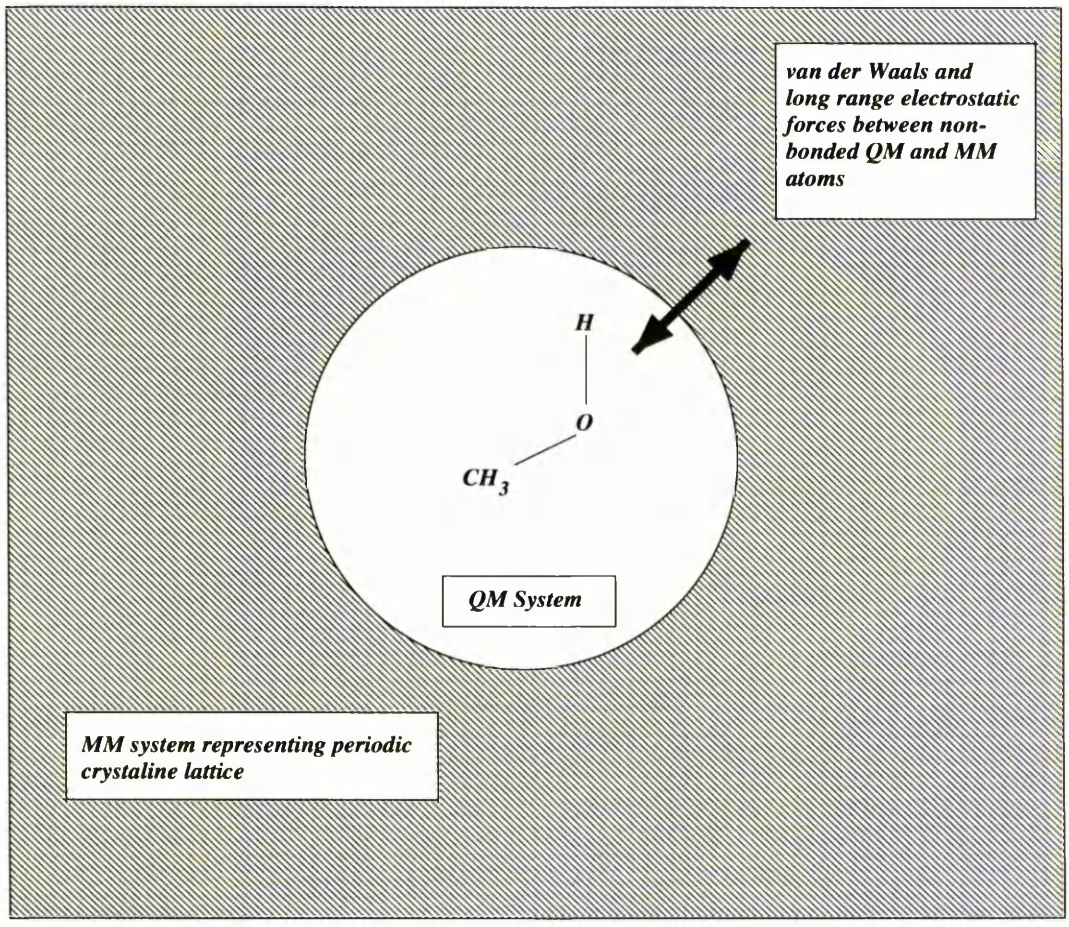

Figure 5.1: Schematic of the partitioning scheme employed in the PQM/MM method when the QM cluster is not covalently bonded to the MM environment

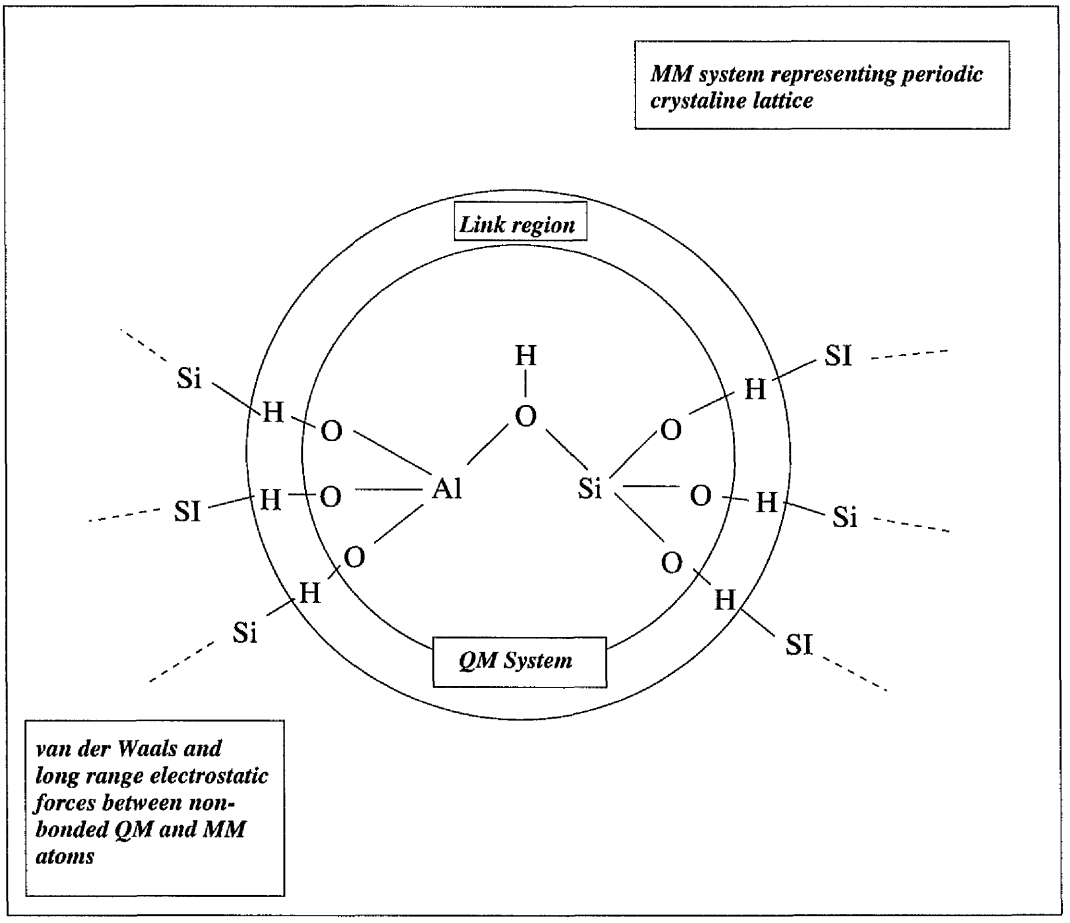

Figure 5.2: Schematic of the partitioning scheme employed in the PQM/MM method when the QM cluster is directly embedded in the MM environment

QM cluster. This would give rise to a charged and often high spin system which would not be representative of the true chemical nature of the cluster. A better representation of the system (although not ideal as will be discussed in 2.4.2) is made by terminating the broken, unsaturated bonds with hydrogens.

5.2 Methodology

Atoms in the QM region are represented as nuclei and electrons. This region contains all those atoms that are involved in chemical processes that cannot be accurately modelled with molecular mechanics techniques *i.e.* bond breaking/bond forming processes. It represents all the regions in which a movement of electron density occurs.

The MM region constitutes the environment in which the QM atoms are embedded. These atoms are included as although they may not play a direct part in the reaction, they exert a significant influence on the behaviour of the QM system. These atoms cannot be involved in the making or breaking of bonds due to the previously mentioned limitations of the MM method.

The periodic electrostatics can be summed in 2 ways:

- Using a standard classical approach, the interaction of the periodic environment with a classical point charge is calculated. *c.f.* ONIOM, IMMOM. Note that the QM region is not polarised by the MM region. The QM region is just embedded in the electrostatic influence of the surrounding environment.
- Using the QMEwald method as described in Section 5.3. The Madelung potential due to the classical periodic environment directly interacts with the QM basis functions, perturbing the QM Hamiltonian (*c.f.* MUQMMM).

5.3 Ewald theory

5.3.1 Introduction

This section describes in more detail the computational implementation of the Ewald methodology described in section 4.6. The Ewald code presented here was not written by the author of this thesis. It was originally written by Nygren et al[158] as a stand alone package, but was implemented at the University of Manchester as a link for Gaussian94.[159] This work has remained unpublished and as such, is reported in brief in this thesis.

5.3.2 The Ewald summation

In the non-periodic case, the total energy for ions in a unit cell can be written as

$$E_{cell} = \sum_i q_i V(r_i) \tag{5.1}$$

where the electrostatic potential V is written as

$$V(\boldsymbol{r}) = \sum_{\boldsymbol{R}} \sum_i \frac{q_i}{|\boldsymbol{R} + \boldsymbol{r}_i - \boldsymbol{r}|} \tag{5.2}$$

where $\boldsymbol{R}$ equals the position of the unit cell and the lower case letters (*i.e.* $\boldsymbol{r}_i$) refer to ion positions with respect to the origin of that unit cell.

Due to the requirement of a sum over terms to infinite values of R_i (for an infinite number of unit cells), it is impossible using the previously defined methods to perform evaluations of periodic electrostatics.

The Ewald method allows the efficient calculation of $E(r)$ where $r \rightarrow \infty$ (U_{Ewald}) by splitting the $1/r$ potential function into two separate, absolutely convergent

components, a short range and a long range term according to equation 5.3.

$$\begin{aligned} \frac{1}{r} &= \frac{f(\boldsymbol{r})}{\boldsymbol{r}} + \frac{1-f(\boldsymbol{r})}{\boldsymbol{r}} \\ &= \frac{erfc(\gamma \boldsymbol{r})}{\boldsymbol{r}} + \frac{erf(\gamma \boldsymbol{r})}{\boldsymbol{r}} \end{aligned} \tag{5.3}$$

which utilises the following relationship

$$\begin{aligned} 1 &= erfc(\gamma \boldsymbol{r}) + erf(\gamma \boldsymbol{r}) \\ &= \frac{2}{\sqrt{\pi}} \int_0^{\infty} exp[-t^2]dt \\ &= \frac{2}{\sqrt{\pi}} \int_0^{\gamma r} exp[-t^2]dt + \frac{2}{\sqrt{\pi}} \int_{\gamma r}^{\infty} exp[-t^2]dt \end{aligned} \tag{5.4}$$

This simple change transforms the problem from a slowly, conditionally convergent summation to the summation of two new absolutely convergent terms representing the short and long range components of the 1/r potential respectively.

The γ term in the error function (equation 5.4) is calculated in the following equation and is chosen to maximise the computational efficiency of the calculation whilst maintaining accuracy of results.

$$\gamma = \frac{16}{V^{2/3}} \tag{5.5}$$

where V = unit cell volume

The potential of the system can now be written as

$$\begin{aligned} V(\boldsymbol{r}) &= V_{sr}(\boldsymbol{r}) + V_{lr}(\boldsymbol{r}) \\ &= \sum_{\boldsymbol{R}} \sum_i \frac{q_i}{|\boldsymbol{R} + \boldsymbol{r_i} - \boldsymbol{r}|} erfc(\gamma |\boldsymbol{R} + \boldsymbol{r_i} - \boldsymbol{r}|) \\ &+ \sum_{\boldsymbol{R}} \sum_i \frac{q_i}{|\boldsymbol{R} + \boldsymbol{r_i} - \boldsymbol{r}|} erf(\gamma |\boldsymbol{R} + \boldsymbol{r_i} - \boldsymbol{r}|) \end{aligned} \tag{5.6}$$

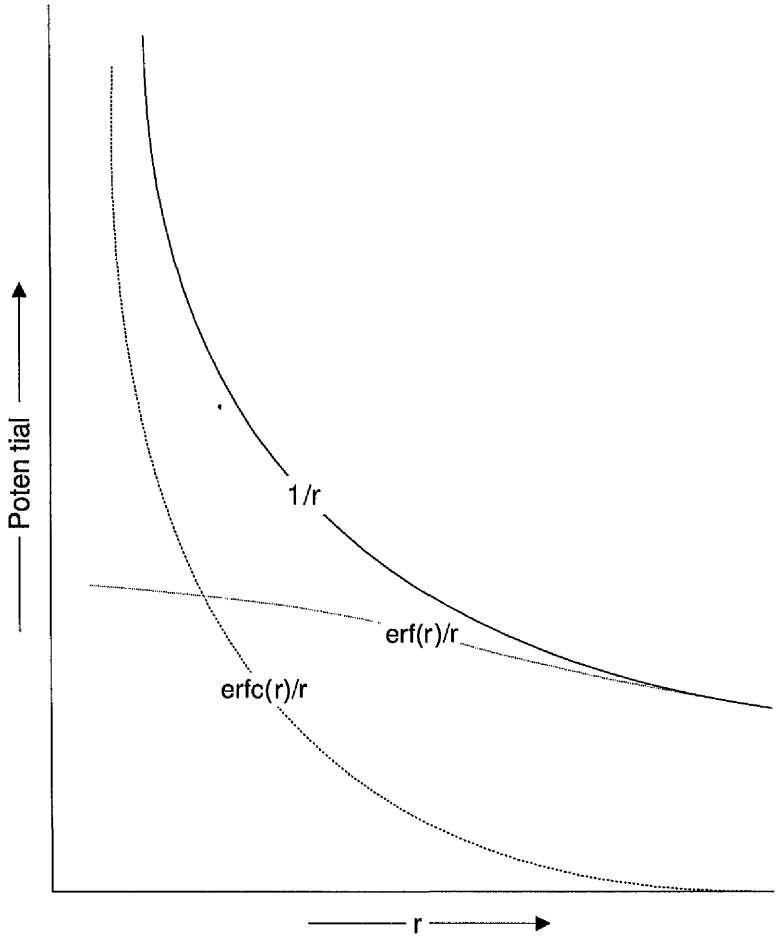

Figure 5.3: Schematic representation of the decomposition of the slowly converging 1/r potential into a short and a long range term

The short range component decays exponentially with increasing r and is absolutely convergent, it is summed in real space and a cut-off of r_{max} employed. The long range component decays more slowly so the interactions are summed in Fourier space.

These relationships can now be used to calculate the nuclear and electronic contributions of the periodic potential to the overall wave function

5.3.3 The Nuclear contribution

The Reciprocal space contribution

The long range nuclear contribution to our Ewald summation is calculated as the interaction of a periodic set of point charges interacting with the nuclear centres of the cluster. As periodic summations are computationally impossible to solve directly, the summation is performed in reciprocal space. Due to the nature of the reciprocal summation method, the summation must be of a central cell interacting with a periodic array of exact replica cells. Therefore, the self-interaction of the central cluster of interest that we are embedding in the periodic environment is unavoidably included in the summation. To circumvent this problem, the contribution must be removed in a separate calculation.

In equation 5.6, the long range potential has been decomposed into the second term, which contains the error function erf.

$$V_{lr}(\boldsymbol{r}) = \sum_{\boldsymbol{R}} \sum_{i} \frac{q_i}{|\boldsymbol{R} + \boldsymbol{r_i} - \boldsymbol{r}|} erf(\gamma|\boldsymbol{R} + \boldsymbol{r_i} - \boldsymbol{r}|) \tag{5.7}$$

From figure 5.3 it can be seen that the potential varies slowly in direct space. This suggests that there will only be a few low-frequency contributions to its Fourier transform.[158] The back-transformation from reciprocal to real space will

be the summation

$$V_{lr}(\boldsymbol{r}) = \sum_{\boldsymbol{K}} A_{\boldsymbol{K}} exp[\boldsymbol{K}i.\boldsymbol{r}] \tag{5.8}$$

The Direct space contribution

As the Ewald method was constructed to avoid problems in summing an infinite number of *long* range interactions, it is surprising to find that the *short* range nuclear term is the more difficult contribution to calculate.

Due to the fact that the short range contribution dies off rapidly with increasing r, it can be dealt with by using a cut-off radius. The short range potential acting on each cluster site is calculated by summing the interactions between the nuclear centre of the cluster ion and each of the charges lying within the cut-off space. The cut-off radius is calculated from γ, introduced in equation 5.6, as shown in equation 5.9

$$R_{Cut-off} = 1/\gamma\sqrt{|log(EPSR\sqrt{\pi})|} \tag{5.9}$$

where $EPSR = 1$ x 10^{-10}

The interaction between the cluster ions and the lattice charges is calculated between the cluster and all charges that lie with the cut-off sphere, unit cell translations being performed as necessary to generate periodic ion images that lie within the boundary.

The short range potential term that is used for this is the second term in equation 5.6.

$$V_{sr}(\boldsymbol{r}) = \sum_{\boldsymbol{R}} \sum_{i} \frac{q_i}{|\boldsymbol{R} + \boldsymbol{r_i} - \boldsymbol{r}|} erfc(\gamma|\boldsymbol{R} + \boldsymbol{r_i} - \boldsymbol{r}|) \tag{5.10}$$

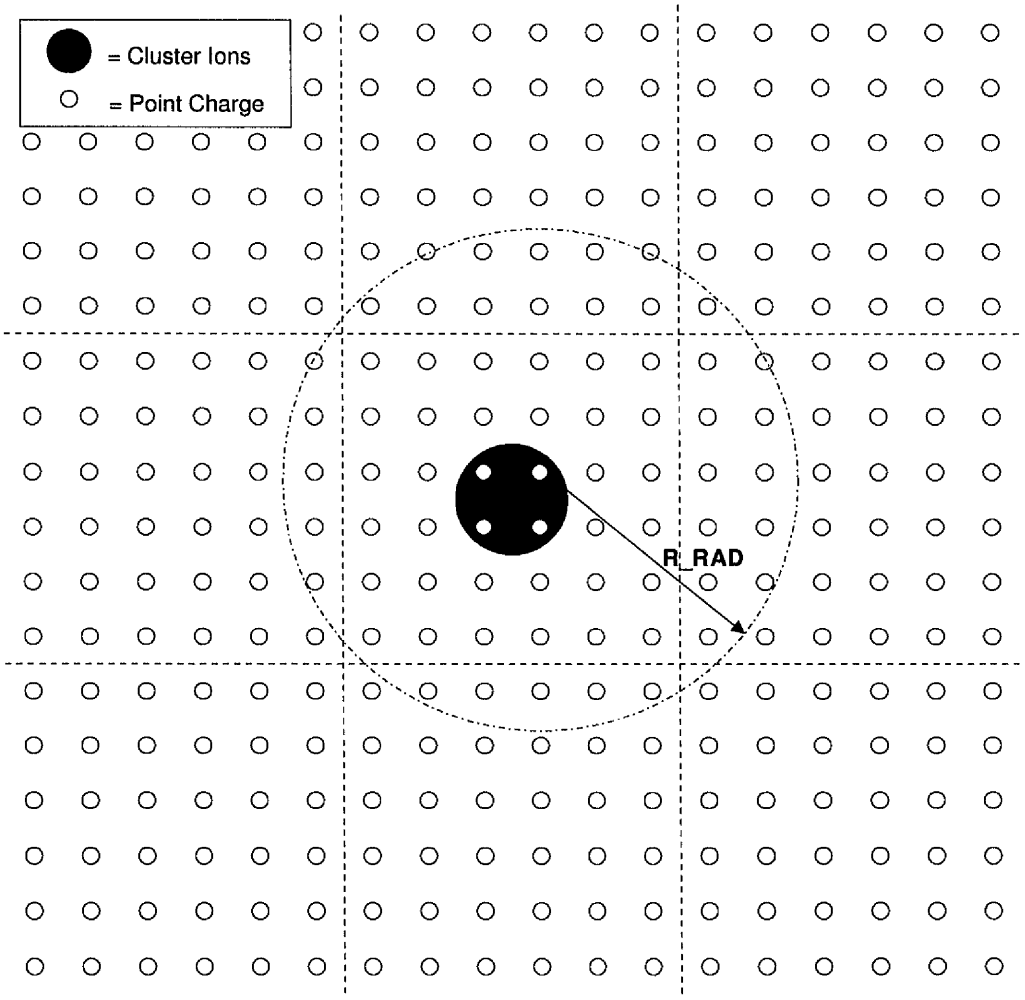

Figure 5.4: Example of ion centred cut-off sphere for short range interactions

It is worth noting here that self interactions of the charges on the cluster ions are not included in this summation. This is also an ideal point at which to correct the reciprocal nuclear contribution to remove the self interaction of the cluster. As the direct space summation is being performed over the cluster ions, it is a trivial task at this point to add in the correction term for the reciprocal space.

$$V_{lr\ corr}(\boldsymbol{r}) = \sum_{i_{(cluster)}} -q_i \frac{erf[\gamma|\boldsymbol{r}_i - \boldsymbol{r}|]}{|\boldsymbol{r}_i - \boldsymbol{r}|} \tag{5.11}$$

5.3.4 The Electronic contribution

The Reciprocal space contribution

As with the nuclear summation, the reciprocal space summation consists of a fully periodic set of point charges interacting with the finite cluster. As with the previous example it contains an extra self-interaction term which must be removed to prevent double counting (by QM code). Again this removal is commonly performed elsewhere for convenience.

The Direct space contribution

The direct space electronic contribution is calculated differently to the nuclear direct space contribution. This contribution is calculated in a similar way to the reciprocal contributions where the interaction of the cluster is calculated with all ions within the direct space cut-off, including self-interactions. The difference in this method is that the self-interactions for the short-range electronic term are not removed. In fact they are left in to compensate, somewhat neatly, for the short range component of the reciprocal space summation.

Using the relationship $erf = 1 - erfc$, the short range electronic contribution

can be written as the operator

$$V_{elec\ sr}(\boldsymbol{r_i}) = \frac{erf[\sqrt{\xi}|\boldsymbol{r_{ii}} - r|] - erf[\gamma|\boldsymbol{r_{ii}} - \boldsymbol{r_i}|]}{|\boldsymbol{r_{ii}} - \boldsymbol{r_i}|} \tag{5.12}$$

This must now be corrected to remove the electronic short range cluster contribution. Rather than remove it all, only part of it is removed

$$V_{sr\ elec\ corr}(\boldsymbol{r_i}) = \frac{erf[\sqrt{\xi}|\boldsymbol{r_{ii}}_{(cluster)} - \boldsymbol{r_i}|]}{|\boldsymbol{r_{ii}}_{(cluster)} - \boldsymbol{r_i}|} \tag{5.13}$$

cleverly, this leaves an extra contribution that requires removing

$$\frac{-erf[\gamma|\boldsymbol{r_{ii}}_{(cluster)} - \boldsymbol{r_i}|]}{|\boldsymbol{r_{ii}}_{(cluster)} - \boldsymbol{r_i}|} \tag{5.14}$$

which is exactly, the contribution that requires removing to correct the long range term, thus all the required corrections have been made and the summation is complete. The total interaction can now be summed as

$$\begin{aligned} < \phi_i|V(\boldsymbol{r_i})|\phi_j > &= < \phi_i|V_{sr}(\boldsymbol{r_i}) + V_{lr}(\boldsymbol{r_i})|\phi_j > \\ &= < \phi_i|V_{sr}(\boldsymbol{r_i})|\phi_j > + < \phi_i|V_{lr}(\boldsymbol{r_i})|\phi_j > \end{aligned} \tag{5.15}$$

5.3.5 Integration with Gaussian94

There are 3 main areas in which the addition of an external potential will have an effect in the Gaussian94 package.[121] Information about Gaussian overlays is given below, additional information about the link structure can be found in Appendix A.

- The calculation of the $1e^-$ integrals

- Evaluation of the integral first and second derivatives with respect to the nuclear coordinates *i.e.* evaluation of the forces and second derivatives
- The final energy

Overlay 3

The 1-electron integrals are calculated by Gaussian94 in link 302 using the PRISM routine. As the Ewald contribution is a simple "correction" to the unperturbed wavefunction, the Ewald contribution can be added at any point after link 302. The Ewald code is in practice called as link 307 (or 320) but due to the way that the Gaussian deck is processed, unless a route card is generated by hand, the extra links are left until last to be executed so the link number is somewhat irrelevant.

Overlay 7

The integral first derivatives are calculated by Gaussian in link 702 and again the perturbation is added after this link. The Ewald first derivatives and forces (second derivatives were not available at the time of writing) are calculated in link 708, the forces being stored in the cartesian frame (note that no symmetry is used). Using the standard method of adding links to Gaussian would mean that no matter what link number was used, the Ewald code would be executed after the standard Gaussian link 716. Link 716 converts Cartesian forces and force constants to internal coordinates and computes harmonic vibrational frequencies and normal modes from the force constants. It also transforms all derivative information from the symmetry orientation back to the input orientation. The transformation to internal coordinates would mean that the forces would be in the wrong format for addition of the addition of the Ewald contribution. It is this reason that the use of a non-standard route card is required, and the numbering

the Ewald link as Link 708. This then causes link 708 to be executed in the correct order, before Link 716.

5.4 The Hamiltonian of the system

An appropriate effective Hamiltonian, H_{eff} must be formed, which describes the system to allow the calculation of the energy of the total system and the forces on each atom. Once we have the Hamiltonian we solve the time independent Schrödinger equation to obtain the energy E_{tot}, and the electronic wavefunction

$$\hat{H}_{eff}\Psi(\mathbf{r};\mathbf{R}_\alpha,\mathbf{R}_M) = E(\mathbf{r};\mathbf{R}_\alpha,\mathbf{R}_M)\Psi(\mathbf{r};\mathbf{R}_\alpha,\mathbf{R}_M) \tag{5.16}$$

The wave function ψ is a function of the position of the electrons, $\mathbf{r}$ and parametrically dependent on the QM nuclear coordinates, $\mathbf{R}_\alpha$, and the MM coordinates, $\mathbf{R_M}$. The geometry dependent energy is calculated as

$$E = \left\langle \Psi \middle| \hat{H}_{eff} \middle| \Psi \right\rangle \tag{5.17}$$

The effective Hamiltonian for the PQM/MM system can be written as the sum of three terms, the total energy being the sum of the expectation values of the operator

$$\hat{H}_{eff} = \hat{H}_{QM} + \hat{H}_{MM} + \hat{H}_{PQM/MM} \tag{5.18}$$

where $\hat{H}_{QM}$ = QM Hamiltonian $\hat{H}_{MM}$ = MM Hamiltonian $\hat{H}_{PQM/MM}$ = PQM/MM Hamiltonian

5.4.1 The MM Hamiltonian

The molecular mechanical Hamiltonian is a function of the positions of the MM atoms but it does not depend on the coordinates of the QM cores and electrons, we can therefore write

$$\hat{H}_{MM} = E_{mm} = E_{bond} + E_{angle} + E_{dihedral} + E_{coulomb} + E_{van\ der\ Waal} \quad (5.19)$$

$$E_{tot} = \left\langle \Psi \middle| \hat{H}_{QM} \middle| \Psi \right\rangle + \left\langle \Psi \middle| \hat{H}_{PQM/MM} \middle| \Psi \right\rangle + E_{MM} \quad (5.20)$$

5.4.2 The QM Hamiltonian

$$\hat{H}_{QM} = -\frac{1}{2}\sum_{i} \nabla_i^2 + \sum_{ij} \frac{1}{r_{ij}} - \sum_{i\alpha} \frac{Z_\alpha}{r_{i\alpha}} + \sum_{\alpha\beta} \frac{Z_\alpha Z_\beta}{r_{\alpha\beta}} \quad (5.21)$$

Where Z_α is the charge on nucleus α r_{ij} is the distance between particles i and j and the subscripts i,j and α, β refer to the electrons and nuclei respectively.

5.4.3 The PQM/MM Hamiltonian

The PQM/MM Hamiltonian is dependent on the coordinates of the electrons, $\mathbf{r}$, and parametrically depends on the location of the QM atomic cores, $\mathbf{R}_\alpha$, the MM atoms $\mathbf{R}_M$ and on the type of interaction between the QM and the MM regions. In the case where the QM and MM regions interact via electrostatic and Buckingham interactions, the Hamiltonian can be written as

$$\hat{H}_{PQM/MM} = -\sum_{iM} \frac{q_M}{r_{iM}} + \sum_{\alpha M} \frac{Z_\alpha q_M}{r_{\alpha M}} + \sum_{\alpha M} \left\{ A e^{-r_{\alpha M}/\rho_{\alpha M}} - C_{\alpha M} r_{\alpha M}^{-6} \right\} \quad (5.22)$$

The first term is a Coulomb interaction between the electrons and the MM atoms. The middle term is a Coulomb interaction between the nuclei and the MM atoms

whilst the final term is represents the van der Waal interaction between the two regions.

The interaction Hamiltonian, $\hat{H}_{PQM/MM}$ in equation 5.22 is the exact Hamiltonian for the interaction of QM atoms with the partially charged van der Waals spheres. The first and the last term of equation 5.22 are constant depending only on PQM/MM geometry and can be calculated and added directly into the total energy. The second term in equation 5.22 involves electronic positions and so must be incorporated into the Quantum Mechanical formalism. This is achieved by calculating the one-electron integrals over the operator $V_{(r)}$ (which represents the interaction of an electron with the periodic Madelung potential) and including them in the one-electron matrix H as described in section 5.3. It must be noted at this point that the periodic QM/MM Hamiltonian does not differ in any way to its non-periodic counterpart, the only difference is that the summation of the electrostatic interactions are over an infinite separation, this being dealt with mathematically as documented in section 5.3.

The wavefunction Ψ is a function of the coordinates of the electrons, $\mathbf{r}$, and parametrically depends on the location of the QM atomic cores, $\mathbf{R}_\alpha$, and the MM atoms $\mathbf{R}_M$. The energy is calculated for each geometry according to

$$E_{tot} = \left\langle \Psi \middle| \hat{H}_{QM} \middle| \Psi \right\rangle + \left\langle \Psi \middle| \hat{H}_{MM} \middle| \Psi \right\rangle + \left\langle \Psi \middle| \hat{H}_{PQM/MM} \middle| \Psi \right\rangle \tag{5.23}$$

Given that Ψ in equation 5.23 is normalized, the forces acting on the QM and MM atoms can be calculated as the derivatives of the energy.

$$\mathbf{F}_\alpha = -\frac{\partial E_{tot}}{\partial \mathbf{R}_\alpha} \tag{5.24}$$

and

$$\mathbf{F}_M = -\frac{\partial E_{tot}}{\partial \mathbf{R}_M} \tag{5.25}$$

$$I_{\mu\upsilon} = -q_M \int \varphi_\mu \frac{1}{r_{iM}} \varphi_\upsilon d\mathbf{r}, \tag{5.26}$$

where φ_μ and φ_υ are the atomic basis functions. The Hartree-Fock equations can be solved in the standard way except that the system now corresponds to one that depends on the external field due to the presence of the periodic MM atomic partial charges.

The one-electron integral of equation 5.26 can be evaluated analytically for both Gaussian and Slater-type orbitals, and this type of treatment would be appropriate for *ab-initio* calculations.

Chapter 6

MUPPET - Manchester University Periodic Potential Environment

6.1 Introduction

MUPPET - Manchester University Periodic Potential Environment is the name for the implementation of several methods for the calculation of crystal clusters embedded (mechanically and electronically) in the potential due to a periodic environment.

In the MM region the atoms are represented using GULP[102] (General Utility Lattice Program), a periodic molecular mechanics program utilising a chosen potential. The QM region is represented using Gaussian 94 and an additional plug-in module, QMEwald,[159] is available which allows the evaluation of the periodic electrostatic potential and its interaction with the central explicitly defined QM region.

6.2 General methodology

The existing QM/MM code, MUQMMM,[160] was written for use with Gaussian94 and AMBER, a molecular mechanics code used extensively in the study of large proteins. AMBER has a distinctive and somewhat unusual method of working due to the way that a protein may be input as amino-acid residues. As such, the original QM/MM code was tightly integrated to the package making porting of the code for use with other molecular mechanics packages difficult.

A natural future progression for this program (although out of the scope of this thesis) would be to integrate it with a program for surface calculations such as MARVIN. This was a driving factor in the decision to make the code as portable as possible so that the method could be implemented with other MM packages. The program was written with as much data passing as possible performed using flat files written to disk. The information required to be passed from the MM code to the PQM/MM code is the updated atomic coordinates, the cluster forces, the periodic forces and the energy contribution. These are then evaluated and information passed to the QM code. Passing of updated coordinates from the QM code is again done by updating an input deck on disk.

To change the MUPPET to work with another MM program would just require a new module that was able to interpret the new programs input deck format and the ability to obtain the MM energy and forces and write them to disk, a facility available in most programs. Although this is not the most efficient method due to the latency involved in disk based I/O, recent increases in disk and I/O sub-system performance has greatly reduced the impact of such a methodology. The advantages of using this methodology are huge due to the increased portability for future work.

6.2.1 Indexing of atoms

In the area of keeping track of the atoms, the Periodic QM/MM method differs greatly to its non-periodic counterpart. In the standard QM/MM method, the position of the atoms, QM or MM, is found by examining the MM input deck. A simple list of atom numbers is held together with a number relating to the atom type. This indexing method is then used to link each atom to its atom type and its co-ordinates. For QM atoms and termination atoms, whose co-ordinates do not directly appear in the MM deck, the indexing points to the QM deck to obtain the co-ordinates.

For the periodic case, it is not as simple. Due to periodic boundary conditions, an atom which is to become a termination atom, or any other QM atom for that matter, may not appear in the MM input deck, although its periodic image may. This occurs frequently in small unit cells and systems where the area of interest lies near the edge of a cell. In addition to this, an atom that lies within the cell at the beginning of a calculation may move out of the cell (and back in at the opposite side) during the course of the optimisation. These problems may be overcome with a strategic choice of unit cell and QM cluster but in certain systems cannot be avoided without either the use of a very large unit cell (*e.g.* 2x2x3 in the case of CHA) or extra code within the program to search for the 'missing' atom by regenerating the periodic repeat from the cell data.

The cross-referencing of atom types and coordinates is done in a similar way to that in the MUQMMM code. The only source of coordinates for all calculations, QM and MM, is from the MM input deck. Atoms are indexed in the QM input deck according to their position in the MM input deck and the atom type (frozen framework atom = 31, frozen = 15, free to move = 0). Additionally, if the atom is to become a termination atom, the number indexing the position in the MM deck is made negative for example.

```
 0      31
 0      31
 0      31
 1      0
 2      0
 3      0
 4      0
 10     15
-11     15
-22     15
```

In the example above, the first three entries would reference atoms that do not appear in the MM deck (such as dummy atoms), the 31 atom type referring to frozen, framework atoms. The following two lines represent atoms which are free to move and can be found at positions 1,2,3 and 4 in the MM input deck. Line eight represents a fixed atom whose coordinates can be found from line 10 in the MM input deck. Similarly the final two lines are fixed atoms with a link to the MM coordinates but this time, the negative value indicates that this atom is to become a termination atom in the QM cluster.

In the MM input deck, there is a second indexing to the QM atoms. Any atoms which are to appear in the QM deck, cores and any associated shells, are indexed in the MM deck by prefixing the atom type line with a 'q'.

```
Na    qcor 5.6391356 8.4587035 8.4587035 1.00000000 1.0000 1.00000 1 1 1
Cl    qcor 8.4587035 5.6391356 5.6391356 0.98400000 1.0000 1.00000 1 1 1
.      .       .         .         .          .         .      .    . . .
.      .       .         .         .          .         .      .    . . .
Na    core 0.0000000 2.8195678 2.8195678 1.00000000 1.0000 1.00000 1 1 1
Cl    core 5.6391356 2.8195678 5.6391356 0.98400000 1.0000 1.00000 1 1 1
```

The MM input deck is always treated as the master input file and initial coordinates for the system are always taken from this deck. On optimisation of the QM cluster, all updates are made to the MM input deck so that any subsequent restarts can be made from the MM input deck.

6.2.2 Core-Shell charges

Usually in this type of work, solids are treated as ionic systems employing a Buckingham potential to describe the interactions. Although solids behave largely ionically, they may also exhibit partial covalent behaviour, for this reason and to allow for polarisation effects the core-shell method of Dick and Overhauser[93] is implemented. This gives rise to a much more accurate representation of the system but with it brings more difficulties for the PQM/MM code.

The QM code has no concept of MM shells (although their effect is similar to the polarisability of p-orbitals on oxygen atoms), it only knows about the atomic centres. When the atomic centres are moved during the QM optimisation cycle, the respective shells have to be displaced by the same amount. This displacement will leave the cores in a non-optimal position so that the force on the core and the force on the core due to the shell must be added to the total force in the next cycle. These forces are not directly additive but are dependent on the restoring force joining them. To avoid this problem, on each cycle, the position of the shells is optimised before any other calculations are performed. When the forces on the shells are zero, it can be assumed that the total force on the ion site is that found on the cores alone.

6.2.3 Charges remaining on termination of a dangling bond

The advantage of using core-shell potentials is that the parameterisation of the potential is done using charges on the ion site (core and shell) that add up to the total ionic charge *e.g.* 4^+ in the case of silicon. When cluster termination occurs in the standard QM/MM method, due to the fact that the terminating hydrogen is placed 1Å along the broken bond, it is usually placed close to what would have been an atomic site, but has been made a point charge. This unnatural placement of a charge near to an atomic site can give rise to unnatural distortions around the termination boundary. This is solved by removal of the charge and redistribution across the neighbouring point-charge sites. When using the PQM/MM methodology for the evaluation of zeolites, this effect is greatly enhanced as truncation of the zeolite cluster at the oxygen as is commonly performed, gives rise to a total of 3 Si^{4+} ions (when using the core-shell potential) dangling unnaturally close to the terminating hydrogens. This gives rise to unphysical polarisation of the atoms around the boundary of the cluster. Simple removal of the charges would not solve the problem as this would give rise to an "unshielding" of the electrostatic effect of three neighbouring O^{2-} ions. The effect of this 6^- charge, even an extra layer away from the terminated cluster, would have a significant effect. Previous studies have attempted to address this inadequacy. For their study on methanol interacting with H-ZSM-5, Vetrivel et al presented a modification whereby all charges, which form part of a dangling bond, were scaled by 50%. Although somewhat empirical, this was done to reduce the unphysical polarisation by taking into consideration the partial covalency of the zeolite structure. In fact, these reduced charges correlate better with Mulliken population analysis studies of small zeolite clusters and periodic Hartree-Fock calculations.[161,162]

Another solution to this problem was to utilise a force-field which contained parameters derived from *ab-initio* data. As these charges were fitted to *ab-initio* data, their values tended to reproduce the Mulliken populations more closely and hence remove some of the problems associated with the use of ionic charges .

The work of Kramer et al[163] details the generation of such a force-field. The use of such a force-field makes the calculation much simpler as the problem of optimising shell positions is removed and the smaller charges cause less problems as the polarisation effect of the charges on the termination atoms and their near neighbours is much more natural.

6.3 Implemented methods

The flexible way in which the MUPPET code allows other methods to be incorporated in to the program easily will aid future development of the code to include new methodologies.

Currently there are several *hybrid methods* implemented within the code that may be of use in the modelling of crystalline solids. The methods are described schematically in the following figures according to the information in the key, figure 6.1. For example, figure 6.2 describes an embedding method where the energy and forces of the cluster are calculated using the MM methodology and subtracted from those of the larger environment, also calculated using the MM methodology. To this, the forces and energy of the cluster and terminating hydrogens, calculated using a QM method, are added. Electrostatic interactions between the 2 regions are calculated using MM methods *i.e.* classically.

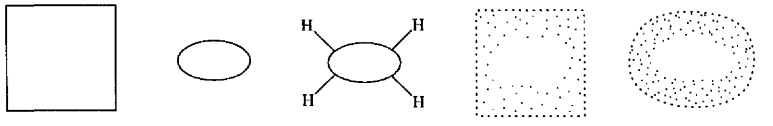

Figure 6.1: Key to figures

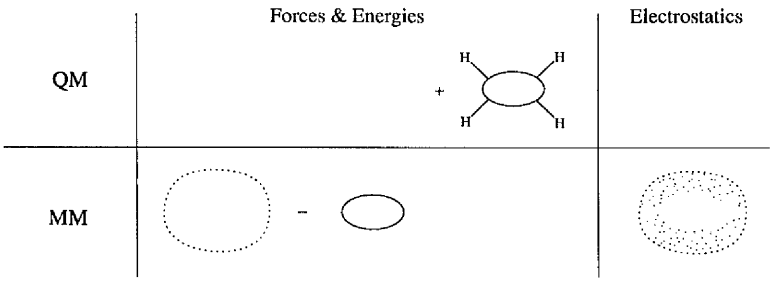

Figure 6.2: QM cluster embedded in a finite MM region. Long range electrostatic interactions are evaluated with the MM equivalents of the QM cluster atoms (*cf. ONIOM, IMOMM).*

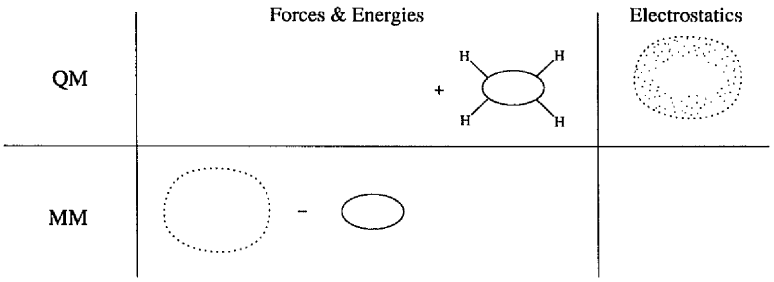

Figure 6.3: QM cluster embedded in a finite MM region. Long range electrostatics interact directly with the QM cluster (*cf. MUQMMM).*

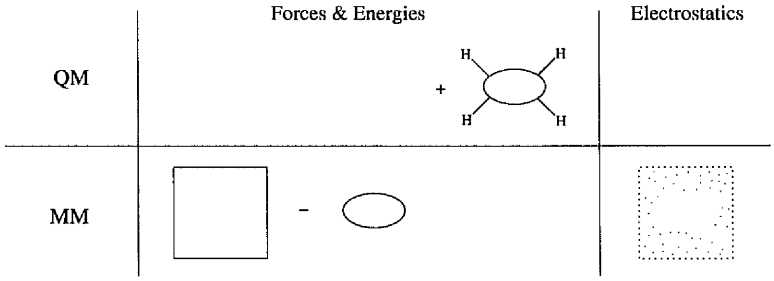

Figure 6.4: QM cluster embedded in a periodic MM environment. Long range electrostatic interactions are evaluated with the MM equivalents of the QM cluster atoms

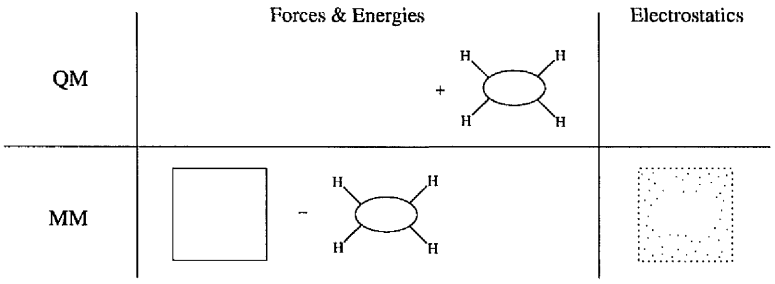

Figure 6.5: QM cluster embedded in a periodic MM environment. Long range electrostatic interactions are evaluated with the MM equivalents of the QM cluster atoms. The MM cluster which is subtracted from the periodic system contains the terminating hydrogens that appear in the QM cluster.

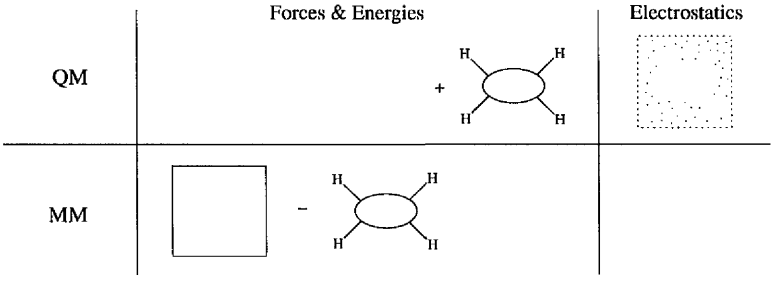

Figure 6.6: PQM/MM - QM cluster embedded in a periodic MM environment. Long range electrostatics interact directly with the QM cluster.

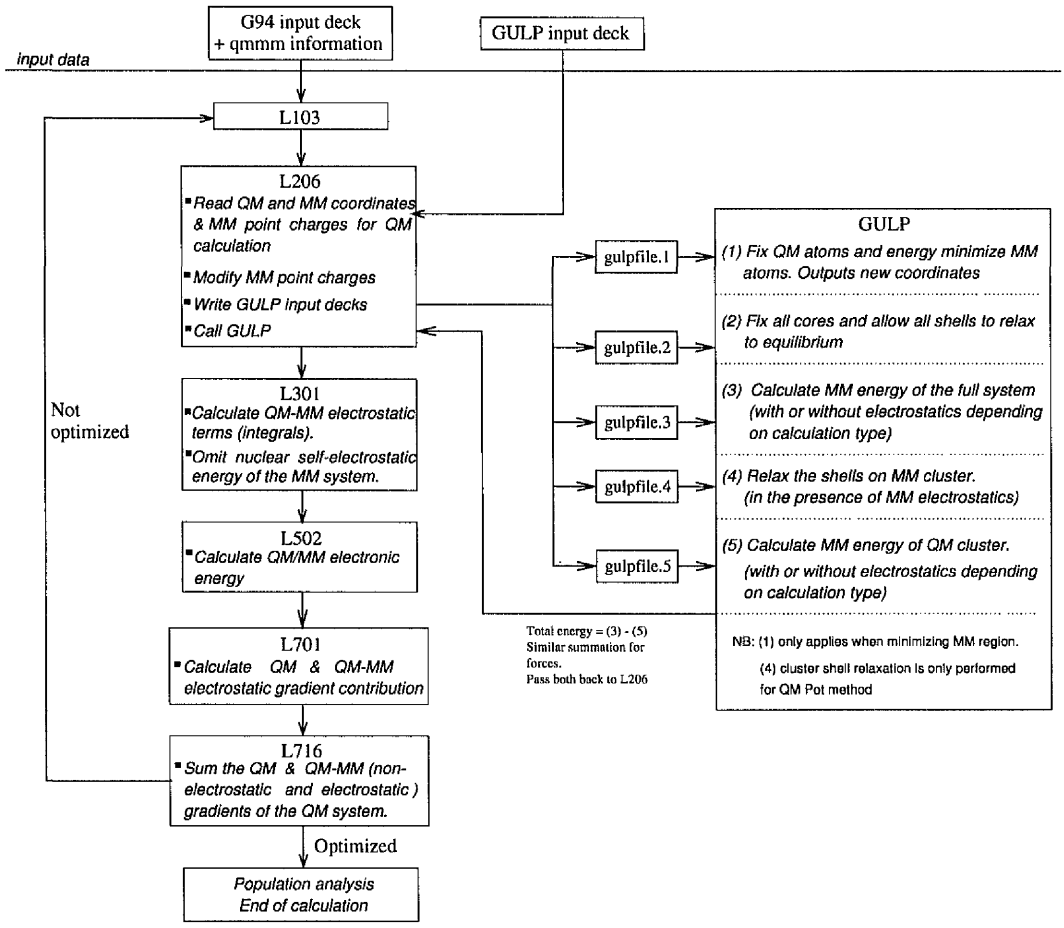

Figure 6.7: Flow diagram of the PQM/MM code (only the modified links are shown)

6.4 The PQM/MM implementation

As mentioned earlier, the PQM/MM code has been written to be as portable as possible. The design methodology allows the currently chosen packages to be replaced whilst keeping the program design and flow exactly the same. Figure 6.7 documents the flow of the code and how the packages are integrated, in particular, how data is passed back and forth between the modules.

The input data consists of input decks for the QM and MM codes, these are

unchanged except for the MM mapping information that is stored in the QM deck. On entry into L206, the input decks are parsed and the required decks generated for use with the MM program. These decks are used to calculate the two MM energy contributions shown in figure 6.2. The energy[†]of the whole periodic system calculated MM is evaluated in the first calculation with the MM code. (See MM section, step 2 in figure 6.7). As we are evaluating the periodic electrostatic contribution in a QM fashion (utilising the QMEwald code) we must calculate the effect of all the MM non-electrostatic contributions only. To do this, all charges are removed and the energy re-evaluated, thus avoiding any double counting of the effect of the electrostatic potential. The energy of the QM cluster is being evaluated quantum mechanically so this must also be removed, taking care not to remove the effect of the electrostatics as this has already been done. This is done in steps 4 and 5 of figure 6.7. At this point the master MM deck is updated with the optimised MM coordinates (although the QM atoms have not moved), ready for the next optimisation cycle.

The energies and forces from the MM calculations are passed back to the MUPPET code via file. This allows any MM package, capable of writing its energy and forces to file, a suitable candidate for use with the MUPPET code. The MUPPET code takes the file, subtracts the cluster values from the periodic values and stores them ready for addition to the result QM calculation.

The QM-MM electrostatic integrals and the QM and QM-MM (electronic and electrostatic) gradients of the QM system are evaluated and summed to give the total effect of a QM system feeling the MM force of the local environment and including perturbation of the QM cluster by the periodic electrostatics.

The QM code checks the gradients and the change in the energy to see if the system is at an optimal geometry. If it is, the calculation ends, if not the new QM geometry is updated to the master MM input deck, and the optimisation

[†]Although the cases described here are for energy evaluations, they apply equally to force calculations.

cycle continues.

Chapter 7

Validation and comparison of computational methods

The aim of the PQM/MM method, was to combine the accuracy of QM methods with the computationally inexpensive MM method by embedding a truncated QM fragment in a periodic potential due to the extended crystal. Before its use in performing reliable structure calculations, the PQM/MM method described in Chapter 5 must be validated to ensure correct results. In order to validate the code, test calculations were chosen and calculated, comparisons being made to literature reported experimental and theoretical results.

7.0.1 A PQM/MM study of bulk NaCl

NaCl provides an excellent test case for the PQM/MM code. It is well studied both computationally and experimentally so there is a plethora of information with which to compare results with. Secondly it is highly ionic and can therefore be studied without the presence of termination atoms.

	Na-Cl	4(Na-Cl)
Experimental (Bulk)[a]	2.820	2.820
Periodic MM (Bulk)[b]	2.820	2.820
QM[c]	2.433	2.709
QM plus point charges[d]	2.889	–
PQM-MM[e]	2.820	2.858
PQM/MM[f]	2.811	2.833

Table 7.1: Comparison of bulk NaCl bond lengths predicted by different methods. *a*) Taken from the work of Binks[1] *b*) The potentials of Binks[1] were used to describe the interactions between the Na^+ and Cl^- ions (see Appendix C). *c*) Calculated with the HF/LANL2DZ level of theory. *d*) Cluster is embedded in the centre of 6x6x6 cell of point charges, totalling 200 point charges in 2 layers surrounding the cluster. *e*) Calculated with the HF/LANL2DZ level of theory for the cluster and the potentials of Binks[1] for the MM region. Electrostatic interactions were calculated between the environment and the cluster classically. *f*) Calculated with the HF/LANL2DZ level of theory for the cluster and the potentials of Binks[1] for the MM region. Electrostatic interactions were calculated between the environment and the cluster using the periodic QM Ewald method.

The first test was to verify that the PQM/MM methods could accurately predict the equilibrium geometry of the bulk crystal. For this we used 2 different clusters; a simple isolated Na-Cl and a single 8 atom cell comprising of 4 sodium and 4 chlorine ions. Full geometry optimisations were performed on both bare and embedded clusters, in different environments to represent the *true* periodic potential. The results of these calculations are shown in table 7.1.

The MM potentials chosen to study this system combine the long-range electrostatics, represented by a Coulomb term and a short-range pair interaction, represented by a Buckingham potential as described in Chapter 2 section 2.3.1. To allow the polarisation of the anions, the shell model was employed (figure 2.3).

The method with the best correlation with experimental results is the Periodic MM bulk method. This is hardly surprising as the force field parameters used

were fit to reproduce experimental results.[1] Bare QM calculations grossly underestimate the Na-Cl bond length in both cases although the discrepancy decreases with increasing cluster size. To allow the embedding of Na-Cl in an array of point charges, the QM cluster had to be enlarged to include all nearest neighbour ions to the original cluster. The neighbouring ions were fixed in space and the remaining ions added in as point charges. This was required to stop the QM region from crashing into the point charges. This method can not be fairly compared to the other calculations as it has the advantage of having a larger QM cluster. The conclusion that can be made from this result is that even with a larger QM cluster and the embedding effect of the local point charges there is still a lack of agreement with experiment and there is an over estimation in the bond length.

The PQM-MM method exactly reproduces experimental results for the small cluster case and is in reasonable agreement ($< 1.5\%$) with experiment for the larger cluster. The real success with this method, however is with the use of the periodic Ewald summation for the evaluation of the long range electrostatics. Both results are within 0.015Å agreement with experiment and this with fewer empirical parameters being required.

7.0.2 A PQM/MM study of bulk chabazite

The next progression in validation is to validate a system which contains termination atoms. Introduction of termination atoms adds the possibility of errors due to introduction of the foreign atom to the environment. The system under study is chabazite (CHA), which was chosen due to its small unit cell and the fact that it has been extensively studied and well characterised.

From these results it can be again seen that the pure MM methods accurately reproduce the experimental results. This is due to the method by which the MM force-field was generated, using experimental results as the source from which

	Si-O	Si-O-Si
Experimental (Bulk)[a]	1.642	149.20
Periodic MM frozen cell (Bulk)[a]	1.623	151.70
Periodic MM relaxed cell (Bulk)[a]	1.600	146.63
QM[c]	1.614	139.97
QM in point charges[d]	1.631	153.45
PQM-MM[b],[e]	1.637	164.78
PQM/MM[b],[f]	1.644	155.54

Table 7.2: Comparison of CHA bond lengths and angles predicted by different methods. *a*) Not pure Si zeolite. Geometry elucidated from a structure containing 31% Al.[2] *b*) Calculation using MM potentials of Schröder et al[3] (see Appendix C). *c*) T3 cluster calculated at the HF/3-21G level. *d*) T3 cluster calculated at the HF/3-21G level and surrounded by 720 point charges. *e*) Calculated with the HF/3-21G level of theory for the QM cluster. Electrostatic interactions were calculated between the environment and the cluster classically. *f*) Calculated with the HF/3-21G level of theory for the QM cluster. Electrostatic interactions were calculated between the environment and the cluster classically. Electrostatic interactions were calculated between the environment and the cluster using the periodic QM Ewald method.

	Al-O(H)	Al-O(Si)	O-H	Al-O(H)-Si
Periodic MM frozen cell (Bulk)[a]	1.934	1.700	0.967	139.67
QM Cluster[b]	1.880	1.678	0.983	128.60
QM in Potential derived charges[b,c]	1.985	1.714	0.981	127.40
Periodic QM [a,d]	-	-	0.960	-
PQM/MM	1.911	1.710	0.979	134.89

Table 7.3: Comparison of CHAH, bond lengths and angles predicted by different methods. Cluster calculations and QMMM methods use a T3 cluster containing 1 Al. Protonation is performed at the most stable oxygen site (O1). *a*) MM calculations performed using the potentials of Schröder et al[3] (see Appendix C). *b*) QM calculation performed at the HF/3-21G*. *c*) Results reproduced from Greatbanks et al.[4] *d*) Periodic *ab-initio* calculations were taken from the work of Teunissen et al[5] and were performed using the HF/6-31G(d) basis set for the Al and Si, 6-311G(d) on the acidic oxygen, 6-31G on all other oxygens and 3-1G on the acidic proton

to generate parameters. The bare QM cluster underestimates the bond lengths and the Si-O-Si angle. This is attributed to the neglect of the local environment and replacement of a neighbouring Si with a terminating proton. Addition of point charges to the system appears to resolve this problem and gives results not too dissimilar to the experimental values. The QMPot method is again in good agreement with the experimental bond lengths although the Si-O-Si angle is somewhat different to the experimental values. This has been attributed to the use of a basis set that differed to that used to parameterise the QMPot MM potentials. This is a known drawback of the QMPot method. The PQM/MM method is in good agreement with experimental data for the Si-O-Si angle but it deviates furthest of all the methods from the experimental results for the Si-O bond lengths. Nevertheless, the difference in bond length is still only around 0.02Å.

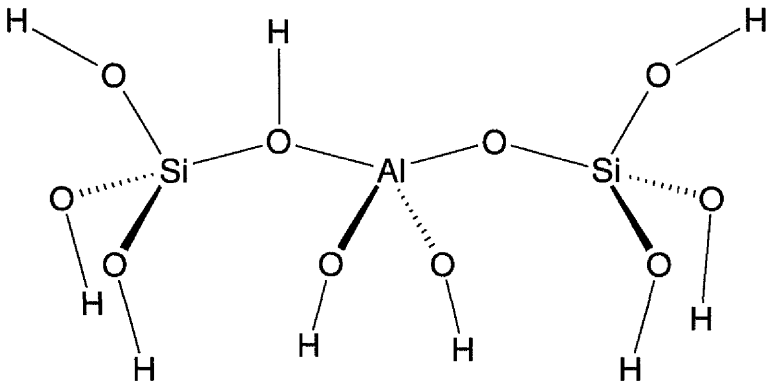

Figure 7.1: Si-OH terminated T3(H) zeolite cluster

7.0.3 A PQM/MM study of Al substituted chabazite

There is little direct experimental structure information of protonated zeolites due to the problems in detecting the absolute position of the substituted aluminium and balancing protons, especially at low concentrations. For this reason, MM techniques commonly rely on data gleaned from electronic structure calculations for development of their force-field parameters. This brings with it all of the inaccuracies associated with the particular electronic structure method but enables the evaluation of more complex systems. The lack of direct structure information also complicates validation as there is no experimental data with which validation can be compared to. In this case comparison must be made with a trusted theoretical method.

The major feature to compare in these calculations is the length of the OH bond length. The acidity of the proton is one of the most important features of the zeolite and this can be partially related to the bond strength (and hence length). Taking the *ab-initio* work of Teunissen et al[5] as the reference point, it can be seen that all methods are in reasonable agreement both MM and the PQM/MM methods giving similar results (within 0.01Å).

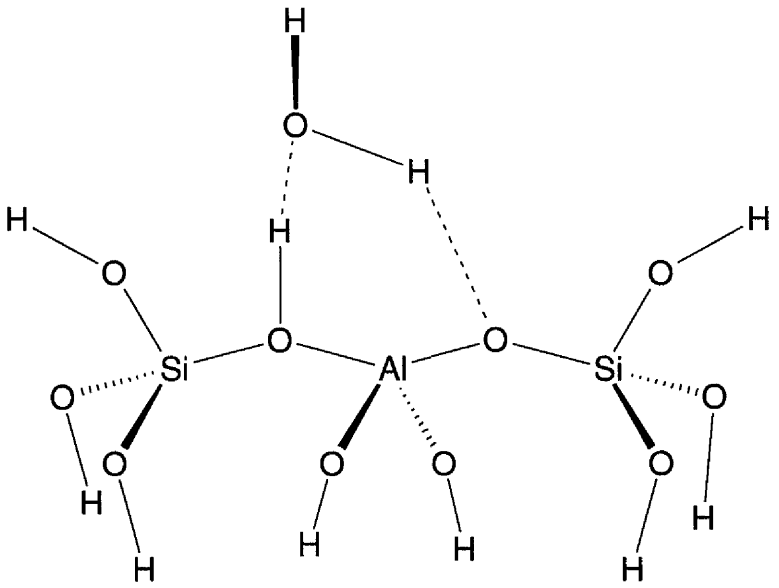

Figure 7.2: Water bound to Si-OH terminated T3(H) zeolite cluster

7.0.4 A PQM/MM study of water binding to H-chabazite

As discussed in section 1.3, it is common for molecular probes to be used to indirectly measure proton affinity. This way, direct comparison to experimental data can be used. Due to its extensive study and characterisation, the molecular probe water, was chosen

The point of note in this study is the gross errors that occur when the long range potential is neglected. In the case of the bare STO-3G calculation, the relative stabilities of the water and the hydroxonium ions are reversed compared to the other methods. The Periodic, STO-3G calculation is deemed to be the standard by which these other methods are to be compared to and all methods except the previously mentioned bare cluster calculation, reproduce the trends of the periodic method. The PQM/MM method improved on the Potential derived charge method by predicting energies that are closer to those of the periodic QM method. The only point of concern is that the energy difference between

	Binding energy kJ mol^{-1}	
	H_2O	H_3O^+
QM (STO-3G)[a]	-39.748	5.021
QM in a PDC field (HF/STO-3G//STO-3G)[b]	-57.739	-64.434
PQM/MM HF/6-31G[c]	-65.689	-71.965
Periodic/STO-3G[d]	-76.567	-90.374

Table 7.4: Binding energy of water to a zeolite cluster. *a*) Evaluation of T3 cluster as shown in figure 7.2 *b*) Results reproduced from Greatbanks et al.[4] *c*) PQM/MM calculation performed at the HF/6-31G* level of theory. MM region represented by th forcefield of Schröder et al[3] with water van der Waal potentials taken from the Amber force-field. *d*) Results reproduced from Greatbanks et al.[4]

the water bound to the zeolite and the hydroxonium ion bound to the zeolite, does not improve. in the periodic case, the difference is 13.8kJ mol^{-1} , this has dropped to 6.3kj in the PDC method. It would have been expected that the PQM/MM method would have found achieved similar energy difference to that of the periodic method but unfortunately this was found not to be the case. In fact the energy difference was found to be only 5.9kJ mol^{-1} .

7.0.5 Conclusion

From the test cases in this chapter, it can be seen that the PQM/MM method is a valuable tool in the modelling of zeolite structure and reactivity and provides an accurate alternative to cluster or point charge embedding methods. Even so, there are still results which require further verification and refinements of the code required.

Chapter 8

Additional Computational Methods for the Incorporation of Periodic Electrostatic Potential in Cluster Calculations

8.1 Introduction

Previous chapters have introduced and demonstrated methods for the inclusion of the infinite electrostatic potential into the calculation of crystal properties. One such method was that of Greatbanks et al[149] in which a cluster potential was subtracted from a periodic, *ab-initio* electrostatic potential and this new **difference potential** resolved to a set of point charges, used to embed the cluster in further calculations. This allows optimisations to be performed in the presence of a potential that represents the periodic environment.

Another such method for including an *extended* Madelung potential, more suited

to but not limited to solvent / surface interfaces, is the SCREEP (Surface Charge Representation of the Electrostatic Potential) method introduced by Stefanovich et al.[164]

8.2 Methodology

The SCREEP method provides a system where by the potential generated by an infinite (or very large) point charge lattice, can be represented by a finite set of point charges. This is done by resolving the effect of the potential of the periodic lattice onto a mesh surrounding a cluster under study (*cf.* Greatbanks et al. where the potential is resolved into a set of point charges located on a cubic grid surrounding the cluster). The mesh is generated by first choosing the cluster that is to be studied. Spheres are drawn around each of the cluster atom sites using a radius large enough to include the surrounding volume in which reaction chemistry may take place. The spheres interlock and an external surface is generated which is subsequently divided into segments called tesserae each of which contains a poin at which the potential is evaluated.

To do this the system is partitioned as follows.

Region I, the QM region is the region in which the studied chemistry of interest occurs *i.e.* bond breaking and/or forming, and is usually treated with a QM formalism. The cluster usually consists of several lattice ions from the first and second surface layer of ions and one or more solvent molecules. The size of the region, level of theory and basis set are as usual, dictated by the computational resources available.

Region II is known as the buffer region. It can consist of 10-100 crystal lattice ions and several solvent molecules which surround the QM region. This region describes the short range forces between the nuclei and electrons in the QM region

(I) and the surrounding ions. In highly ionic systems, the simplest representation of the buffer region is by point charges. On its own, this method proves not to be accurate due to the neglect of Pauli exclusion effects which give rise to unphysical charge delocalisation of the cluster wave function. It can be observed that charge leaks out from the QM cluster. This can be resolved with the strategic use of effective core pseudo-potentials (ECP) to describe the interaction of ions in the buffer zone (particularly cations) with the cluster electrons. These pseudo-potentials act as a cap to stop the QM charge density leaking out into the buffer zone.

Region III is the peripheral region containing the remaining point charges and possibly a dielectric continuum as an approximation to the Madelung and long range solvent polarisation potentials interacting with the QM cluster. In order to achieve an accuracy in the region of 1%, several hundred point charges are required in this region. For the purposes of this thesis, this region provides the potential due to the remaining, infinite, electrostatic potential.

Once the partitioning of the system has been performed, the SCREEP charges must be generated from the periodic potential. To do this, the following procedure is followed:

1. construct the SCREEP surface around the QM cluster
2. calculate Madelung potentials V_j on the surface
3. solve linear equations to obtain representative charges from the potential

Construction of the SCREEP surface

The SCREEP method can only provide a correct representation of the external potential *within* the generated surface. For this reason, a large enough volume must be chosen so that the cluster wavefunction is fully contained within the

surface and therefore influenced by the potential. The surface is controlled by R_a, the radius of the *atomic spheres* used to generate the surface. As a rule of thumb the larger the value of R_a, the more accurate the results. The surface (S) must subsequently be divided up into surface elements in a similar way to the panels of a football. The finer the surface elements, the more accurate the results but with a trade-off for computational expense.

The results can further be improved if the ions directly surrounding the cluster (and therefore the surface) are treated explicitly, their effect inside the cluster evaluated and the subtracted from the SCREEP potential. This is most simply achieved by use of a cutoff radius R_{cut} ($R_{cut} > R_a$). For example.

Calculation of the potentials on the surface mesh

Consider a region of space C, filled with an ideal grounded metallic conductor, and where charge density is zero and the electrostatics in the region are produced by a charge distribution $\rho(r)$ lying outside of region C. Gauss' Law of Electrostatics states that whatever the charge distribution $\rho(r)$ outside the boundary C, its resultant electrostatic potential $\nu_{el(r)}$ inside C can be replaced by a surface charge density $\theta(r)$ located on boundary S of the volume C. According to Gauss' Law, the presence of the ideal grounded metallic conductor within the volume C makes the electrostatic potential within the volume become zero and hence independent of the external potential $\nu_{el(r)}$.

The potential due to the charge density $\rho(r)$ on the surface S, exactly compensates for the external potential $\nu_{el(r)}$ for all points r on the surface S and all points within.

This relationship can be written as:

$$\nu_{el(r)} - \oint_s \frac{\rho(r\prime)}{|r - r\prime|} d^2r = 0 \tag{8.1}$$

Where r and $r\prime$ are points of evaluation on the surface S. This assumption only holds true for points within the boundary S and outside of the volume C, the electrostatic potential will not necessarily be reproduced correctly.

Linear equations

To simplify matters further, the surface S is divided into M smaller elements, S_j (known as tessera). The charge density can now be represented as a set of m point charges q_j, located at the centre of the tessera r_j by using the following approximation

$$q_{(j)} \approx \rho(r_j)S_j \tag{8.2}$$

This holds true when the surface S and the charge distribution $\rho(r)$ are sufficiently smooth and the number of surface points M is large enough so that the charge distribution does not vary greatly across the area of the tessera r_j. If this is true and the charge distribution is truly homogeneous, the charge at the point r_j is approximately equal to the charge density at that point multiplied by the area.

Equation 8.1 can now be simplified to the following matrix equation

$$\nu - \mathbf{A}q = 0 \tag{8.3}$$

where ν is a vector containing the external electrostatic potential at r_j and A is the MxM nonsingular matrix

$$\mathbf{A}_{ij} = \frac{1}{|r_j - r_i|} \text{ for } j \neq i \text{ and } \mathbf{A}_{jj} = 1.069(4\pi/S_j)^{1/2} \tag{8.4}$$

S_j is the surface area of the tessera, centred at point j

The non-diagonal elements A_{ij} represent a generic Coulomb interaction between elements r_i and r_j. The diagonal elements A_{ij} describe the self interaction of r_j. The coefficient 1.07 is a parameter fitted by Klamt et al.[165] Further details about the parameter and its fitting procedures may be found within that reference and references therein.

The linear equations can now be solved to give the vector of the surface charges by utilising the matrix inversion method.

$$q = \mathbf{A}^{-1}\nu \tag{8.5}$$

The ability to simplify the calculation from one of a charge distribution $\rho(r)$ to a charge density on a closed finite surface is advantageous as the calculation has been changed from one of a large (possibly infinite) number of ions to one of a cluster with a relatively small number of point charges on a surface.

8.3 Implementation

The SCREEP method was implemented as a subset of the MUPPET program and as such, utilises many of the same pieces of code. It was constructed as a link to Gaussian and uses the QMEwald code to generate the potential due to the periodic environment. The steps involve in running a SCREEP calculation follow the method in Section 8.2.

1. A surface is generated around the QM cluster and any reacting or solvent molecules deemed to play a part in the reaction.

2. The Madelung potential V_j due to the periodic electrostatics is calculated at the centre of each tessera on the SCREEP surface.

3. The potentials are corrected to remove the effect of any point charges that have been specified explicitly.

4. Linear equations are solved to obtain representative charges from the potential

5. QM calculation is performed in the presence of the SCREEP charges

8.3.1 Validation of the SCREEP potential

The NaCl system was chosen due to the fact that it is experimentally, a well characterised system and a relatively simple system to study computationally. A 3x3 slab of NaCl excised from the 001 surface, centred on an Na^+ ion was chosen as the test system. A SCREEP surface was generated around the 9 ions in the slab and a fictitious layer that would have sat above that layer in bulk NaCl, this allowed enough space for ions such as Na^+ and Cl^- or small molecules such as water to bind to the NaCl slab. The surface was generated using a van der Waals surface from interlocking spheres of fixed radius R_a using the GEPOL93 algorithm.[166]

Before committing computational expense to the optimisation of ions or small molecules such as water on the NaCl surface, it is prudent to confirm that the SCREEP charges correctly reproduce the periodic electrostatic potential. This was done by evaluating the potential at chosen points above the central Na^+ion (figure 8.1) and comparing the results to other methods.

The SCREEP charges were generated on a 720 point mesh surrounding the 3x3 NaCl cluster and an additional 3x3 'layer' that would have existed above the cut surface. In order to confirm that the SCREEP charges were correctly contributing to the potential correction, for this evaluation only, the SCREEP calculation was performed without the use of explicit charges. The Ewald potential evaluation was performed at the B3LYP/3-21G level using the QMEwald module for

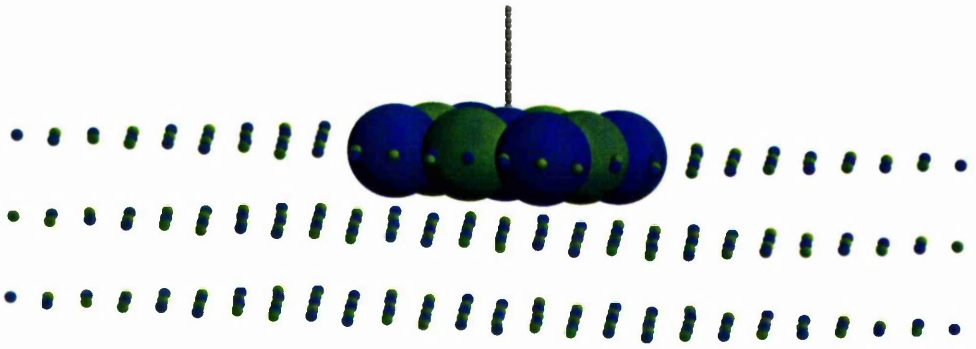

Figure 8.1: 21 points above the central Na of the 3x3 NaCl cluster at which the potential was evaluated.

Gaussian94 and the potential due to the periodic environment evaluated at the 720 grid points. The generated charges were included in a QM potential evaluation at 21 points from 1Å to 5Å above the central Na^+ ion of the cluster using Gaussian94.[121]

The SCREEP potentials were directly compared to the potentials due to a bare 3x3 NaCl cluster and to the NaCl cluster embedded in the periodic electrostatic (Ewald) environment.

From this graph, it can clearly be seen that the bare cluster underestimates the electrostatic potential substantially. This is understandable due to the lack of surrounding electrostatic environment. The SCREEP potential is in much better agreement with the Ewald potential although it slightly overestimates the electrostatic potential in the regions between point four and eight. The reason for this slight disagreement with the expected results is due to the placement of the SCREEP surface. positions one to four correspond to distances between 1.0Å and 1.8Å from the central Na^+ ion centre. At these short distances, the potential is largely defined by the local structure and the potential will be dominated by that of the cluster. At greater distances from the cluster, the influence of the cluster subsides and the effect of the long range electrostatics begins to play a

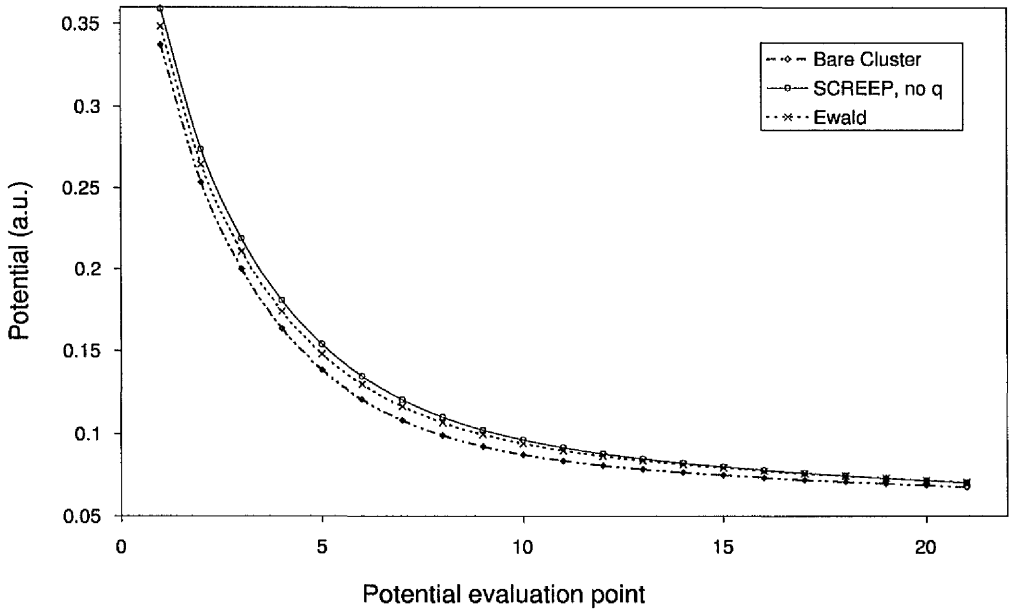

Figure 8.2: Graph of potential due to the SCREEP method and selected comparison methods, evaluated at 21 points above the central Na^+ of the 3x3 NaCl cluster.

greater part in the overall potential. The region on the potential plot with the greatest deviation from the 'exact' Ewald values lies between points four and eight. This region of the evaluation is the furthest away from the surface on which the SCREEP charges are located and hence is the region in which the SCREEP method finds it most difficult to reproduce the exact potential. At points nine and above, the potential converges to almost exactly the same values as in the Ewald evaluation.

8.4 Water binding to an NaCl surface

Once the SCREEP potential above the NaCl surface had been proven to reproduce the Ewald values effectively, the method was used to evaluate the binding energy of water to the NaCl surface. Calculations were performed using a similar method and level of theory to that used by Stefanovich et al..[164] The NaCl surface was described by Hay-Wadt effective core pseudo-potentials (ECP) and a valence double-zeta basis set.[167] The water oxygen atom was described by the SBK ECP with the CEP-31+G* basis set.[168] The 311+G** basis was used for the oxygen hydrogens. In the study by Stefanovich et al.,[164] basis functionless frozen core Hay-Wadt ECPs were used for Na^+ in a buffer region surrounding the study cluster. The aim of this was to cap the electron density of the QM cluster and prevent it from 'leaking' out into the surrounding environment.

The quantum mechanical 3x3 NaCl cluster ($5Na^+4Cl^-$) was surrounded by 720 SCREEP charges as described earlier in the chapter and shown in figure 8.3. To increase the accuracy of the method 131 explicit point charges were included in the evaluation and their effect removed from the SCREEP potential contribution.

The SCREEP evaluation with explicit charges closely mimics both the energy an the geometry of the Ewald method. The distance of the water oxygen from the NaCl surface is reproduced with an accuracy of 0.0001Å and the water OH bond

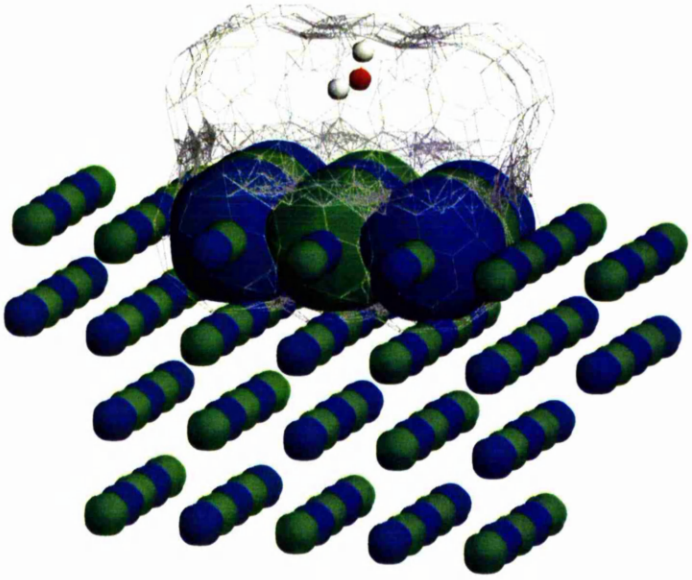

Figure 8.3: 3x3 NaCl cluster surrounded by a 131 point charges (blue = Na = +1, green = Cl = -1). Included in the diagram is the screep mesh of 720 points at which the periodic potential is evaluated.

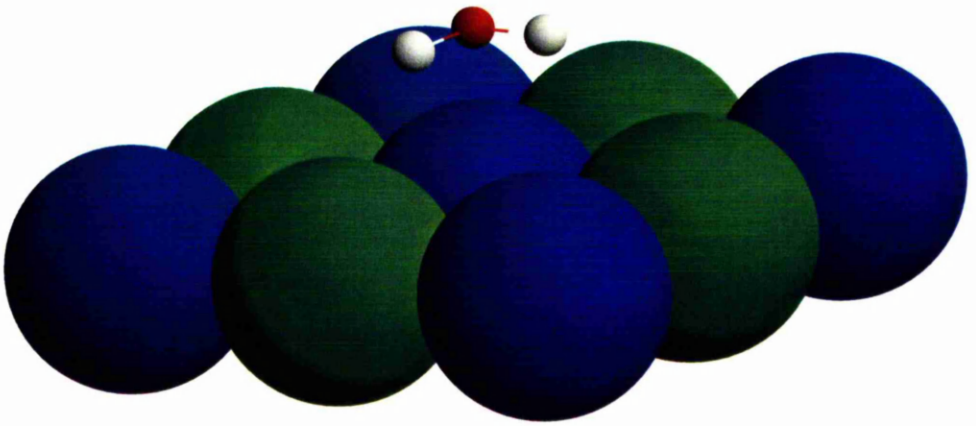

Figure 8.4: Water bound to the NaCl surface

	Bare cluster	8x8x4	SCREEP 131 exp q	Ewald
Water adsorption				
O_z	2.4157Å	2.4338Å	2.4432Å	2.4431Å
$O_x = O_y$	0.4932Å	0.4020Å	0.4812Å	0.4814Å
OH	0.9496Å	0.9527Å	0.9512Å	0.9512Å
HOH angle	106.42°	106.22°	105.94°	105.88°
Adsorption energy (kcal mol^{-1})	-6.9887	-7.4684	-7.3640	-7.3301

Table 8.1: Comparison of geometries and adsorption energies of water binding to a NaCl (001) surface

lengths are exact within the given numerical accuracy. The water HOH angle shows the greatest deviation, even so this is still only 0.0600° and has negligible effect on the overall energy as this is still within 0.035kcal mol^{-1} of the exact Ewald value.

The true value of this method is shown on comparison of the SCREEP values with the bare cluster and the 8x8x4 point charge embedded values. The bare cluster underestimates the NaCl surface/water separation by almost 0.03Å, this is reduced by 0.02Å by embedding of the cluster in point charges, but still disagrees with the Ewald method by almost 0.01Å, compared with the SCREEP method. The adsorption energies also prove to be in disagreement with the Ewald method, in fact, this is where the bare cluster method has its greatest failing. The energy of adsorption of the water onto the NaCl surface is almost 0.35kcal mol^{-1} higher than that of the Ewald method, a significant deviation from the exact value. Addition of the point charges overestimates the energy but reduces the deviation to 0.14kcal mol^{-1} again a significant improvement on the bare cluster values but still a long way from the accuracy shown by the SCREEP method. When it is considered that the point charge embedding method and the SCREEP method are comparable in computational expense, this further exemplifies the value of the SCREEP method.

8.5 Conclusion

The bare cluster method has been proven to follow basic geometric and energetic trends but disagrees with the absolute values when compared with the exact Ewald method. Addition of point charges to the evaluation goes a long way to resolve the deficiency in the method and shows that clusters embedded in finite arrays of point charges are a valid starting point for computational studies. The SCREEP method allows accuracy approaching that of the Ewald method, for

little extra expense. The only extra cost incurred in this method is the initial generation of the SCREEP charges which requires an Ewald potential evaluation. Subsequent evaluations such as optimisations of molecules within the SCREEP boundary require nothing more than the evaluation of the cluster and chosen molecule in a field of point charges. Although this is the methods strongest point, it is also the source of its greatest failing. The drawback with this method is that on addition of a molecule to the system, a normal QM system would respond by polarising the molecule and the molecule would polarise the QM system. With the SCREEP method, the molecule is polarised by the SCREEP charges and the QM cluster is polarised by the molecule. The only effect missing is the response of the SCREEP charges to the molecule which in a real system corresponds to the molecules effect on all atoms outside of the explicit cluster. One way of resolving this would be to generate new SCREEP charges on each optimisation cycle. This would require an Ewald evaluation per cycle and hence would negate and advantage over the Ewald method. This said, the effect of neglecting this contribution is small and can be further minimised by choice of a quantum mechanical region which fully encompasses the adsorbate and the use of a buffer region containing explicit point charges. The method has proved to be a suitable choice for the modelling of zeolite systems and has been used in several studies on the adsorption of NH_3 on Chabazite,[169] Methane on zeolite H-Y,[170] and carbon monoxide on H and Li forms of FAU[171] and ZSM-5.[172]

chapterAdsorption of carbon monoxide on zeolite clusters

8.6 Introduction

Acid catalysed reactions using protonated zeolites are driven by the nature of the bridging hydroxyls [≡Si(OH)Al≡] which generate the Brønsted acidity. As was discussed in Section 1.2.2, directly defining the nature of a zeolite acid site is a difficult procedure due to the fact that the position of the proton cannot be accurately obtained and that protons may be unevenly distributed throughout the zeolite. For this reason, it is often more advantageous to use a molecular probe and indirectly measure the Brønsted acidity from the effect on the environment has on the probe and the probe has on the bridging hydroxyl. Carbon monoxide is one of the most widely used molecular probes for FTIR spectroscopy in surface chemistry and as such, it is often applied in to the study of zeolites .[173,174,34] It is used in preference to other available probes due to the sensitivity of its stretching mode to the acid centres in the zeolite.[175,176]

Even so, a recent study by Otero Areán et al[174] stressed the lack of research into the interaction of CO with zeolites, in particular, the interaction of the probe molecule with cations, hydroxyl groups and the active centres present within the zeolite channels and cavities. Their work focused on the effect of interacting the CO probe with alkali-metal cations present in the Na-ZSM-5 zeolite leading to $Na^{+}\cdots CO$ adducts.

Previous theoretical studies have shown that either end of the carbon monoxide molecule can act as the nucleophile. Simple models of the Brønsted acid sites have shown that although interaction via the carbon is preferential, the interaction via the oxygen is significant and cannot be ignored .[177]

A question that has been largely ignored in this type of work is the possibility of

the carbon monoxide oxygen interacting with a basic zeolite framework oxygen and the carbon interacting with an acid site. This "double-point" adsorption would be geometrically possible and in small pore zeolites (pore diameters < 10Å), interactions could even take place between two Brønsted sites (from a steric point of view).

An investigation on this subject was undertaken, in collaboration with co-workers at UMIST,[178] to ascertain the effect of binding the CO probe to a zeolite framework by both the C and the O and also the effect of binding both simultaneously, via the so called *double point adsorption.*

Due to the fact that this area of zeolite chemistry had previously been neglected, a study was undertaken to compare the effects on the energy and the CO and zeolite proton harmonic stretching frequency shifts when interacting a carbon monoxide probe with:

- A single zeolite Brønsted acid site via the carbon.
- A single zeolite Brønsted acid site via the oxygen.
- A zeolite Brønsted acid and a basic site (in both orientations).
- Two zeolite Brønsted acid sites.

A great deal of work has been undertaken to evaluate the effect of varying levels of theory, basis set, zeolite geometry,[179] cluster size,[144,180,181] on the protonation energies , vibrational frequencies and adsorption energies of adsorbates interacting with the zeolite framework. As the author was unaware of such a study relating to CO interacting with a zeolite cluster, this was investigated prior to performing a full set of calculations in order to determine the most efficient method for undertaking subsequent work.

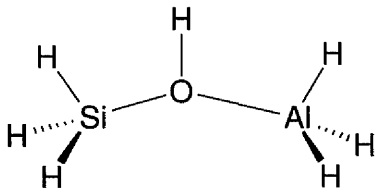

Figure 8.5: Model 1 in table 8.2, $H_3Si(OH)AlH_3$

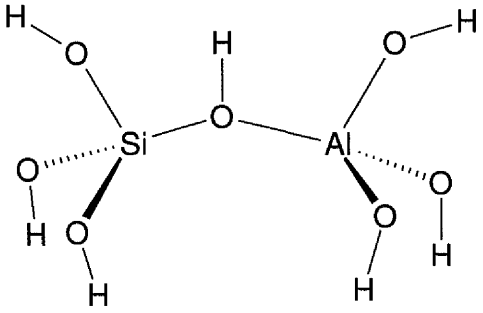

Figure 8.6: Model 2 in table 8.2, $(HO)_3Si(OH)Al(OH)_3$

8.7 Preliminary study

8.7.1 Results

An initial study was made into the effect of computational method, basis set and cluster size and composition on the interaction energy and vibrational frequency. Small clusters containing 2-3 T-sites terminated with hydrogens and hydroxyls were evaluated at varying levels of theory to provide information on the most appropriate method for evaluation of such systems.

All calculations were performed using the Gaussian94 suite of programs.[121]

The interaction energies between the carbon monoxide and the small clusters (table 8.2) were calculated using Hartree-Fock methods and a range of basis sets.

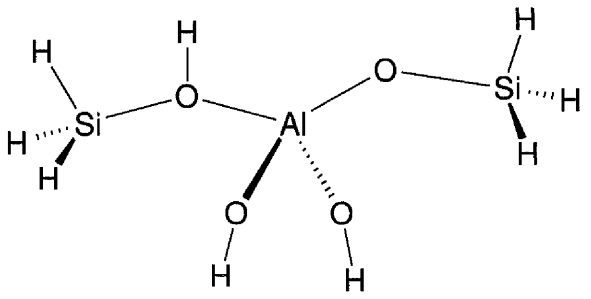

Figure 8.7: Model 3 in table 8.2, $H_3SiOAl(OH)_2(OH)SiH_3$

	Interaction energy[a]/kJ mol^{-1}		Frequencies and shifts[b] on complexing with CO/cm^{-1}			
Model cluster	HF	MP2	ν_{OH}	$\Delta\nu_{OH}$	ν_{CO}	$\Delta\nu_{CO}$
$H_3Si(OH)AlH_3$	14.68	23.79	4016	-74	2474	+35
$(HO)_3Si(OH)Al(OH)_3$	16.07	25.13	3982	-96	2470	+31
$H_3SiOAl(OH)_2(OH)SiH_3$	14.23	25.13	3992	-72	2473	+34

[a]Uncorrected for BSSE. Calculated at the HF/6-31G* level.

Table 8.2: Interaction of carbon monoxide with bridged hydroxyls (C_s symmetry, 6-31G* basis set)

	Interaction energy[a]/kJ mol^{-1}			Frequencies and shifts[b] on complexing with CO/cm^{-1}				
Basis set	HF	BSSE	MP2	ν_{OH}	$\Delta\nu_{OH}$	ν_{CO}	$\Delta\nu_{CO}$	$\nu^c_{CO(gas)}$
6-31G*	14.69	5.10	23.79	4016	-74	2474	+35	2439
D-95**	13.39	-	21.82	4080	-91	2459	+35	2424
6-311G**	10.40	-	18.54	4073	-75	2468	+28	2440
6-311 + G**	9.61	-	17.51	4068	-77	2461	+29	2432
6-311 ++ G**	9.58	-	17.62	4066	-78	2461	+29	2432

Table 8.3: Interaction of carbon monoxide with bridged hydroxyls in structures containing two tetrahedra $H_3Si(OH)AlH_3$, (C_s symmetry)

Electron correlation was approximated with the MP2 method. CO frequency shifts were calculated by comparing the vibrational mode with greatest stretching character in the complex with that of the optimised CO at the HF/6-31G* level. OH frequency shifts were again calculated by comparing complexed and free zeolite clusters at the HF/6-31G* level. Hartree-Fock interaction energies were corrected for basis set superposition error (BSSE) using the method of Boys and Bernardi[182] using the following equation.

$$\begin{aligned} BSSE &= \{E_{dimer\ A,\ no\ ghost\ B} + E_{dimer\ B,\ no\ ghost\ A}\} \\ &- \{E_{dimer\ A,\ ghost\ B} - E_{dimer\ B,\ ghost\ A}\} \end{aligned} \tag{8.6}$$

Where A and B are the infinitely separated zeolite clusters and carbon dioxide molecules and $E_{dimer\ A,\ no\ ghost\ B}$ refers to the energy of the zeolite cluster at the complex geometry without ghost functions on the carbon monoxide molecule (B). $E_{dimer\ B,\ no\ ghost\ A}$ is defined similarly for the carbon monoxide. $E_{dimer\ A,\ ghost\ B}$ refers to the energy of the zeolite cluster at the complex geometry with ghost functions in the position of the carbon monoxide molecule (B). A ghost function is the basis function that would have been found on an atomic centre but without the atom it would have been centred on. The purpose of these functions is to allow the polarisation of the electrons in one of the molecules into the basis functions of the other. $E_{dimer\ B,\ ghost\ A}$ is defined similarly for the carbon monoxide.

By the way BSSE is defined, BSSE is positive and as such, results in a reduction in the interaction energy.

8.7.2 Discussion

From the results in table 8.2, it can be seen that the interaction energy is highly sensitive to the cluster size and the termination, rendering small cluster calculations unreliable. Even with these preliminary calculations, the interaction energy exhibits the properties of an energy, oscillating about the true periodic energy with increasing cluster size as discussed in Chapter 4. The interaction energy also proves to be sensitive to the quality of the basis set used but up until a limit. The interaction energy decreases when increasing the quality of the basis set up until the 6-311G** basis, after which, increasing of the quality of the basis set has little effect relative to the increase in computational cost.

The shifts in the C-O stretching frequency (ν_{CO}), on complexing *via* the the C atom, are all positive (blue shifted) which corresponds to a shortening, and hence a strengthening of the C-O bond. Shifts in the hydroxyl stretch (ν_{OH}) are all negative (red shifted) corresponding to an increase in the bond length, and hence a weakening of the bond strength. The results in tables 8.2 and 8.3 show that change in vibrational frequencies on complexing the CO with the zeolite cluster, $\Delta\nu_{CO}$ and $\Delta\nu_{OH}$ are relatively invariant with increasing cluster size and basis set despite the absolute values for ν_{CO} and ν_{OH} being over-estimated by all basis sets (as is true of all HF calculations). On comparison with experimental results, the calculated absolute values of the stretching frequencies prove to be over-estimated by $14-16\%$ for ν_{CO} and $10-36\%$ for ν_{OH}. These errors are not propagated into the frequency shift on complexing ($\Delta\nu$) as they are subtracted and effectively cancel each other out. On comparison of the values for the CO blue frequency *shifts* with typical experimental results,[183–185] it can be seen that the values are reproduced with good accuracy with all basis sets tested (Experimental ν_{CO} = 27-32 cm^{-1}, Theoretical ν_{CO} = 29-35 cm^{-1}). However, red shifts for the hydroxyl stretch ν_{OH} are 25% of the experimentally observed values[186,183,34] for all

basis sets. Using the 6-31G* basis set, ν_{OH} is particularly poorly predicted and, in fact, gives results that are typically 300 cm^{-1} further from the experimental values than the smaller 3-21G basis set.[179]

8.7.3 Conclusion

The main focus of interest in this study was to be the change in frequencies of the CO and the zeolite OH bond stretch and the interaction energy of the probe with the zeolite.

In table 8.3, the BSSE energy at HF/6-31G* level was large in comparison to the interaction energy being calculated although for larger basis sets, it is expected that this value will decrease rapidly to the point where at the HF/6-311++G** level, it would become negligible. On comparison of the interaction energy at HF/6-31G*, corrected for BSSE with the energy at HF/6-311++G** the values are almost exactly the same ($E_{(HF/6-31G^*)} = 9.59$, $E_{(HF/6-311++G^{**})} = 9.58$). For this reason the 6-31G* basis set, with corrections made for BSSE, would seem to be a valid basis set for prediction of interaction energies. This basis also provided accurate values for the C-O stretch frequencies (ν_{OH}), on comparison with experimental results. The only area in this study in which this basis set proved to be flawed was in prediction of the O-H stretching frequency (ν_{OH}). As ν_{OH} was found to be closer to the experimental value at the lower 3-21G level, it was decided that this frequency would be evaluated in all cases at the lower level of theory in an attempt to reproduce more closely, the experimental results. This way, the choice of calculation method was based on the most appropriate method to give the best result for interaction energy and frequencies whilst maintaining computational efficiency.

8.8 Study of double point adsorption of CO on zeolite clusters

The results of the preliminary study were extrapolated and used in the subsequent study of the larger systems. The computational expense consumed by the preliminary study was easily recovered from the savings made from the calculations in this section. Larger, 5 tetrahedra clusters were used for the subsequent calculations, all optimisations being performed at the HF/6-31G* level of theory. Further energy evaluations using higher levels of theory such as MP2, B-LYP and B3-LYP were performed at the HF/6-31G* geometry in order to account for electron correlation. Frequencies were calculated at the HF/6-31G* level for C-O stretch and HF/3-21G for O-H stretch for reasons discussed in Section 8.7.2.

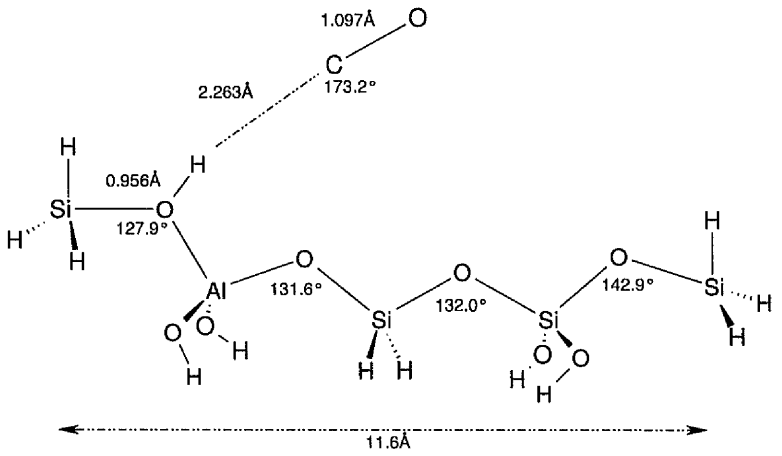

Figure 8.8: Single point interaction of CO (*via* carbon) with 5 'T' atom units (one Al atom). Distance of the terminal Si atoms fixed at 11.6Å (6-31G*/C_s).

8.8.1 Results

For the larger cluster shown in Figures 8.8- 8.12, optimisations and vibrational frequency calculations were performed at the HF/3-21G and HF/6-31G*.

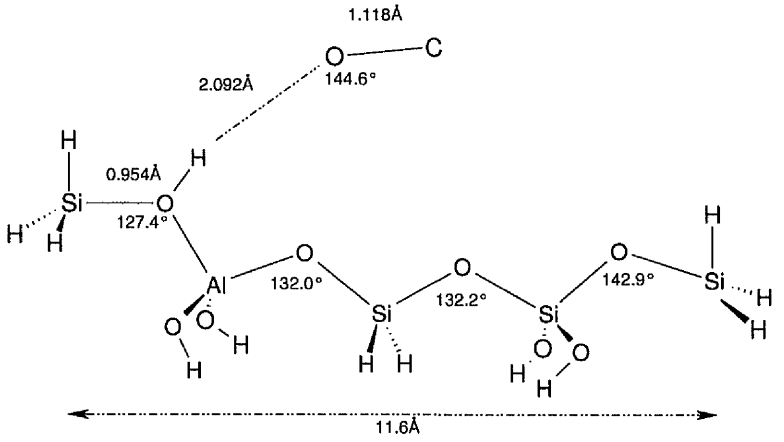

Figure 8.9: Single point interaction of CO (*via* oxygen) with 5 'T' atom units (one Al atom). Distance of the terminal Si atoms fixed at 11.6Å (6-31G*/C_s).

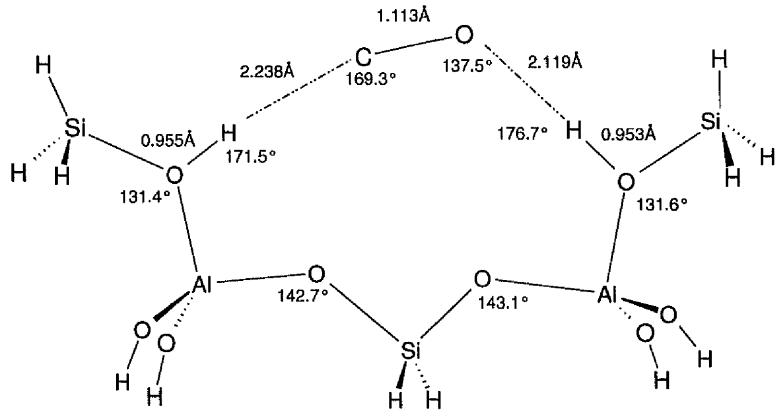

Figure 8.10: Double point interaction of CO (*via* oxygen) with 5 'T' atom units (two Al atoms). (Fully optimised at 6-31G*/C_s) Distance between acidic protons 4.98Å.

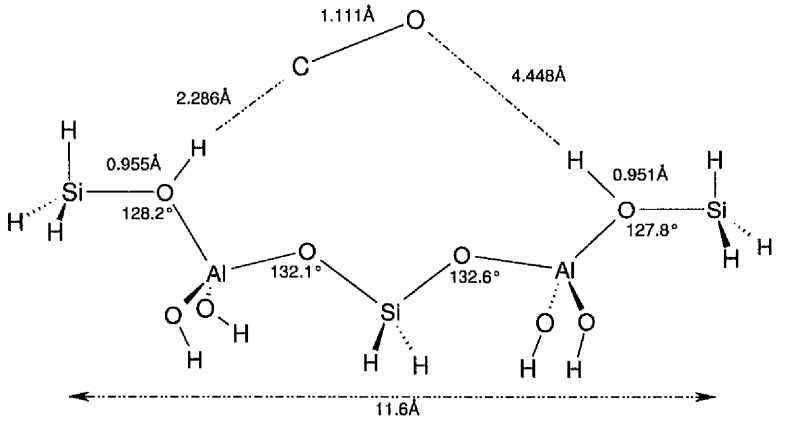

Figure 8.11: Single point interaction of CO (*via* carbon) with 5 'T' atom units (two Al atoms). Distance of the terminal Si atoms fixed at 11.6Å (6-31G*/C_s). Distance between acidic protons 7Å.

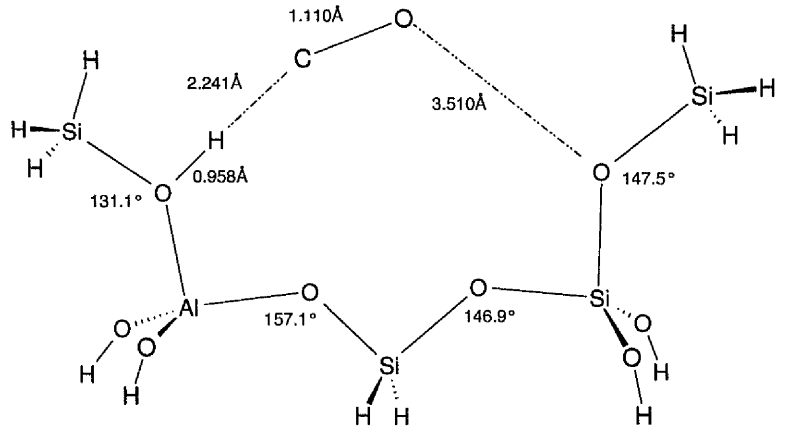

Figure 8.12: Interaction of CO (*via* carbon) with 5 'T' atom units (one Al atom), (Fully optimised at 6-31G*/C_s).

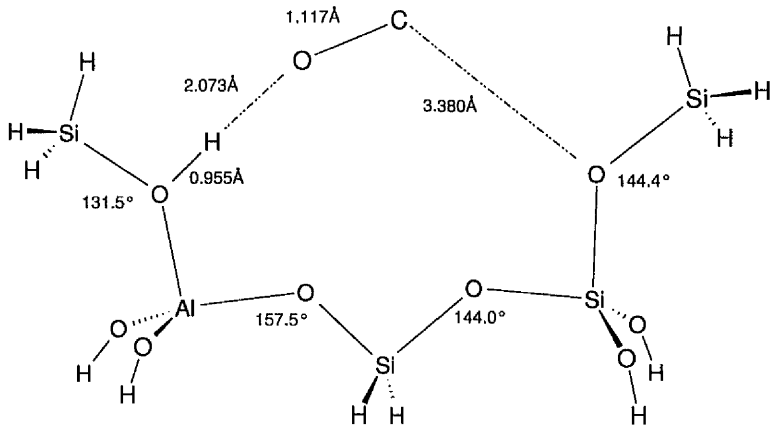

Figure 8.13: Interaction of CO (*via* oxygen) with 5 'T' atom units (one Al atom), (Fully optimised at 6-31G*/C_s).

			Interaction energies[a]/kJ mol^{-1} at the HF/6-31* geometry					Frequency shifts/cm^{-1}	
	'T' atom	CO linkage	HF	(BSSE)	MP2	B-LYP	B3-LYP	$\Delta\nu_{CO}$ 6-31G*	$\Delta\nu_{OH}$ 3-21G
1[b]	4Si,1Al	'C'(1)	18.5	11.3	31.9	30.8	31.0	+36	-136
2[b]	4Si,1Al	'O'(1)	16.3	10.4	17.9	14.9	17.9	-39	-130
3[c]	3Si,2Al	'C' and 'O'(2)	25.0	14.5	37.6	32.0	34.9	+ 4	-97
4[b]	3Si,2Al	'C'(1)	19.5	11.7	31.7	30.0	31.7	+27	-135
5[c]	4Si,1Al	'C'(2)	17.2	8.6	33.8	28.6	28.4	+39	-
6[c]	4Si,1Al	'O'(2)	15.1	8.3	20.7	15.6	17.3	-29	-

[a]Models 1-6 correspond to Fig. 1-6. [b] Terminal Si...Si distance fixed at 11.6Å.
[c]Terminal Si...Si optimised at 6-31G* basis.
[d]Linkage: single point (1), double point (2).
[e]BSSE calculated at the HF/6-31G* level.
[f]Shift in ν_{OH} for second hydroxyl linked *via* oxygen.

Table 8.4: Interaction of carbon monoxide with bridged hydroxyl (C_s symmetry, 6-31G* basis set)

8.8.2 Discussion

The first point to note from these calculations is the asymmetry that arises on optimisation of the cluster and the CO. On optimisation, the linear carbon monoxide - hydroxyl linkage (Z-O-H·····C-O) breaks symmetry. This is attributed to the asymmetry of the surrounding electrostatic environment of the extended zeolite cluster.

For clusters in table 8.4 which contain a single aluminium ion, and hence acidic proton (clusters 1,2,5 and 6) results are similar to those in table 8.2 and 8.3, the results of the smaller systems. In all cases, the energy of complexing *via* the carbon is greater than when complexing *via* the oxygen, in addition, the shifts observed on complexing *via* the carbon are positive whilst the shifts on complexing *via* the oxygen are negative. For all clusters, the energies of interaction at HF/6-31G* are consistently lower than when calculated at the higher levels of theory (MP2, B-LYP, B3-LYP). The higher levels of theory, B-LYP and B3-LYP give results that are comparable to MP2 values.

Comparison of Models 1 and 4 shows the effect of substitution of a second aluminium into the cluster. The substitution has a small effect on the energy (+1 kJ mol^{-1} at the HF/6-31G* level) and the O-H frequency (-7 cm^{-1} at the HF/6-31G* level). The Al substitution has the least effect on the C-O frequency which varies by only 1 cm^{-1} at the HF/3-21G* level.

8.8.3 Conclusion

The sorption of carbon monoxide onto zeolite acids is a well researched subject.[186,183,34,179] Even so, the complex infrared spectra for zeolites associated with carbon monoxide have proven to be difficult to characterise and uncertainty has arisen about the origin of several of the bands. This work has failed to identify

the experimentally observed 2106cm^{-1} and 2124cm^{-1} bands seen in steamed mordenite. It is clear that this work would benefit from study using the PQM/MM method as ν_{CO} shifts for CO in zeolites have been shown to be greatly influenced by local electrostatic fields[187] and this may help elucidate the remaining unidentified spectral bands.

Chapter 9

Conclusion

As was shown in chapter 1, the study of zeolite chemistry is one of both scientific and economic importance. The lack of understanding of the chemical processes that take place within the zeolite pores during catalytic reactions, such as cracking and the MTG process, makes these systems ideal candidates for study with computational techniques. Due to the failings of some of the computational techniques described in chapter 2, it soon became clear that a novel method was required for accurate modelling of these systems.

9.1 Summary of work

On reviewing the existing methods for modelling of periodic systems, it became clear that the one method that was not available was a periodic implementation of the QM/MM methodology, a non-periodic version of which had previously been created within the group (section 2.4). It was felt that such an implementation would be of scientific benefit due to the enhanced accuracy whilst retaining computational efficiency. This method was implemented using the Ewald methodology for the evaluation of periodic electrostatics, and although was written to

interface with the Gaussian suite of programs, was written with the objective of being independent to both the QM and MM codes utilised. In order to verify the accuracy and efficiency of the code, other methods for performing hybrid calculations were also implemented, such as the Sauer et al. mechanical embedding method QMPot (section 4.5.2) and the SCREEP potential method of Truong et al. (chapter 8).

In a study of NaCl, it was found that the PQM/MM method accurately modelled the geometric properties of the bulk crystal, even with a limited number of explicit QM ions. These results were a large improvement on the bare cluster results, and the embedding of the cluster in point charges. In this case, the PQM-MM method in which the QM cluster feels the force due to a set of periodic classical charges, also performed well. More central to the thesis was the next study of the geometric properties of chabasite. The PQM/MM method once again reproduced experimental results well, although with some minor discrepancies attributed to the presence of termination atoms and too small a cluster under study.

Overall, the PQM/MM implementation and the full MUPPET code was successful in achieving this thesis objective which was to create a novel code capable of accurately modelling zeolite chemistry.

9.2 Future work

There are many opportunities in which to expand the capabilities of the code. The thesis of Hindle,[111] presents a method for the replacement of termination hydrogens with a frozen localised orbital. This would allow the truncation of a zeolite cluster without the use of the perturbing hydrogen termination atoms. The truncation of covalent bonds has been shown to give rise to perturbations of the local environment. Their presence close to the charges of MM environment gives rise to such large interactions that the charges have to be arbitrarily scaled.

Replacing these termination atoms with a frozen localised MO would remove (or greatly reduce) this interaction and remove the need for arbitrary charge scaling.

The MUPPET code was written with the aim of being portable to other MM and QM packages. The GULP code which was utilised in this work is a 3-dimensional molecular mechanics package, lending itself to the study of zeolites. Another important area in solid-state chemistry is surface modelling. The MM code MARVIN is one of the most popular 2-dimensional surface analysis packages and it would be a relatively trivial task to interface it into the MUPPET code.

As has been shown, the MUPPET code is a valuable tool in determining the structure of zeolite systems. Further calculations are required to completely validate the code, an ideal candidate being the CO work presented in chapter 8.5 which was only performed using standard QM methods due to time restrictions. Once this validation has been completed, further areas of interest would be the area of chiral modification of zeolites discussed in chapter 3. This intriguing area of zeolite chemistry, was shown to be poorly described by finite QM methods due to the high dependence on the periodic electrostatic environment, making it an ideal case for treatment with the PQM/MM methodology.

Appendix A

Gaussian94 Overlays

Overlay 0: Is concerned with program control. It includes the root segment on machines with classical overlaying. On UNIX machines it includes a start-up link (Link 0). Link 0 performs the machine-dependent actions required to start the program. This overlay also includes Link 1, which reads the job type input section, forms the detailed route, and sets up files and some general tables. The source for Link 1 is divided into machine-dependent and independent sections.

Overlay 1: Reads geometry input sections and controls manipulation of nuclear coordinates and numerical differentiation, including optimization procedures, numerical frequency and polarizability computations, linear synchronous transit, reaction path following, and numerical SCRF.

Overlay 2: Computes Cartesian coordinates of the nuclei, derives symmetry related information and brings the molecule to a standard orientation for optimal use of symmetry.

Overlay 3: Sets up the basis set and evaluates one-electron integrals (and $2e^-$ integrals for conventional SCF).

Overlay 4: Performs semi-empirical calculations, both as independent methods and in order to generate the initial guess to the SCF wave function, and generates data for the CI phase of MCSCF.

Overlay 5: Determines the SCF wave function.

Overlay 6: Does analysis and output of the SCF wave function and computes electron density and electrostatic properties.

Overlay 7: Evaluates integral first and second derivatives with respect to nuclear coordinates and uses their contributions to evaluate forces and second derivatives. Link 716 converts Cartesian forces and force constants to internal coordinates and computes harmonic vibrational frequencies and normal modes from the force constants. It also transforms all derivative information from the symmetry orientation back to the input orientation.

Overlay 8: Transforms the two-electron integrals and internal derivatives to the basis of molecular orbitals, after setting up the window (frozen-core) information.

Overlay 9: Calculates the correlation energy either by perturbation theory or by configuration interaction. It also checks the stability of the Hartree-Fock determinant and produces a new guess for a wave function with fewer constraints and can also perform CIS calculations of electronic excited states and propagator calculations.

Overlay 10: Forms the derivatives of the Hartree-Fock and Kohn-Sham density matrices with respect to perturbations (electric field, nuclear coordinates), and computes the density derivative term in the post-SCF contribution to MP2, CI, and QCI gradients and dipole moments, which is also used to produce correlated density matrices. Also performs coupled perturbed CI-Singles to produce CIS analytic frequencies.

Overlay 11: Forms the one and two-electron integral derivative contributions

to the Fock matrix derivatives with respect to nuclear coordinates in a form suitable for solution of the CPHF problem, as well as the integral derivative contribution to the dipole derivatives. In CI and QCI gradient evaluations, it forms the correlation contribution to the two-particle density matrix. In CI and QCI gradient evaluations it back transforms the two-particle density matrix to the AO basis and contracts it with the integral derivatives. It also forms most of the terms in MP2 second derivatives.

Overlay 99: Is a termination overlay. It produces a summary of the results of the calculation for archiving and reformats arrays for input to other programs.

Appendix B

Code Optimisation

The use of the QMEwald code allowed us to calculate the effect of a periodic classical electrostatic potential, interacting with a set of QM basis functions. This is not implemented in standard codes such as Gaussian94 and was developed in part at the University of Manchester. Being an 'in development code' it could be expected that bugs and inefficiencies would be found in the code and initial use of the code proved this to be the case. Calculations on small systems (2 ions) embedded in a high symmetry system took a small amount of time but on larger systems, 20 ions, a few hundred basis functions and a large unit cell (700 charges) took an excessive amount of time.

A subsequent profiling study of the code was undertaken with timing routines added to the standard code to allow the elucidation of programming bottlenecks. The results of this study are shown in figure B.1.

From the information depicted in figure B.1, it can be seen that for link 307, the integral code, 92% of the total time spent in the link was spent in the subroutine rec3d.f. Furthermore, it was found that most of the time was spent in the function call cosdp.f a simple routine containing a few lines of logic and a *cosine* call. Although this seemed innocuous, cosdp was embedded in a loop over the basis

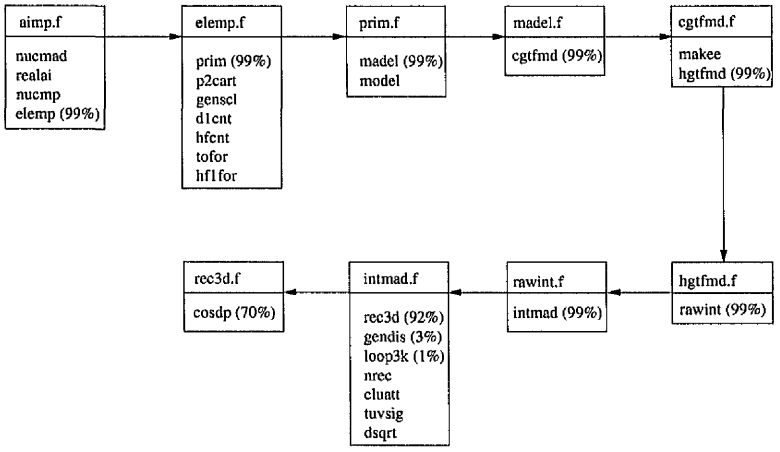

Figure B.1: Sub-routine timing trace of QMEwald code

functions, the number of k vectors in the reciprocal summation and the number of ions in the unit cell. When multiplied together it was found that this routine in certain circumstances could be called over 200,000 . If for example we were studying a system containing 8 unit cell ions, 1000 k-vectors in the reciprocal summation and 100 basis functions in the QM cluster this would cause the cosdp routine to be called 8*1000*100 = 800000 times. Any inefficiency in this routine would case a massive multiplication of the bottleneck and slow the code down.

The original code is shown in figure B.2 and it can be seen that for every use of the *cosdp* function, the function has to be loaded into memory for what will be a very short length of time as the function only performs a simple *sin* or *cosine* evaluation on a number that it is passed. A second problem with this piece of code is that a logic evaluation is performed on each call to cosdp. The logic is dependent on the value of MTUV which is constant during the whole of the section of code in rec3d.f. It was decided that 2 simple changes could be made to the code to improve performance.

- Move the logic check so that it is only performed once per call to rec3d

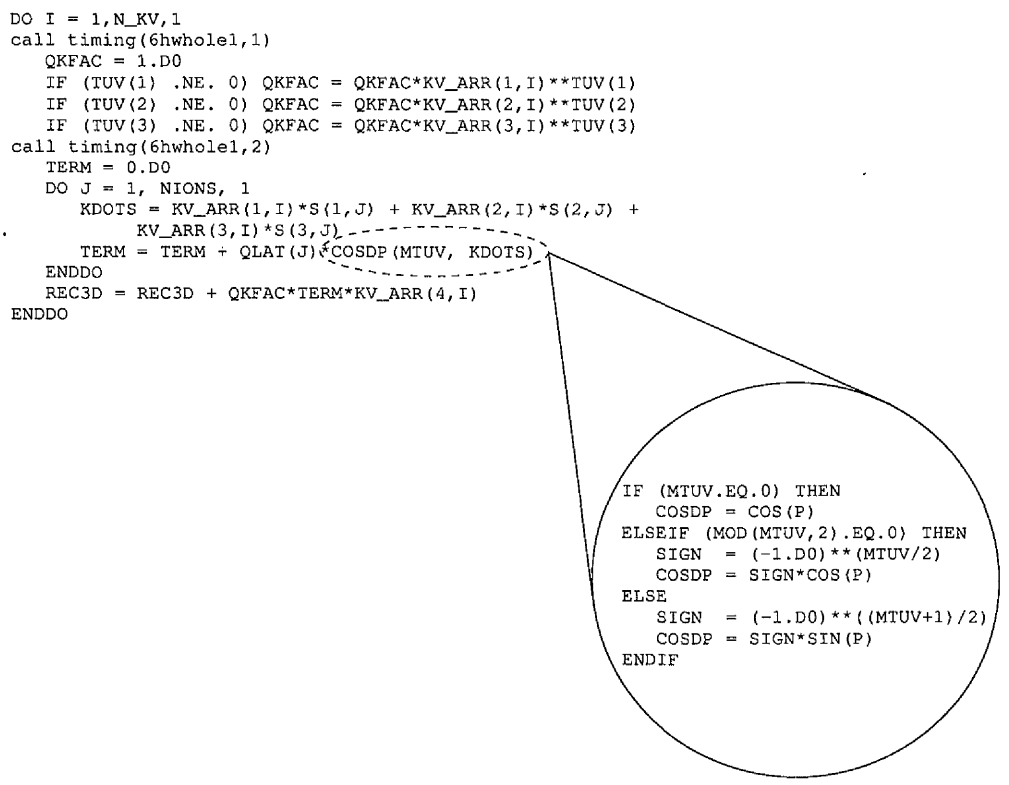

Figure B.2: Original code taken from QMEwald: subroutine rec3d.f and function cosdp

- Inline the code from cosdp to remove any slow down due to the time taken to load the cosdp into memory for every call to it *i.e.* "start-up" time.

The re-written code is shown in figure B.3

The speed-up due to these small changes made a huge difference

We intended to perform the same optimisation for l708, the first derivative code but on profiling it quickly became obvious that the bottleneck was in exactly the same routine so the previous fix worked for both cases. Here though the speedup was even more impressive.

In an attempt to reduce execution time even further, the remaining logic (if(docos))

```
if(MTUV.eq.0)then
   SIGN=1.0D0
   docos=.TRUE.
elseif (MOD(MTUV,2).eq.0)then
   SIGN=(-1.D0)**(MTUV/2)
   docos=.TRUE.
else
   SIGN  = (-1.D0)**((MTUV+1)/2)
   docos=.FALSE.
endif

DO I = 1,N_KV,1
   QKFAC = 1.D0
   IF (TUV(1) .NE. 0) QKFAC = QKFAC*KV_ARR(1,I)**TUV(1)
   IF (TUV(2) .NE. 0) QKFAC = QKFAC*KV_ARR(2,I)**TUV(2)
   IF (TUV(3) .NE. 0) QKFAC = QKFAC*KV_ARR(3,I)**TUV(3)
   TERM = 0.D0
   DO J = 1, NIONS, 1
      KDOTS = KV_ARR(1,I)*S(J,1) + KV_ARR(2,I)*S(J,2) +
.             KV_ARR(3,I)*S(J,3)

      if(docos)then
         TERM = TERM + QLAT(J)*SIGN*cos(KDOTS)
      else
         TERM = TERM + QLAT(J)*SIGN*sin(KDOTS)
      endif

   ENDDO
   REC3D = REC3D + QKFAC*TERM*KV_ARR(4,I)
ENDDO
```

Major part of logic removed from the loop

Subroutine call removed to reduce "start-up" time

Figure B.3: Optimised code for QMEwald: A replacement for the original rec3d.f and cosdp

was moved out of the loop at the expense of duplicating the code. The improvement, although not as great as previous optimisation, still manages to reduce the optimisation time by 5.5% and 3.3% for l307 and l708 respectively. In total, this simple profiling and optimisation procedure has given over a 43% speed up in our test case.

	Total time of execution for l307 (s)
Original code	20.92
Optimised code	13.10
Speed up	7.82 (37.4%)

Table B.1: Times of execution for Link 307

	Total time of execution for l708 (s)
Original code	133.35
Optimised code	77.36
Speed up	55.99 (41.98%)

Table B.2: Times of execution for Link 708

Appendix C

Molecular Mechanics Potentials

C.0.1 NaCl potentials

NaCl potentials of Binks et al.[1]

(available online from http://www.ri.ac.uk/Potentials/)

	Charge (e)	
	Core	Shell
Na	1.000000	
Cl	0.984000	-1.984000

		Short range repulsion	
		A(eV)	ρ(Å)
$Na_{(core)}$	$Na_{(core)}$	1788.1890	0.158600
$Cl_{(shell)}$	$Cl_{(shell)}$	3296.5700	0.328900
$Na_{(core)}$	$Cl_{(shell)}$	482.6300	0.358100

	Core-Shell Interaction $k(eV\AA^{-2})$
Cl	17.520000

C.0.2 Zeolite potentials

Zeolite potentials of Schröder et al.[3]

	Charge (e)	
	Core	Shell
Si	4.00000	
Al	3.00000	
O	1.06237	-3.06237
O_H	1.23944	-3.23944
H	1.00000	

		Short range repulsion	
		A(eV)	ρ(Å)
$Si_{(core)}$	$O_{(shell)}$	1550.950	0.30017
$Si_{(core)}$	$O_{H(shell)}$	2078.349	0.28130
$Al_{(core)}$	$O_{(shell)}$	1068.711	0.32260
$Al_{(core)}$	$O_{H(shell)}$	887.969	0.32377
$H_{(core)}$	$O_{(shell)}$	452.466	0.21143
$H_{(core)}$	$O_{H(shell)}$	6758.796	0.20511

	Core-Shell Interaction $k(eV\AA^{-2})$
O	112.7629
O_H	137.0634

	Three-Body Interaction	
	$k(eV\ rad^{-2})$	θ_0(deg)
Si	0.18397	109.47
Al	0.64984	109.47

Zeolite potentials of Tsuneyuki et al.[188]

	Charge (e)
Si	2.4
O	-1.2

			Short range parameters	
		A(eV)	b(Å^{-1})	$C(eV$Å$^6)$
O	O	1753.80	2.82641	214.3700
Si	O	10703.95	4.79593	70.6100
Si	Si	861588000.00	15.22070	23.2603

References

1. D. J. Binks. Thesis, Ph.D. thesis, University of Surrey (1994).
2. M. Calligaris, G. Nardin, L. Randaccio and P. Chiaramonti. actac, **B38**, 602 (1982).
3. K. Schröder and J. Sauer. J. Phys. Chem., **100**, 11043 (1996).
4. S. Greatbanks. Theoretical Studies of Zeolite Catalysis, Ph.D. thesis, Department of Computational and Theoretical Chemistry, University of Manchester (1995).
5. E. H. Teunissen, R. A. Vansanten, A. P. J. Jansen and F. B. Vanduijneveldt. J. Phys. Chem., **97**, 203 (1993).
6. A. Cronstedt. Akad. Handl. Stockholm, **18** (1756).
7. R. Barrer. Proc. Roy. Soc. (1938).
8. V. Gramlich and W. M. Meier. Z. Kristallogr., Kristallgeometrie, Kristallphys., Kristallchem., **133**, 134 (1971).
9. J. Dwyer. An Introduction to Zeolite Molecular Sieves, John Wiley & Sons (1988).
10. Loewenstein. Am. Mineral., **39**, 92 (1954).
11. D. Breck. Zeolite Molecular Sieves: Structure, Chemistry and Use, John Wiley, London. (1974).

12. L. King, D. Campbell, E. Collins, J. B. Knauer and R. Wallace. Proceedings of the 6th Intenational Zeolite conference, Butterworths, Guildford (1984).

13. A. Zorpas, T. Constantinides, A. Vlyssides, I. Haralambous and M. Loizidou. Bioresource Technology, **72**, 113 (2000).

14. T. Gaffney. Curr. Opin. Solid State Mat. Sci., **1**, 69 (1996).

15. S. Meisel, J. McCullogh, C. Lechthaler and P. Weisz. Chem. Tech., **6** (1976).

16. F. Hasse and J. Sauer. J. Am. Chem. Soc., **117**, 3780 (1995).

17. F. Hasse and J. Sauer. J. Phys. Chem., **98**, 3083 (1994).

18. S. R. Blaszkowski and R. A. Vansanten. J. Am. Chem. Soc., **119**, 5020 (1997).

19. S. R. Blaszkowski and R. A. Vansanten. J. Phys. Chem. B, **101**, 2292 (1997).

20. R. Shah, M. Payne, M.-H. Lee and J. Gale. Science, **271**, 1395 (1996).

21. J. Gale, C. Catlow and C. J.R. Chem. Phys. Lett., **216**, 155 (1993).

22. A. G. Pelmenschikov, G. Morosi and A. Gamba. J. Phys. Chem., **96**, 2241 (1992).

23. C. Zicovich-Wilson, P. Viruela and A. Corma. J. Phys. Chem., **99**, 13224 (1995).

24. F. Hasse and J. Sauer. Microporous and Mesoporous Materials, **35-35**, 379 (2000).

25. J. Gale, R. Shah, M. Payne, I. Stich and K. Terakura. Catal. Today, **50**, 525 (1999).

26. T. Narbeshuber, A. Brait, K. Seshan and J. Lercher. aca, **146**, 119 (1996).

27. A. Corma, J. Planelles, J. Sanchez-Marin and F. Thomas. jcat, **93**, 30 (1985).

28. C. Mota, P. Estaves, A. Ramirez-Solis and R. Hernan-Dez-Lamoneda. jacs, **119**, 5193 (1997).

29. R. Parrillo, D.J. Gorte. J. Phys. Chem., **97**, 8786 (1993).

30. M. Sonnemans, C. den Heijer and M. Crocker. J. Phys. Chem., **97**, 440 (1993).

31. M. Crocker, R. Herold, M. Sonnemans, C. Emeis, A. Wilson and J. van der Moolen. J. Phys. Chem., **97**, 432 (1993).

32. W. Jacobs, J. , van Wolput and van Santen R.A. J. Chem. Soc., Faraday Trans., **89**, 1271 (1993).

33. M. Makarova, A. Ojo, K. Karim, M. Hunger and J. Dwyer. J. Phys. Chem., **98**, 3619 (1994).

34. M. Makarova, K. Al-Ghefaili and J. Dwyer. J. Chem. Soc., Faraday Trans., **90** (1994).

35. A. Zecchina, S. Bordiga, G. Spoto, D. Scarano, G. Petrini, G. Leofanti and M. Padovan. J. Chem. Soc., Faraday Trans., **88**, 2959 (1992).

36. W. Earl, P. Fritz, A. Gibson and J. Lunsford. J. Phys. Chem., **91**, 2091 (1987).

37. A. Pelmenschikov, R. van Santen, Jänchen and E. Meijer. J. Phys. Chem., **97**, 11071 (1993).

38. R. Pelmenschikov, J. van Wolput, A. Jänchen, and R. van Santen. J. Phys. Chem., **99**, 3612 (1995).

39. R. Jackson and C. Catlow. Molec. Simul., **1** (1988).

40. B. Smit and C. den Ouden. J. Phys. Chem., **92**, 7169 (1988).

41. S. Auerbach, N. Henson, Cheetham and H. Metiu. J. Phys. Chem., **99**, 10600 (1995).

42. F. Jousse, L. Leherte and D. Vercauteren. Molec. Simul., **17**, 175 (1996).

43. L. Bull, N. Henson, A. Cheetham, J. Newsam and S. Heys. J. Phys. Chem., **97**, 11776 (1993).

44. S. Yashonath and P. Santikary. J. Phys. Chem., **98**, 6368 (1994).

45. M. Duer, H. He, W. Kolodziejski and J. Klinowski. J. Phys. Chem., **98**, 1198 (1994).

46. J. Nicholas, F. Trouw, M. J.E., L. Iton and A. Hopfinger. J. Phys. Chem., **97**, 4149 (1993).

47. H. Brand, L. Curtiss, L. Iton, F. Trouw and T. Brun. J. Phys. Chem., **98**, 1293 (1994).

48. A. Kyrlidis, S. Cook, A. Chakraborty, A. Bell and D. Theodorou. J. Phys. Chem., **99**, 1505 (1995).

49. S. Greatbanks, I. Hillier, N. Burton and I. Hillier. J. Chem. Phys., **105**, 3770 (1996).

50. H. Koller, G. Engelhardt, A. Kentgens and J. Sauer. J. Phys. Chem., **98**, 1544 (1994).

51. R. Ramprasad, W. Schneider, K. Hass and J. Adams. J. Phys. Chem. B, **101**, 1940 (1997).

52. E. Teunissen, C. Roetti, C. Pisani, A. de Man, A. Jansen, R. Orlando, R. van Santen and R. Dovesi. Modelling Simul. Mater. Sci. Eng., **2**, 921 (1994).

53. E. Schrö dinger. Ann. Physik, **79**, 361 (1926).

54. W. Pauli. Annals de Institut Henri Poincare, **6**, 137 (1936).

55. W. Pauli. Phys. Rev., **58**, 716 (1940).

56. D. Hartree. Proc. Cambr. Phil. Soc.,, **24** (1928).

57. V. Fock. Z. Physik, **61** (1930).

58. C. Roothaan. Rev. Mod. Phys., **23** (1951).

59. G. Hall. Proc. Roy. Soc., **A205** (1951).

60. C. Møller and M. Plesset. Phys. Rev., **46**, 618 (1934).

61. R. Parr and W. Yang. J. Am. Chem. Soc., **106**, 4049 (1984).

62. J. Casanovas, F. Illas and G. Pacchioni. Chem. Phys. Lett., **326**, 523 (2000).

63. H. Xian, Z. Cao, X. Xu and X. Lu. Chem. Phys. Lett., **326**, 485 (2000).

64. M. Bankhead, G. Watson, G. Hutchings, J. Scott and D. Willock. Appl. Catal. A-Gen., **200**, 263 (2000).

65. M. Sierka and J. Sauer. J. Chem. Soc., Faraday Trans., **106**, 1 (1997).

66. S. Blaskzowski, M. Nascimento and R. v. Santen. J. Phys. Chem., **100**, 3463 (1996).

67. S. Blaskzowski and R. v. Santen. J. Phys. Chem., **99**, 11728 (1995).

68. L. Barbosa, G. Zhidomirov and R. van Santen. Phys. Chem. Chemical Physics, **2**, 3909 (2000).

69. K. Shrivastava, R. Belosludov, N. Zhanpeisov, S. Takami, M. Kubo and A. Miyamoto. Chem. Phys. Lett., **325**, 1 (2000).

70. J. Nicholas. Topics in Catal., **9**, 181 (1999).

71. G. Valerio, A. Goursot, R. Vetrivel and D. Salahub. Microporous Mesoporous Mat., **30**, 111 (1999).

72. R. Deka, R. Vetrivel and S. Pal. J. Phys. Chem. A, **103**, 5978 (1999).

73. P. Hohenberg and W. Kohn. Phys. Rev. B, **136**, 864 (1964).

74. R. Parr and W. Yang. Density-Functional Theory of Atoms and Molecules, Oxford University Press, New York (1989).

75. W. Kohn and L. Sham. Phys. Rev. A, **140**, 1133 (1965).

76. A. Becke. Phys. Rev. A, **38**, 3098 (1988).

77. C. Lee, N. Yang and R. Parr. Phys. Rev. B, **37** (1988).

78. A. Becke. J. Chem. Phys., **98**, 1372 (1993).

79. P. Stephens, F. Devlin, C. Chabalowski and M. Frisch. J. Phys. Chem., **98**, 11623 (1994).

80. S. Boys. prs, **A200** (1950).

81. R. Pariser and R. G. Parr. J. Chem. Phys., **21**, 466 (1953).

82. J. N. Murrell and A. J. Harget. Semi-empirical Self-consistent Field Molecular Orbital Theory of Molecules, Wiley-Interscience (1972).

83. J. A. Pople and G. A. Segal. J. Chem. Phys., **44**, 3289 (1966).

84. M. J. S. Dewar and G. Klopman. J. Am. Chem. Soc., **89**, 3089 (1967).

85. J. A. Pople, D. L. Beveridge and P. A. Dobosh. J. Chem. Phys., **47**, 2026 (1967).

86. J. A. Pople, D. P. Santry and G. A. Segal. J. Chem. Phys., **43**, S129 (1965).

87. M. J. S. Dewar and W. Thiel. J. Am. Chem. Soc., **99**, 4899 (1977).

88. J. J. P. Stewart. J. Computer-Aided Mol. Design, **4**, 1 (1990).

89. M. J. S. Dewar, E. G. Zoebisch, E. F. Healy and J. J. P. Stewart. J. Am. Chem. Soc., **107**, 3902 (1985).

90. J. J. P. Stewart. J. Comp. Chem., **10**, 209 (1989).

91. J. J. P. Stewart. J. Comp. Chem., **10**, 221 (1989).

92. Fujitsu Limited. MOPAC 93 Manual (1993).

93. B. Dick and A. Overhauser. Phys. Rev. B, **112**, 90 (1958).

94. K. Schröder and J. Sauer. J. Phys. Chem., **100**, 43 (1996).

95. E. de Vos Burchart, V. Verheij, H. van Bekkum and B. van de Graaf. Zeolites, **12** (1992).

96. J. R. Hill and J. Sauer. J. Phys. Chem., **98**, 1238 (1994).

97. J. Hill and J. Sauer. J. Phys. Chem., **99**, 9536 (1995).

98. J. Maple, U. Dinur and A. Hagler. Proc. Natl. Acad. Sci., **85**, 5350 (1998).

99. E. de Vos Burchart, H. van Bekkum, B. van de Graaf and E. Vogt. J. Chem. Soc., Faraday Trans., **88**, 2761 (1992).

100. B. Baekelandt, W. Mortier and R. Schoonheydt. Modelling of Structure and Reactivity in Zeolites, Academic Press, London (1992).

101. K. van Genechten, W. Mortier and P. Geerlings. J. Chem. Phys., **86**, 5063 (1987).

102. J. D. Gale. GULP (the General Utility Lattice Program), Royal Institution/Imperial College, UK (1992-1994).

103. M. Brandle and J. Sauer. J. Mol. Cat. A: Chem., **119**, 19 (1997).

104. P. K. Weiner and P. A. Kollman. J. Comp. Chem., **2**, 287 (1981).

105. A. Warshel and M. Levitt. J. Mol. Biol., **103**, 227 (1976).

106. U. C. Singh and P. A. Kollman. J. Comp. Chem., **7**, 718 (1986).

107. S. Humbel, S. Sieber and K. Morokuma. J. Chem. Phys., **105**, 1959 (1996).

108. F. Maseras and K. Morokuma. J. Comp. Chem., **16**, 1170 (1995).

109. M. Frisch, G. Trucks, H. Schlegel, G. Scuseria, M. Robb, J. Cheeseman, V. Zakrzewski, J. Montgomery, R. Stratmann, J. Burant, S. Dapprich, J. Millam, A. Daniels, K. Kudin, M. Strain, O. Farkas, J. Tomasi, V. Barone, M. Cossi, R. Cammi, B. Mennucci, C. Pomelli, C. Adamo, S. Clifford, J. Ochterski, G. Petersson, P. Ayala, Q. Cui, K. Morokuma, D. Malick, A. Rabuck, K. Raghavachari, J. Foresman, J. Cioslowski, J. Ortiz, A. Baboul, B. Stefanov, G. Liu, A. Liashenko, P. Piskorz, I. Komaromi, R. Gomperts, R. Martin, D. Fox, T. Keith, M. Al-Laham, C. Peng, A. Nanayakkara, C. Gonzalez, M. Challacombe, P. Gill, B. Johnson, W. Chen, M. Wong, J. Andres, C. Gonzalez, M. Head-Gordon, E. Replogle and J. Pople. Gaussian 98, Gaussian, Inc., Pittsburgh PA, 1998. (1994).

110. X. Assfeld and J.-L. Rivail. Chem. Phys. Lett., **263**, 100 (1996).

111. S. A. Hindle. A new Quantum Mechanical/Molecular Mechanical method for modelling biological and solid state systems, Ph.D. thesis, University of Surrey (1994).

112. H. Schlegel. Adv. Chem. Phys., **67**, 249 (1987).

113. A. Szabo and N. Ostlund. Modern Quantum Chemistry, McGraw-Hill, New York, first edn. (1989).

114. H. Schlegel. J. Comp. Chem., **3**, 214 (1982).

115. P. Pulay. Mol. Phys., **17**, 197 (1969).

116. P. Pulay. Mol. Phys., **18**, 473 (1970).

117. P. Pulay, G. Fogarasi, F. Pang and J. Boggs. J. Am. Chem. Soc., **101**, 2550 (1979).

118. P. Pulay and G. Fogarasi. J. Chem. Phys., **96**, 2856 (1992).

119. F. G., Z. X., P. Taylor and P. Pulay. J. Am. Chem. Soc., **114**, 8191 (1992).

120. C. Peng, P. Ayala, H. Schlegel and M. Frisch. J. Comp. Chem., **17**, 49 (1996).

121. M. Frisch, G. Trucks, H. Schlegel, P. Gill, B. Johnson, M. Robb, J. Cheeseman, T. Keith, G. Petersson, J. Montgomery, K. Raghavachari, M. Al-Laham, V. Zakrzewski, J. Ortiz, J. Foresman, J. Cioslowski, B. Stefanov, A. Nanayakkara, M. Challacombe, C. Peng, P. Ayala, W. Chen, M. Wong, J. Andres, E. Replogle, R. Gomperts, R. Martin, D. Fox, J. Binkley, D. DeFrees, J. Stewart, M. Head-Gordon, C. Gonzalez and J. Pople. GAUSSIAN 94, Gaussian Inc., Pittsburgh, PA (1994).

122. E. Wilson, J. Decius and P. Cross. Molecular Vibrations, McGraw-Hill, New York (1955).

123. C. Broyden. J. Inst. Math. Appl., **6**, 76 (1970).

124. R. Fletcher. Comput. J., **13**, 317 (1970).

125. D. Goldfarb. Math. Comput., **24**, 23 (1970).

126. D. Shanno. Math. Comput., **24**, 647 (1970).

127. J. Bofill. J. Comp. Chem., **15**, 1 (1994).

128. M. Powell. Math. Prog., **1**, 26 (1971).

129. B. Murtagh and R. Sargent. Comput. J., **13**, 185 (1972).

130. J. Baker. J. Comp. Chem., **7**, 385 (1986).

131. J. Newsam, M. Treacy, W. Koetsier and C. deGruyter. Proc. Roy. Soc., **420**, 375 (1998).

132. G. Hutchings, P. Page and F. Hancock. Chemistry in Britain, pp. 46–48 (July 1997).

133. G. Hutchings, R. Wells, S. Feast, M. Siddiqui, D. Willock, F. King, C. Rochester, D. Bethell and P. Bulman Page. Catal. Lett., **46**, 249 (1997).

134. P. Jacobs. Nature, **369**, 543 (1994).

135. D. Willock, D. Bethell, S. Feast, G. Hutchings, F. King and P. Bulman-Page. Topics in Catal., **3**, 77 (1996).

136. S. Feast, M. Siddiqui, R. Wells, D. Willock, F. King, C. Rochester, D. Bethell, P. Bulman Page and G. Hutchings. J. Catal., **167**, 533 (1997).

137. S. Feast, D. Bethell, P. Bulman Page, C. Rochester, M. Siddiqui, D. Willock and G. Hutchings. J. Mol. Cat. A: Chem., **107**, 291 (1996).

138. S. Feast, D. Bethell, P. Bulman-Page, M. Siddiqui, D. Willock, G. Hutchings, F. King and C. Rochester. Stud. Surf. Sci. Cat., **101**, 211 (1996).

139. S. Feast, D. Bethell, P. Bulman Page, F. King, C. Rochester, M. Siddiqui, D. Willock and G. Hutchings. J. Chem. Soc., Chem. Comm., pp. 2409–2411 (1995).

140. U. Fleischer, K. Kutzelnigg, A. Bleiber and J. Sauer. J. Am. Chem. Soc., **115**, 7833 (1993).

141. L. Curtiss, H. Brand, J. Nicholas and L. Iton. Chem. Phys. Lett., **184**, 215 (1991).

142. R. A. Vansanten. Stud. Surf. Sci. Cat., **85**, 273 (1994).

143. M. Stave and J. Nicholas. J. Phys. Chem., **97**, 9630 (1993).

144. H. Brand, L. Curtiss and L. Iton. J. Phys. Chem., **96**, 7725 (1992).

145. K. Fuchs. J. Mol. Cat. A: Chem., **119**, 449 (1997).

146. C. Pisani, R. Dovesi and C. Roetti. Crystal 92 User's Manual, Gruppo di Chimica Teorica, Universitá di Torino and SERC Laboratory (1992).

147. Roetti. The CRYSTAL code, Gruppo di Chimica Teorica, Universitá di Torino and SERC Laboratory (1996).

148. V. Saunders, C. Freyria-Fava, L. Salasco, R. Dovesi and C. Roetti. Mol. Phys., **77**, 629 (1992).

149. S. Greatbanks, P. Sherwood and I. Hillier. J. Phys. Chem., **98**, 8134 (1994).

150. U. Eichler, C. M. Kolmel and J. Sauer. J. Comp. Chem., **18**, 463 (1996).

151. M. Brandle and J. Sauer. J. Am. Chem. Soc., **120**, 1556 (1998).

152. M. Brandle, J. Sauer, R. Dovesi and N. Harrison. J. Chem. Phys., **109**, 10379 (1998).

153. M. Sierka and J. Sauer. Faraday Disc., pp. 41–62 (1997).

154. U. Eichler, M. Brandle and J. Sauer. J. Phys. Chem. B, **101**, 10035 (1997).

155. D. Nachtigallova, P. Nachtgall, M. Sierka and J. Sauer. Phys. Chem. Chemical Physics, **1**, 2019 (1999).

156. E. Madelung. Phys. Z., **19**, 524 (1918).

157. P. Ewald. Ann. Phys, **64**, 253 (1921).

158. M. Nygren. Theoretical Studies of Metal CLusters and Oxidic Surfaces, Ph.D. thesis, Department of Physics, University of Stockholm (1995).

159. M. Nygren and R. Hall. Implimentation of the ECPAIMP package for Gaussian94, University of Manchester, UK (1998-2000), Modifications by C.M. Windsor & L. Salsi.

160. M. Harrison, N. Burton and I. Hillier. J. Am. Chem. Soc., **119**, 12285 (1997).

161. J. White and A. Hess. J. Phys. Chem., **97**, 8703 (1993).

162. J. White and A. Hess. J. Phys. Chem., **97**, 6398 (1993).

163. G. J. Kramer, N. Farragher, B. van Beest and R. A. Vansanten. Phys. Rev. B, **43**, 5068 (1991).

164. E. Stefanovich and T. Truong. J. Phys. Chem. B, **102**, 3018 (1998).

165. A. Klamt and G. Schüürmann. J. Chem. Soc., Perkin Trans., **2**, 799 (1993).

166. J. Pascual-Ahuir, E. Silla and I. Tuñon. J. Comp. Chem., **15**, 1127 (1994).

167. W. Wadt and P. Hay. J. Chem. Phys., **82**, 284 (1985).

168. W. Stevens, H. Basch and J. Krauss. J. Chem. Phys., **81**, 6026 (1984).

169. J. Vollmer, E. Stefanovich and T. Truong. J. Phys. Chem., **103**, 9415 (1999).

170. J. Vollmer and T. Truong. J. Phys. Chem., **104**, 6308 (2000).

171. J. Limtrakul, S. Jungsuttiwong and P. Khongpracha. J. Phys. Chem., **525**, 153 (2000).

172. J. Limtrakul, P. Khongpracha, S. Jungsuttiwong and J. Truong. J. Mol. Cat. A: Chem., **153**, 155 (2000).

173. I. Senchenya, E. Garrone and P. Ugliengo. J. Mol. Struct. (Theochem), **368**, 93 (1996).

174. E. Garrone, B. Fubini, B. Bonelli, B. Onida and C. Otero Areán. Phys. Chem. Chemical Physics, **1**, 513 (1999).

175. G. Della-Gatta, B. Fubini, G. Ghiotti and C. Morterra. J. Catal., **43**, 90 (1976).

176. E. Paukshtis, S. R.I. and Y. E.N. React. Kinet. Catal. Lett., **19** (1982).

177. J. Dwyer and S. P. Bates. J. Chem. Phys., **97**, 5897 (1993).

178. A. Khodakov, S. P. Bates, J. Dwyer, C. M. Windsor and N. A. Burton. Phys. Chem. Chemical Physics, **1**, 507 (1999).

179. P. J. O' Malley and D. J. Chem. Phys. Lett., **143**, 97 (1988).

180. K. Hass and W. Schneider. J. Phys. Chem., **100**, 9292 (1996).

181. W. Schneider, K. Hass, R. Ramprasad and J. Adams. J. Phys. Chem., **100**, 6032 (1996).

182. B. S. F. and B. F. Mol. Phys., **19** (1970).

183. N. Echoufi and P. Gelin. J. Chem. Soc., Faraday Trans., **88**, 1067 (1992).

184. V. Gruver and J. J. Fripiat. J. Phys. Chem., **98**, 8549 (1994).

185. J. Szanyi and M. T. Paffett. Microporous Materials, **98**, 8549 (1994).

186. L. M. Kustov, V. Z. Kazansky, S. Beren, L. Kubelkova and J. Jiru. J. Phys. Chem., **91**, 5247 (1987).

187. C. Angell and P. Schaffer. J. Phys. Chem., **148**, 526 (1966).

188. S. Tsuenyuki, M. Tsukada, H. Aoki and Y. Matsui. Phys. Rev. Lett., **61**, 869 (1988).